CRANFIELD UNIVERSITY

FIASAEL ALSHIMMERI

Diagnosis of Low-Speed Bearing Degradation Using Acoustic Emission Techniques

School of Engineering

PhD Thesis
Academic Year: 2016 -2017

Supervisor: Dr. Abdulmajid Addali
Supervisor: Dr. Amaral Teixeira, Joao

January 2017

CRANFIELD UNIVERSITY

School of Engineering

PhD Thesis

Academic Year 2016 -2017

FIASAEL ALSHIMMERI

Diagnosis of Low-Speed Bearing Degradation Using Acoustic Emission Techniques

Supervisor: Dr. Abdulmajid Addali
Supervisor: Dr. Amaral Teixeira, Joao
January 2017

ABSTRACT

It is widely acknowledged that bearing failures are the primary reason for breakdowns in rotating machinery. These failures are extremely costly, particularly in terms of lost production. Roller bearings are widely used in industrial machinery and need to be maintained in good condition to ensure the continuing efficiency, effectiveness, and profitability of the production process. The research presented here is an investigation of the use of acoustic emission (AE) to monitor bearing conditions at low speeds.

Many machines, particularly large, expensive machines operate at speeds below 100 rpm, and such machines are important to the industry. However, the overwhelming proportion of studies have investigated the use of AE techniques for condition monitoring of higher-speed machines (typically several hundred rpm, or even higher). Few researchers have investigated the application of these techniques to low-speed machines (<100 rpm), This PhD addressed this omission and has established which, of the available, AE techniques are suitable for the detection of incipient faults and measurement of fault growth in low-speed bearings.

The first objective of this research program was to assess the applicability of AE techniques to monitor low-speed bearings. It was found that the measured statistical parameters successfully monitored bearing conditions at low speeds (10-100 rpm).

The second objective was to identify which commonly used statistical parameters derived from the AE signal (RMS, kurtosis, amplitude and counts) could identify the onset of a fault in either race. It was found that the change in AE amplitude and AE RMS could identify the presence of a small fault seeded into either the inner or the outer races. However, the severe attenuation of the signal from the inner race meant that, while AE amplitude and RMS could readily identify the incipient fault, kurtosis and the AE counts could not. Thus, more attention needs to be given to analysing the signal from the inner race.

The third objective was to identify a measure that would assess the degree of severity of the fault. However, once the defect was established, it was found that of the parameters used only AE RMS was sensitive to defect size.

The fourth objective was to assess whether the AE signal is able to detect defects located at either the centre or edge of the outer race of a bearing rotating at low speeds. It is found that all the measured AE parameters had higher values when the defect was seeded in the middle of the outer race, possibly due to the shorter path traversed by the signal between source and sensor which gave a lower attenuation than when the defect was on the edge of the outer race. Moreover, AE can detect the defect at both locations, which confirmed the applicability of the AE to monitor the defects at any location on the outer race.

Keywords:

Condition monitoring, low-speed bearing, acoustic emission, vibration analysis, signal processing, statistical parameters

ACKNOWLEDGEMENTS

My ultimate thanks are to ALLAH almighty that created me and gave me strength and knowledge.

I would deeply like to express my gratitude and appreciation to my supervisors Dr. Abdulmajid Addali and Dr. Joao Amaral Teixeira for their advice, comments, and patience.

Also, as written in the Quran, “ALLAH has decreed that you do not worship except Him, and to parents, good treatment". I am particularly indebted to my father, Mr. Mubarak Nashmi Al-Shammarri, The Paradise of the Earth (My Mother A. Al-Dabbous) and my brothers, Dr. Nashmi Al-Shammarri, Dr. Saoud Al-Shammarri, Dr. Sajer Al-Shammarri, and Dr. Mosab Al-Rashed, for their enthusiasm, encouragement, support and co-operation. May ALLAH bless them in all their endeavours as, without their unreserved support, completion of this study would not have been possible.

I would also like to express my gratitude to the many people for their help. Particular mention goes to those individuals and bodies listed below:

The Paradise of the Earth (My Mother Awatef Al-Dabbous)

Mr. Fayez Saoud Al-Dabbous

Mr. Yousef Mohammad Al-Harbi

Dr. Abdulrahman Al-Enezi

Dr. Abdulrahman Al-Mutairi

Dr. Hamad Al-Hajeri

Also, I want to thanks the Kuwait Foundation for the Advancement of Sciences (KFAS) who partially funded my project under the project code “P116-65EE-01.”

Finally, hope to be and death as those mentioned by the messenger, “the God makes the way to heaven easy for him who treads the path in search of knowledge".

TABLE OF CONTENTS

LIST OF FIGURES

LIST OF TABLES

LIST OF EQUATIONS

LIST OF ABBREVIATIONS

CM	Condition Monitoring
AE	Acoustic Emission
EDM	Electrical Discharge Machine
PLDT	Peak Level Differential Technique
SST	Slow-Speed Technology
ANN	Artificial Neural Network
A/D	Analogue to Digital
ASL	Average Signal Level
RMS	Root Mean Square
FFT	Fast Fourier Transform
ANC	Adaptive Noise Cancellation
RBC	Rotating Biological Contractors
CF	Crest Factor
ASL	Average Signal Level
EI	Energy Index
SI	Separation Index
STFT	Short-Time Fourier Transform
SK	Spectral Kurtosis
WT	Wavelet Transform
CWT	Continuous Wavelet Transform
MRA	Multi-Resolution Analysis
LPF	Low-Pass Filter
dB	Decibels
HT	Hilbert Transform
HHT	Hilbert-Huang Transform
IMF	Intrinsic Mode Functions

Chapter One

1 Introduction

1.1 Background and Motivation

Condition monitoring (CM) is the process of monitoring physical parameters that demonstrate a machine's operational condition, give a measure of its integrity, and possibly, predict likely time before the operation has to be interrupted for repair and maintenance. Many industries use CM, especially for expensive, heavy machines and equipment such as generators, compressors, and turbines. This is because the monitoring process maintains the operational health of the plant and maximizes production volume. It also helps in detection of faulty conditions at an early stage, avoids accidents, and reduces downtime. Furthermore, these CM techniques are used to arrange proactive maintenance and increase the machinery efficiency by reducing downtime.

In machine CM, greatest attention is given to the bearings as they tend to fail more frequently than other components, usually through fatigue. For instance, O'Donell et al. [1] stated that 41% of the failures in induction motors are due to bearing failures. Thus, a large number of studies have concentrated their effort in monitoring these components.

There are two general types of bearings; sliding contact bearings and rolling contact bearings. Sliding contact bearings can be a guide, journal or thrust bearing. Guide bearings are usually used to guide the machine component motion along its length without rotation. Journal bearings have a cylindrical shape and require fluid lubrication. Thrust bearings are used to prevent motion along the shaft axis.

Rolling contact bearings substantially reduce friction between components thus are also known as anti-friction bearings. This type of bearing can have either point contact or line contact with the bearing races. Rolling contact bearings have the ability to carry the radial load (radial ball or roller bearings), thrust (thrust ball bearing), or a combination of both (angular ball and roller bearings). The elements

for rolling contact bearings can be cylindrical, spherical, tapered, or barrel-shaped.

In industry, rolling contact bearings exist in a wide range of applications. They play a major role in rotating machinery, and their failure can require machinery shut down. Hence, research into the successful CM of these bearings is ongoing. Today, the major problem related to CM of bearings is to detect faults in their early stages. The problems related to monitoring these bearings are directly linked with machine complexity. For instance, while it is easy to monitor the bearing condition in an electric motor, the main bearings of aero-engine shafts require advanced signal processing techniques to extract the required signal from background noise.

Rotating machinery can be divided into four categories based on the speed of rotation; high, moderate, low, and extremely low-speed. However, the boundaries for categorization have no universally accepted values. This research separates machine speed into four categories: high-speed (above 60,000 rpm [1 kHz]) as stated by Mba [2], moderate-speed (between 100 – 60,000 rpm [1.67 Hz - 1 kHz]), low-speed (between 10-100 rpm [0.167 - 1.67 Hz]) as mentioned in [3–5], and extremely-low-speed (below 10 rpm [< 0.167 Hz]) as cited by [2,6–8]. In the industrial sector, low-speed machines using bearings can be found in such areas, as sewage treatment plants, cranes, and wind turbines. Due to the high cost of these machines, it is important to monitor those bearings to minimise downtime and likelihood of failures.

Thus, CM of low-speed bearings has become the subject of considerable attention and research, in defining which parameters to use for detecting fault initiation and fault propogation (i.e. fault size). This study investigates the applicability of Acoustic Emission (AE) to the detection of the early stages of bearing defect at low speeds (10-100 rpm).

The main motivation for this study is to improve rolling element bearing reliability in machines. To undertake this task, an experimental investigation has been carried out using AE techniques to detect and monitor defect initiation and propagation in a roller bearing. The key task was to detect incipient faults at the

earliest possible stage. Detecting and diagnosing the fault at this early stage does not necessarily mean immediate replacement. Instead, the fault's development can be tracked, and maintenance activity can be planned to maximize bearing life and minimize downtime.

1.2 Project Scope

In the past, machinery continued in use until it failed and then repairs and maintenance were carried out. Today, such an approach is not possible because run-to-failure is very expensive in terms of lost production, and as machines have become larger and more complex, their parts have become too costly to destroy. Thus, this research program investigates the use of AE as a viable condition monitoring technique to be used with low speed rotating machinery. Such a technique may offer:

- The opportunity for arranging proactive maintenance and increase the efficiency of the machinery by minimizing production stoppages.
- Effective detection of incipient faults.
- Location of the AE sources.
- Identification of the size of bearing defects.

To achieve these goals the first and most important task of this research program is to demonstrate a correlation between AE and defect initiation and propagation in low-speed bearings.

On the basis of a review of CM technologies, a test rig was designed and built for the bearing tests. The AE results were measured, recorded, and analyzed using such statistical parameters from the time domain as maximum amplitude, kurtosis, RMS, and the number of AE counts.

1.3 Aim and Objectives of the Research

The aim of this project is to demonstrate experimentally, the applicability of AE techniques to detect and monitor defect initiation and subsequent propagation on bearings rotating at low speeds.

The objectives of this research are as follows:

- To conduct a set of experiments at low speeds, for different speeds, loads, and different defect sizes in both the inner and outer races of a roller bearing.
- Compare the measurements obtained from both inner and outer races under similar conditions to check the applicability of AE techniques in detecting faults in these parts.
- To investigate the applicability of AE to detect the defect initiation at both inner and outer races of bearings rotating within the low-speed range.
- To consider the effect of defect size on the measured AE statistical parameters.
- To study the applicability of the measured AE statistical parameters in detecting a defect at different locations on the outer race.

1.4 Contribution to Knowledge

An enormous amount of work has been carried out investigating the applicability of AE to the CM of bearings at high speeds. However, only limited studies have investigated the low-speed range. Thus, to date, there is a shortage of knowledge on the applicability of AE to monitor bearing degradation in the speed range between 10-100 rpm. This investigation addresses the applicability of AE techniques to monitor the early stages of bearing degradation in this speed range and so will offer a significant contribution to the existing body of knowledge on the applications of AE.

The main contributions of study are:

- AE is proved to be a suitable technique to monitor bearing conditions at low speeds (10-100 rpm).
- This is the first known attempt to investigate the sensitivity of AE statistical parameters to varying speed and load at low speeds (10-100 rpm).

- This is the first known attempt to examine the sensitivity of AE statistical parameters to the presence of defects and defect size at low speeds (10-100 rpm).

1.5 Thesis Outline

This thesis contains nine chapters. Chapter 2 reviews the relevant literature including an overview of bearing failure and available CM techniques for low-speed bearings. A comprehensive review of vibration analysis is also included, followed by a review of the application of AE to the monitoring of low-speed bearings. Chapter 3 provides a critical review of signal processing techniques. Chapter 4 describes the research methodology and details of the experimental procedure, data acquisition, and calibration.

Chapter 5 is devoted to an investigation of possible AE statistical parameters to be used for monitoring the outer race. The first objective of the chapter is to examine the sensitivity of the statistical parameters to speed and load variations. The second objective is to identify the most sensitive statistical parameters for defect existence and defect size. The same investigation is repeated for the inner race in Chapter 6. A comparison of the outcomes of chapter 5 (outer race case) and Chapter 6 (inner race case) is presented in Chapter 7. The applicability of the AE measured parameters to monitor defects at different locations on the outer race, and the effect of the defect size on the measured parameters are investigated in Chapter 8. This element of the research is restricted to only the outer race due to time constraints on the project. Finally, Chapter 9 provides conclusions and recommendations for future work.

Chapter Two

2 Literature Review

This chapter begins with an overview of the major failures in bearings and their likely causes. Then there is a brief discussion of available CM techniques and their possible application to low speed rotating machinery. Next, the application of vibration analysis to monitor bearing condition is critically reviewed. Finally, an in-depth description is given of the AE techniques used in previous work to monitor low-speed bearing conditions.

2.1 Bearing Failure

The accurate and correct design of rolling element bearings is essential to ensure that a machine performs efficiently in the long term. Furthermore, proper installation, maintenance, and lubrication of bearings ensure machinery longevity and efficiency. However, bearing defects can still arise due to an event such as improper maintenance and/or installation, poor lubrication, overheating, overloading, imbalance, misalignment, incorrect application, and so forth. [8,9]. Moreover, cyclic stresses can lead to crack initiation and propagation, followed by material flaking from the rolling surfaces. Bearing lifetime will be affected, and such bearings will fail earlier than expected [10].

Bearing defects are usually divided into distributed or localised [11]. Distributed defects include, for example, misaligned races or surface roughness and are generally due to manufacturing errors or abrasive wear. Localised defects include cracks, pits, and spalls. Of course, the capability to detect both distributed and localised faults is important, but the focus of this study is localised defects that are usually related to specific and distinct indicators contained in the acquired signals. For example, the harmonic characteristics in machine vibrations generated by the presence of a fault. The emphasis of this research is on localised defects as these will usually start with subsurface cracks and progressively propagate to the surface and present as pits and spalls [12].

Spalling and brinelling are recognised as the most important causes of bearing failure [12]. Spalling can occur at contact points on the rolling elements on either the inner or the outer ring of a bearing, wherever there are an overloading and severe impact. Spalling is a failure due to fatigue and leads to the removal of discrete particles of either ring or the rolling elements themselves, see Figure 2.1 (b). Once started the failure will progress and is always accompanied by increased vibration levels. Brinelling (the development of dents or indentations) is usually due to overloading the bearing beyond the prescribed elastic limit, see Figure 2.1 (a).

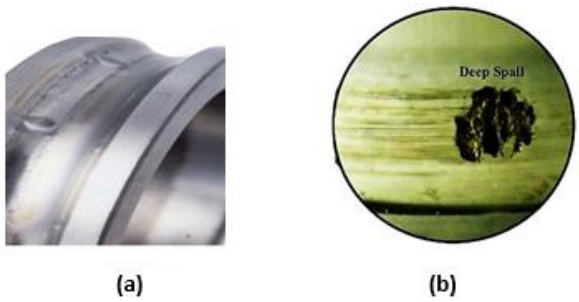

Figure 2.1: Brinelling and Spalling [9]

Researchers have adopted two general approaches to generating local bearing defects in order to study their properties. One is run-to-failure so that defects occur naturally [13–18]. However, to accelerate the process and reduce the time required for the tests, it is usual to apply significant loads or less graded bearing material. The second is to seed artificial defects into the bearing using, for example, an electric discharge machine (EDM) or engraving tool [19–23].

2.2 Condition Monitoring

CM is the process applied to determine the operational health of a machine to detect potential failures before they develop into functional failures. CM usually consists of continuous or periodical data collection, analysis, and interpretation. Today, CM is expected to give an indication of the remaining working life of the component, and it is an integral part of Predictive Maintenance (PM) in which maintenance activities are scheduled only when a functional failure is likely. CM improves the operational efficiency and staff safety. Thus, it is important to find accurate and reliable methods of predicting the remaining working life of in-service machinery.

CM techniques frequently used for rotating machinery include vibration analysis, AE, thermography, and oil analysis [5]. Selecting an appropriate CM method can be quite difficult as there are many factors to consider. The key factors for choosing the best-suited technique are sensitivity, the number of components, monitoring accessibility, the cost of instrumentation, and the size of the machine being monitored. Of course, the capabilities and limitations of each monitoring technique should be understood.

- **Vibration Analysis**

In rotating machinery, vibration analysis is considered to be the most common form of CM method in the industrial field. This technique is used for many kinds of rotating machines, and it is a powerful tool in diagnosing faults [24–26]. Velocity, displacement, and acceleration are the most common parameters monitored in vibrations. There are different types of vibration sensors and they are selected based on the frequency range of interest:

- Accelerometer sensors are used in the high-frequency range
- Velocity sensors are employed in the middle-frequency range
- Displacement sensors are used in the low-frequency range

Various data analysis techniques are used to assess signals and extract specific data or information. The most commonly used techniques for analysing signals

are spectral analysis and cepstral analysis. Moreover, various statistical parameters, such as kurtosis, RMS, and peak value can be used to describe the time domain signals. Vibration analysis can be usefully applied to monitor various machine elements such as bearings, shafts, compressors, turbines (gas and steam), pumps, and gearboxes. The range of frequencies in which vibration analysis is effective is 1 - 50 kHz [27].

- **Acoustic Emission Technology**

AE is considered as a successful technique for monitoring the condition of rotating machines [8]. It is a non-destructive testing as it does not affect the future usefulness of the object being tested. The typical range of AE frequencies is between 50 kHz to 1 MHz [28]. Signal processing techniques are used to measure AE signals and observe the different characteristics of defects. The properties of signals can be found with the help of statistical tools such as mean, standard deviation, skewness, and kurtosis. Details of AE technique are provided in Section 2.4.

- **Thermography**

Thermography is a quick observation technique used to monitor the condition of machines. The hot spots on the body of the machine can be detected by thermal images that are produced by infrared radiation from the surface. This radiation can be detected using the thermographic camera. The performance of a bearing can be determined by simple assessment. Incorrect alignment and other faults will be displayed as thermal patterns as mechanical work is converted into heat.

- **Oil Analysis**

Monitoring machinery based on the condition of the used lubricating oil has been standard operating procedure for more than 50 years and continues to be one of the most widely used techniques in CM. The condition of the spent oil is compared with the virgin oil to determine the condition of the equipment, see Figure 2.2. However, analysing oil and interpreting the data are time-consuming activities.

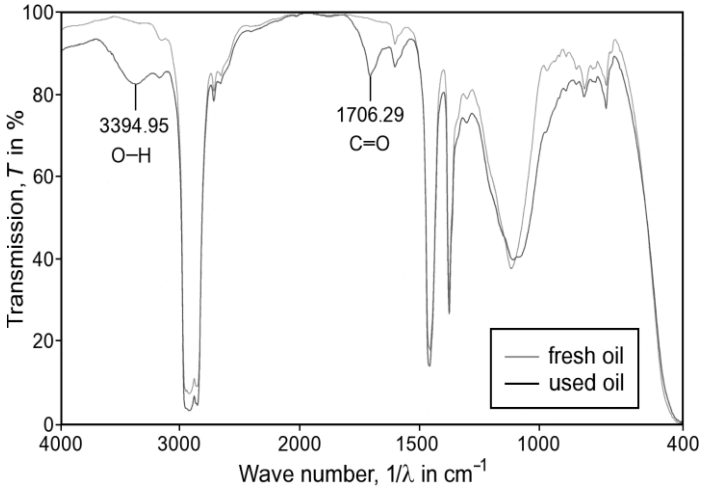

Figure 2.2: Typical Oil Analysis [29]

A comparison between some of the CM methods used for rotating machines is shown in Table 2.1.

Table 2.1: CM Techniques used with rotating machines

Technology	Feasibility	Limitations
Vibration Analysis	Structural components, bearings, shafts and gears	• Detects fully developed defects only • Not useful for very low-speed applications • Signals tend to be of low amplitude
Thermography	Technology involves sensors and electronic control systems	• Run mostly in offline mode • Not able to identify the internal temperature when the medium is isolated by glass, polyethene or other materials • High instrument costs
Oil Analysis	Machine components, such as hydraulic system, bearing, gear, and shaft	• Typically performed offline • Appropriate for a limited number of components which require lubricant • Requires accessibility • Time consuming
Acoustic Emission	Structural components, bearings, shafts, and gears	• Very sensitive to low amplitude signals • Special sensors and signal processing are required

Before this century, researchers tended to focus on monitoring components such as bearings, shafts, gearboxes, and so forth at high-speed machines with limited research on monitoring the condition of low-speed rotating machines [8]. Some previous studies have investigated the applicability of AE, and vibration analysis to monitor bearing conditions at different speeds, see Table 2.2. AE and vibration analysis were chosen owing to their ability to be applied online and their sensitivity to bearing conditions. Table 2.2 divides some of the previous studies according to the speed range, as well as the type of defective method (natural or seeded).

Table 2.2: Applications of AE and Vibration analysis for bearing monitoring

Defect type	**Extremely low speed (S < 10 rpm)**	**Low speed (10 ≤ S ≤ 100 rpm)**	**Moderate and high speeds (S > 100 rpm)**
Natural defect	[2,6,30–32]	[5,13–15,17][33]	[34–41]
Artificially seeded defect	[7,42–44]	[45,46]	[12,19–21,23,33,45,47–64]
Applications	RBC (Rotating Biological Contactor), Steel mills, Paper mills	Passenger ropeway, Wind turbine, Cranes, Sugar packaging machines, Bucket elevator	Jet engine, Car engine, Trains, Rotating motor, Drilling applications

From Table 2.2 it can be seen that only a limited number of researchers covered the low-speed range despite there being many applications.

For a clearer understanding of the use of vibration and AE techniques for bearing CM, the next sections discuss both techniques.

2.3 Vibration Analysis

Vibration analysis is a well-established technique used to monitor bearing degradation [11,65–67]. This technique has the advantage over the other methods in that it can be applied online. Furthermore, analysing time is shorter, and the process is less expensive than other comparable techniques. However, at low rotational speeds, there are numerous limitations which can be divided into four sections [2,68,69]:

1. **Type of sensor required for low rotating speed applications**

The accelerometer is the sensor usually employed in vibration analysis, however, for low rotating speeds displacement sensors are better-suited [2]. This is because the sensitivity of the accelerometer decreases as rotational speed decreases. Figure 2.3 shows the relationships between the responses of the accelerometer, velocity, and displacement sensors with a change in rotational speed.

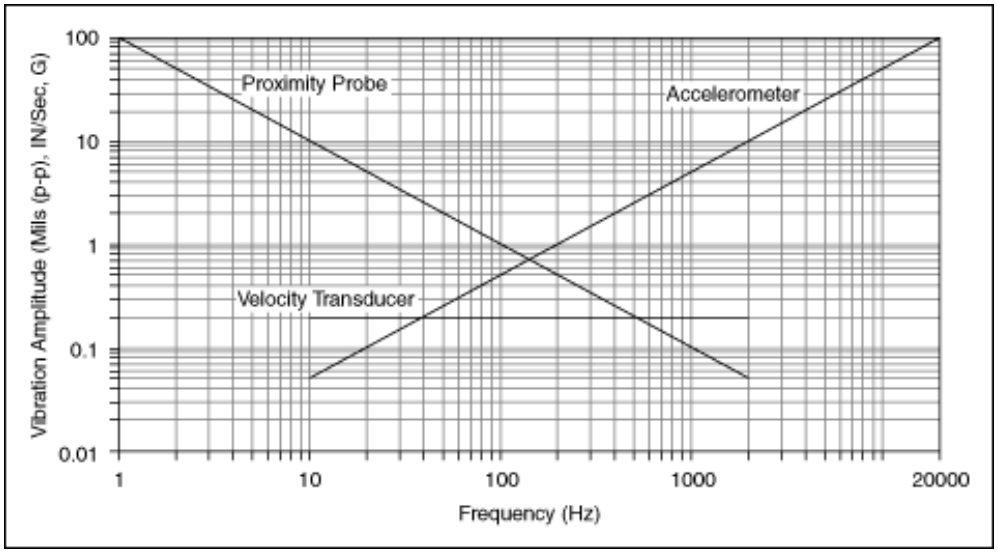

Figure 2.3: Comparison of responses of several types of vibration sensor [70]

Figure 2.3 clearly indicates that the most sensitive sensor that can be used to analyse vibration at medium to high rotational speeds (more than 6,000 rpm, 100 Hz) is the accelerometer. Displacement is the most sensitive parameter at low rotational speed. However, as expected, velocity gives a flat response in that a

peak velocity at 600 rpm is the same to peak velocity at 60,000 rpm. Therefore, velocity sensors are used for setting alarm levels for machines that rotate in the range of 600 to 60,000 rpm [2].

2. **Instruments limitations in low rotating speed applications**

Amplifiers at low rotational speeds cannot separate the signal from the noise, and any source of low-frequency noise will affect the results.

3. **Signal amplitude in low rotating speed applications**

The roll-off filter, which is included in most sensors, has an impact on the magnitude of the signals detected within the range of the roll-off frequency.

4. **Coupling should be taken into consideration in low rotating speed applications**

Coupling between sensor and machine should be taken into consideration. Murphy [68] has suggested that a robust and efficient magnetic clamp be used to attach the sensor to the machine to avoid any rocking effects and to reduce the levels of unwanted noise at low frequencies. Moreover, Robinson and Canada [69] advised using a coaxial cable to reduce any electrical noise, and the dynamic forces applied to the sensor.

Furthermore, as the speed is reduced, the impact energy generated by the relative movement of the components will be reduced. The complexity of this technique and the difficulty of deriving information from the data collected (that relies on technical knowledge) can be noted as a limitation of this technique.

2.3.1 Vibration Analysis for Low-Speed Bearing Fault

The previously highlighted points make vibration monitoring of low-speed rotating machinery difficult, despite this, some attempts have been made. Kuboyama [3] has prepared a summary of the difficulties associated with monitoring low-speed rotating bearings. He has stated that it was possible to monitor the degradation and damage conditions using vibration techniques if the operating speed exceeds 100 rpm. This is because the vibrations produce sufficient energy which can be

monitored over a short period. Conversely, for speeds lower than 100 rpm, smaller amounts of energy are emitted and a longer measurement period is required. Also background noise can distort the vibration signals.

Kuboyama suggested several methods for monitoring extremely low-speed (1 rpm) bearing conditions. The peak level differential technique (PLDT) is one of the recommended techniques. The idea of this technique is to compare between two bearings one healthy and the other faulty (same type and size) and note the acceleration peaks that exceed pre-set threshold levels using a peak picker. The difference in peak levels between the bearings is calculated, if this difference and the number of occurrences are greater than a certain criteria then the bearing was considered as damaged.

Kuboyama [3] carried out a comparison between two pinch bearings rotating at 1 rpm using PLDT. He stated that surface cracking on the inner race of one of the bearings was successfully detected. In his investigation, neither the characteristics of the sensor that was used nor the measuring equipment was described. Furthermore, several alternative techniques were used in his study; including self-correlation and cycle histogram. It was concluded that due to technical difficulties none of these techniques could be applied successfully in the present research program.

Robinson and Canada [69] developed a system known as Slow-Speed Technology (SST) for measuring vibrations on low-speed machinery. This system separates the machine's high-frequency noise from the low-frequency signatures of interest using an analogue integrator. It was noted that analogue integrators distort the low-frequency components, but that was determinist distortion. This system was applied to a variable low-speed rotor unit rotating between 15 to 150 rpm and was shown to give better performance than digital integration. Robinson and Canada claimed that the system could be applied to speeds as low as 10 rpm [69]. However, with the development, recently digital integration shows better performance than the analogue integrators.

Later, Robinson et al. [71] described a development of the PLDT for monitoring the vibration of low-speed machinery, called Peak Value Technique. In this

method, the time-domain vibration signal is separated into different lengths depending on the sampling frequency, and the peak values for contiguous time breaks for processing are obtained by either analogue or digital circuitry until the anticipated standard number is reached.

The experimental investigation of Robinson et al., used low-frequency accelerometers to monitor two drying machines with eight bearings each rotating at 10 rpm. The signal was assumed to be a high-frequency carrier with low-frequency modulation. Envelope analysis which involved both high and low pass filtering as well as rectification was used to separate the two. When this method was applied to the two drying machines, it was found that the envelope of the signal was dependent on machine speed, but sensitivity decreased swiftly with a decrease in machine speed, and the technique became unreliable at low speeds. Robinson et al., claimed that this method was able to detect defects in the inner race one month before failure occurred, but failed to describe the nature of the failure.

Another attempt was conducted by Mechefske and Mathew [4,72] to generate frequency spectra for low-speed (≤100 rpm) roller bearings with three different defects. In this investigation, autoregressive parametric models were used to generate frequency spectra. An important benefit claimed for this technique is that considerably shorter signal lengths are required for fault detection and diagnosis than for conventional techniques. A new index called the probability of fault existence (P_{fe}) based on a statistical distance measure is used to detect bearings defects. It was claimed that this index was easy to apply and was found to be suitable for detection of bearing defects.

Patidar and Soni [73] conducted a review of the applicability of vibration analysis for bearing faults diagnosis. The review concluded that using the high-resolution capabilities of time-frequency techniques, bearing faults could be easily detected. It was also concluded that envelope and wavelet analysis were proved as useful tools for diagnosing the early stages of bearings faults. Furthermore, to detect bearing faults fast and accurately, Artificial Neural Network (ANN) and Fuzzy Logic-Based techniques can be used, and their efficacy has been proven by

many researchers [74–76]. However, at low speeds, background noise can distort the vibration signals. Thus it is hard to apply these techniques to detect bearing degradation at low speeds.

In summary, it appears where faults have been detected in low-speed machines using vibration methods, the time between the successful detection and subsequent failure was short, suggesting well-developed faults, not incipient faults, were detected. This also suggests that faults could develop to the stage where the machine would require costly repairs before being detected. Furthermore, in most of the previously mentioned studies, important information on the equipment (e.g. sensor) used in the investigation is missing.

In conclusion, it can be said that the use of vibration measurements to monitor low-speed bearing conditions is fraught with difficulties: low amplitude signals obscured by background noise is a serious limitation on the use of vibration analysis for CM of low-speed rotating machines. However, this is not the case for AE which is well suited to detecting very small energy release rates. The concept of using AE technique to monitor bearing degradation is presented in the next section.

2.4 Acoustic Emission Technique

In the last few decades, AE has received a great deal of interest and is reported to be a robust and powerful diagnostic tool for CM with the ability to detect even tiny defects [8,19,44]. It is claimed that AE can generate an early warning of machine problems, allowing proactive maintenance activities to be planned, scheduled, and carried out. In this section, AE CM technique is discussed in more detail.

2.4.1 Acoustic Emission Phenomena

Acoustic emission is a phenomenon in which transient elastic waves are generated by local sources within a material [28]. The typical frequency content of AE is in the range between 50 KHz and 1 MHz [28]. Sources of AE in rotating

machinery include friction, cyclic fatigue, cavitation, corrosion and other sources such as crack propagation.

The AE emissions propagate as Rayleigh waves on the surface of the material. Other types of the wave associated with AE propagation include longitudinal, Lamb, and shear waves. AE signals are often divided into two types, continuous and burst (transient). Burst signals are the product of individual random events separated in time; that is one signal ends before the next commences. The beginning and end of a burst signal deviate clearly from the background noise. Continuous signals are produced when there are sufficiently numerous individual AE events to overlap and produce an apparently continuous signal with variations in amplitude and frequency content.

Detection and measurement of these high-frequency elastic waves are achieved by AE sensors coupled to the surface of the structure being investigated. The signals from these AE sensors are fed directly to low-noise preamplifiers, then filtered to remove unwanted noise and then sampled and digitally processed [77].

2.4.2 Advantages of Acoustic Emission Technique

AE can be used in fatigued materials to detect the initiation and propagation of cracks, and it can localise the defect sources. This method is more sensitive than other non-destructive methods, such as vibration analysis. In contrast to vibration analysis, AE covers a frequency range of 50 kHz to 1 MHz. Therefore, an AE signal is unlikely to be influenced by mechanical noise originating in rotating machines, including misalignment and imbalance, which cannot be removed easily and comprehensively. Thus, AE is superior in some areas than vibration, especially for incipient fault detection in rolling element bearings [19].

2.4.3 Limitations of Acoustic Emission Technique

AE CM methods have some significant drawbacks, including the non-repeatability of the AE signal, whereas other techniques can be applied again and again. Attenuation is a major drawback of this technique, and AE sensors have to be close to the signal source. Further, AE is sensitive to insignificant noise and ultrasonic sources. AE measurement needs a high sampling rate, normally

between 1 to 5 MHz [78]. This becomes a shortcoming because at low-speed applications, longer data recording time is required to detect the defect and this can impose a limitation on the hardware in term of memory and data storage.

2.4.4 Applications of Acoustic Emission Technique

For over fifty years, AE techniques has been used to identify discontinuities in pressure vessels and cracks in materials and structures [79]. AE has also been progressively used for CM of engineering assets such as industrial machinery. Mba and Rao have critically reviewed AE and state that AE can help to avoid accidents and damage by playing a significant role in monitoring and detecting faults in structures and machines such as bridges, pipes, and nuclear power plants [8]. The successful implementation of the AE can be seen in various civil and industrial fields as:

- Material testing: including testing materials to analyse their strength and fatigue level, as well as crack testing and corrosion detection [80–83]. AE is also widely applied for the detection of welding defects.
- Civil engineering: structural testing of concrete buildings, bridges, dams, and tunnels. It helps in the continuous monitoring and assessment of repairs required in these structures [84–86].
- Chemical and petroleum industries: integrity testing of pressure vessels, storage tanks, and cryogenic tanks. AE is also used to monitor formation, oscillation, and cavitation of air bubbles in multiphase flow [87–91].
- Electric and power plant industries: monitoring of power plants and diagnosis of high-pressure vessels [92,93].
- Aircraft and aerospace industries: numerous tests such as proof testing, ageing tests, and fatigue tests of aircraft to assess their integrity [85,94].
- Transportation industry: locating and detecting flaws in rails, tanks trucks, and trailers [85,95].

- Medical field: one example is using AE techniques to monitor joint conditions in humans [85,96].

Other applications include detection of bad sectors in hard disks due to cracks, grinding, and machining. This technique is also used in various geological and seismological applications.

2.4.5 Acoustic Emission Sensors

Selecting the right sensor is essential for the success of any CM process. AE sensors detect the motion of a surface that generate AE events and convert this motion into voltage signals in the time domain. These signals are used in all subsequent stages in the AE measurement process.

To detect AE events, a wide range of transducers is available; including laser interferometers, displacement sensors and capacitive transducers. However, the most commonly used AE sensors are piezoelectric transducers. A specially processed ceramic such as Lead Zirconate Titanate (PZT), see Figure 2.4, forms the transduction element [97–99]. The sensor is firmly coupled to the surface of the structure under test to maximise energy transmission into to the piezoelectric element.

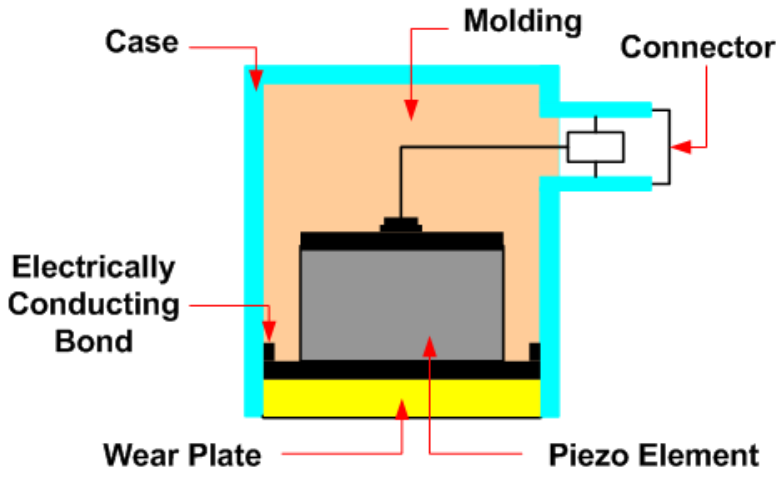

Figure 2.4: AE sensor basic setup [97]

The dynamic strain is transmitted to the piezoelectric element that converts mechanical energy to electrical signals via the piezoelectric effect. Then these electric signals are fed to a preamplifier that can also reduce unwanted

background noise and match sensor impedance to that of the following filter so the signal can be transmitted with minimum energy loss. Traditionally, the preamplifier was connected to the sensor by short, coaxial cables to avoid any electrical or magnetic noise and to decrease the level of interference. Nowadays, to minimise errors, and to make for a more robust system, the pre-amplifier is integrated within the sensor housing.

2.4.6 Acoustic Emission Measurements

In this research program, the AE signals were successfully recorded and analysed using two approaches. The first method was the so-called “classical AE technique” or Hit Driven Data Measurements; the second was a signal based AE technique or Time Driven Data Measurements. Then signal processing was used to extract the required data from the captured signal.

2.4.6.1 Hit Driven Data Measurements

In this method, the signal itself is not stored, although a set of conventional parameters such as amplitude, peak level, rise time, counts, and energy are extracted from the captured signal and stored (conventional AE method). A correlation between one or more of these features and the defect formation can be developed. Figure 2.5 illustrates the commonly used parameters [97].

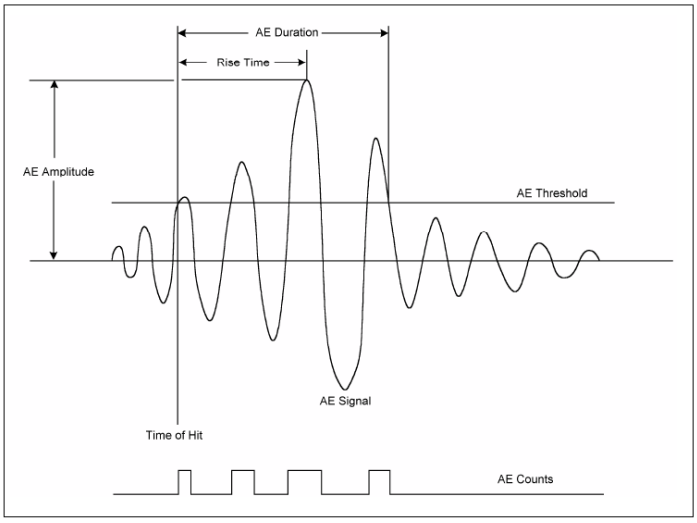

Figure 2.5: Commonly used parameters of AE signals [100]

- AE event: This refers to an elastic wave, produced under load or stress in a material by a micro-structural displacement, whose amplitude exceeds a pre-set threshold level.
- AE count: The number of times the amplitude of the signal exceeds a pre-set threshold level.
- Energy: The total elastic energy emitted by an emission event which is the area under the rectified signal envelope.
- Amplitude: The largest trip peak voltage achieved by the waveform of a signal from an emission event.
- Duration: The time between the signal initially rising above the pre-set threshold level and the last time the signal drops below the threshold level.
- Rise time: The time between the AE signal crossing the pre-set threshold level and reaching its peak amplitude.
- Threshold: A pre-set signal level above which the signal is recognised as an event and counted.

2.4.6.2 Time Driven Data Measurements

In this method, the AE waveform is continuously recorded and stored digitally via an analogue to digital (A/D) converter. Using this approach will allow a more comprehensive analysis of the data. Such an approach was only made possible by the development of high-speed high-storage computers, and the parallel development of highly sensitive wide-band sensors. Such capability is now available with the new AE system that can continuously capture AE waveforms at different sampling rates. Hence, the characteristics of AE sources can be described from the captured waveform. Figure 2.6 shows an example of a typical AE waveform. Nowadays, commercially available signal processing software enables rapid extraction of the AE parameters listed above for defined sampling rates and time constants.

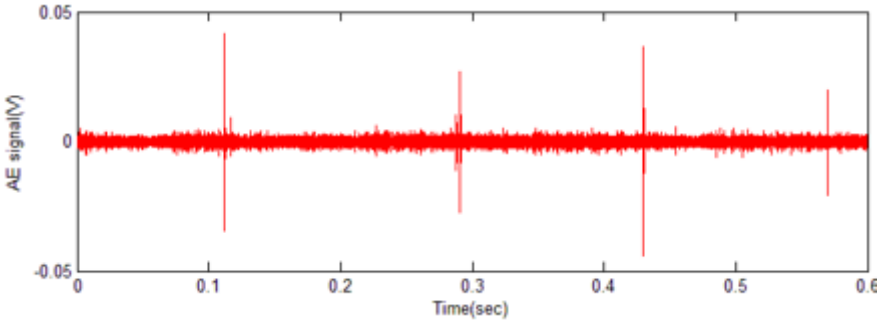

Figure 2.6: Example of AE waveform

2.4.7 Trends of Acoustic Emission in Bearing Fault Diagnosis

During the past 30 years, many researchers have applied AE to the CM of bearings [8,11,101]. Possibly the earliest paper addressed the use of AE technology to identify artificially-induced defects in rolling element bearings was done by Balderston [8,102]. Balderston investigated the applicability of AE to detect seeded defects on the inner race, outer race, and ball elements of a bearing, as well as lack of lubrication. The vibration analysis and AE were compared, and the advantages of AE over vibration were confirmed.

Balderston detected two types of AE signatures; burst-type emissions were detected with seeded defects on the inner and outer races, and ball elements of a bearing, as well as lack of lubrication. Continuous type AE signatures were detected due to lack of lubrication. He also suggested that due to the interconnection of components, any defect that occurs can result in the generation of frequencies that make the results difficult to interpret. It has been mentioned that when the rotational speed was low, the impact energy is low, which suggested that application of vibration techniques would be limited.

Balderston concluded that AE has been applied successfully and offered a direct correlation between amplitude level and defect severity. Furthermore, as more sophisticated sensors were developed, AE would become important practical CM tools.

About ten years later, AE was used in the industrial field by Rogers [55] to monitor low-speed rotating bearings on cranes. The results from AE were compared to those obtained from vibration analysis. Rogers stated that it was hard to apply vibration analysis for online CM because of the low rotational speed of the crane. However, using kurtosis at different frequency rates, AE resonant transducers could be utilised for the online monitoring of the bearings.

Two similar scenarios applied by Sundt [103] to the detection of bearing defects using AE. The first scenario involved the generation of high-frequency signals by a hairline crack on the outer race. The defect frequency detected using AE was above 100 kHz, but was not detectable by vibration analysis. The signal occurred only at an initial stage of crack generation. Subsequently, the bearing appeared to be in a satisfactory condition for normal operation. Sundt then successfully applied AE to detect the presence of particulate matter in pump unit bearings [103]. However, he did not describe the characteristics of the equipment used in the experiments.

Yoshioka and Fujiwara [41] conducted a study and showed that AE techniques could identify defects in a bearing earlier than vibration analysis. AE generating sources were identified during fatigue life tests on ball bearings. Later, Hawman and Galinaitis [47] obtained similar results to Yoshioka and Fujiwara concerning AE's advantages over vibration analysis for the detection of bearing faults. They explained how bearing defects were diagnosed through the modulation of high-frequency AE burst at the defect frequency of the outer race. The AE signatures modulation at frequencies of the bearing defect has also been observed by other researchers [104,105]. Hawman and Galinaitis [47] used Root Mean Square (RMS) and Fast Fourier Transform (FFT) techniques for monitoring the bearing condition and recommended the use of adaptive noise cancelling (ANC) techniques to overcome noise interference.

All the early studies used bearings with seeded defects. The first known attempt to identify natural degradation in bearings was conducted by Yoshioka [106]. The identification of rolling contact, subsurface, and fatigue cracks was the focus of Yoshioka's study. Through time-delay analysis, which related to the AE events

acquired by different sensors, it was demonstrated that AE could locate the defect source. Furthermore, Yoshioka stated that the size of cracks could be identified using the AE techniques.

The tests performed by Yoshioka were restricted to a roller bearing with only three rollers which is not a typical operational bearing. The test measurements were ended after AE activity increased so that the distribution of subsurface defects relative to surface defects was not observed properly. The outcomes of this study indicated that AE is more sensitive than vibration analysis and can detect faults earlier.

Another laboratory study monitoring the condition of extremely low-speed rotating machinery using AE techniques was conducted by Mba [2]. This study consisted of two parts: the first in which AE was used to detect the early stages of loss of mechanical integrity in extremely low-speed bearings; and in the second part, Mba enhanced and improved a monitoring system for a rotating biological contactor (RBC) rotating at 1 rpm. He also evaluated the possibility of using AE to monitor extremely low-speed bearings with diameters between 80 and 125 mm. On a purpose, a test rig was built and he found signs of AE for every fault condition.

Mba considered the use of autoregressive coefficients instead of traditional AE techniques, such as energy, counts, RMS, and amplitude. He concluded that autoregressive coefficients provide useful information about the condition of the RBC. Moreover, the application of AE to the monitoring of extremely low-speed rotating machines was successfully demonstrated.

Later, Jamaludin et al. [44] showed how AE techniques could be used to identify the initial stages of bearing deterioration at a rotational speed of 1.12 rpm. Attempts were made to generate natural defects in the bearing's components, such as running the test bearing for 800 hours without lubrication, but no defects were detected visually on any bearing components. In this experiment, the test bearing was under a load of 55 kN.

Jamaludin and Mba [107] continued their work with the same test rig at speeds of 1.1 and 1.2 rpm to monitor the integrity of the test bearing using AE. In this experiment, autoregression was used and could successfully classify the defect signature of the bearings in both time and frequency domains [6]. Furthermore, it was again demonstrated that AE was more sensitive than vibration analysis for these types of applications. Also, the simplicity of the AE technique and the use of commercially-available equipment made such a monitoring system very attractive [7]. From this study, it was concluded that AE is a successful method for monitoring extremely low-speed bearings.

Miettinen and Pataniitty [32] conducted another experimental attempt to monitor faults at extremely low-speed bearings using AE techniques and compared results with those obtained by vibration measurement. The measurements were taken using a laboratory test rig at rotational speeds ranging from 0.5 to 5 rpm and load of 70 kN. A spherical roller bearing was used and lubricated with grease. Before the tests began, the tested bearing was damaged on its outer race and resulting AE and vibration measurements were compared.

The vibration measurements included the time domain signal, peak values, envelope spectrum and acceleration signal derivation. They used the pulse count method and time signal for AE measurement. It was concluded that the AE was superior to vibration analysis in detecting bearing defects for extremely low-speed rotating machinery [32].

Sato [108] explored the manner in which AE can be used to monitor damage in extremely low-speed bearings and demonstrated that AE could be used to monitor a defective journal bearing rotating at 5.5 rpm. It was noticed that even slight metallic contact led to an increasing in the duration of the AE bursts. Furthermore, growing metal wear resulted in a larger amplitude of the waveform. However, no correlation could be found between the increasing signal strength and wear.

Parizi et al. [33] used AE to compare a healthy bearing and a naturally-damaged bearing at a rotational speed of 60 rpm. These bearings were used in a conveyor that transported ground ironstone. Parizi et al., used wavelets to remove the low-

frequency noise and then compared statistical parameters for normal and defective bearings. Statistical measures used included crest factor, kurtosis, and energy factor. This study provided evidence that statistical parameters are more effective in detecting defects in a low-speed bearing if the data is first transformed by removing low-frequency noise, in this case by using wavelet analysis.

In the investigation of Parizi et al., two balls were removed from the cage of a roller bearing, which meant that the bearing had already reached a state of failure by the commencement of the measurements. Thus, it was easy to distinguish between healthy and faulty bearings using AE techniques. It was reported that no other defects existed on either inner or outer race so the failure could be regarded as due to improper installation. Moreover, it was mentioned that vibration analysis could not detect the bearing failure. Although, there is no description was given either for vibration instrumentation used nor the outcomes of vibration.

Elforjani and Mba [5] conducted a study to validate the application of AE to locate, identify and monitor the initiation and propagation of natural defects in a thrust rolling bearing. To speed up the initiation of a natural crack, a combination of thrust ball bearing and a roller thrust bearing was used with an electric geared motor with a speed of 72 rpm. Traditional parameters were used in this study to monitor the integrity of bearings, such as counts, amplitude, energy, and average signal level (ASL).

It is shown that both RMS and energy dramatically increased at defect initiation. Thus, it was concluded that these AE parameters are sufficiently robust and sensitive to detect crack initiation in low-speed bearings. It was also shown that the AE source could be successfully located during the operation using the AE. This was the first known attempt to correlate AE with the generation of a natural defect and locate the defect in low-speed bearings [13–15,109].

Furthermore, this study compared defect size with burst duration at various load conditions, but no link was found between burst duration and load, although the burst was linked to defect size. However this study employed a combination of a thrust ball bearing and a thrust roller bearing to accelerate natural crack initiation, and this is not representative of a typical operational bearing.

Tavakoli [46] examined the applicability of AE in monitoring radially loaded needle bearings rotating at 80 rpm, under three conditions: 1) with fully-lubricated, healthy bearings, 2) with unlubricated, healthy bearings, and 3) where two adjacent needle elements were missing. Both time and frequency domain analysis were applied to analyse the signal captured.

The experiment demonstrated that the spectral density of the RMS voltage was different for all three conditions. It also showed that the main source of AE in the bearings under all three conditions was friction. Nevertheless, some experimental details were missing from the published paper, and the analysis process applied to the data was not fully explained as the focus of the paper was to present a literature survey of methods used in the CM of bearings.

McFadden and Smith [110] also investigated the application of AE transducers to monitor the conditions of the roller bearing elements at moderate speeds. The basis of the experiment was to insert a fine scratch on the inner raceway and place AE sensors on the bearing housing. The AE transducer had a frequency response beyond 3 MHz but failed to perform at moderate rotational speeds (below 850 rpm).

The findings of McFadden and Smith were confirmed by Smith [111] who carried out an experiment to investigate the response of an AE transducer attached to a bearing housing for a low rotational speed (10 rpm). The AE transducer responded to the minute strains in the housing which appeared as spikes superimposed on the original time domain signal. This study concluded that at low speeds and steady loads, the AE transducer could detect signatures from tiny defects in rolling element bearings.

Couturier and Mba [112] showed that AE activity depends on load and speed variation. Two experiments were performed using a split roller bearing. In one the speed was fixed, and the load varied, and in the other, the load was fixed and the speed varied. The results obtained proved that AE activity depends on speed and load and increases with either or both. It was also observed that AE activity was more sensitive to changes in speed in comparison to load. This result could be

due to the fact that speed contributes more to variation in lubricant oil thickness as compared to load.

According to Oh et al. [113], degradation on fan bearings can be predicted by studying various types of parameters, which include vibration, AE, and lubricant temperature. The investigation was conducted by simulating lubricant starvation. This study showed AE to be the best precursor technique reflecting the condition of dry bearings.

In conclusion, AE has been shown to be a suitable technique for detecting and monitoring bearing degradation. Furthermore, AE is superior to vibration in term of detecting the fault faster and being more sensitive, and vibration tending to detect faults after they have fully developed.

2.5 Closing Remark

Several studies have described the difficulties of applying vibration analysis in monitoring bearing degradation at low speeds, and the lack of any clearly successful investigation in this area speaks volumes.

On the other hand, an enormous amount of practical research has been carried out applying AE to the CM of bearings at moderate to high rotation speeds. Nevertheless, there remains only limited knowledge regarding CM of bearings in the speed range 10 to 100 rpm. There have been only two substantive investigations of the CM of bearings in this speed range, and each had severe limitations. For one study, the bearing was in failure mode as two rollers were dropped from the cage. Thus it could not be said that AE was applied to detect the early stage of failure [33]. The second study suffered from the serious limitation that the researchers did not use a typical operational bearing but combined the races of one bearing type with another.

Accordingly, more research should be undertaken on bearings rotating at low speeds to investigate:

- The applicability of AE to monitor bearing degradation under conditions of low speed (10-100 rpm).

- The ability of AE to detect the early stages of bearing failures bearing under conditions of low speed (10-100 rpm).
- The influence of speed and load on the AE signal at rotational low speeds.
- The influence of a defect size on the AE signal at such low speeds.

To investigate these points, signal processing techniques needs to be applied to analyse the data from captured signals. In the next chapter, several types of the signal processing techniques are demonstrated.

Chapter Three

3 Signal Processing Techniques

An essential requirement for the successfully CM of bearings is to be able to extract fault features from the AE signals in the presence of high levels of background noise. Various techniques are used to identify and interpret specific source within the recorded signals. The parameters to be measured and the sampling rate of the sensor signal are important considerations.

3.1 Sampling Rate

Figure 3.1, presents the aliasing effect in the time domain. Sample at a too low rate and a high-frequency signal could appear to have a lower frequency. This problem is resolved by use of the Nyquist theorem which states that a signal must be sampled at more than twice the maximum frequency of interest [114].

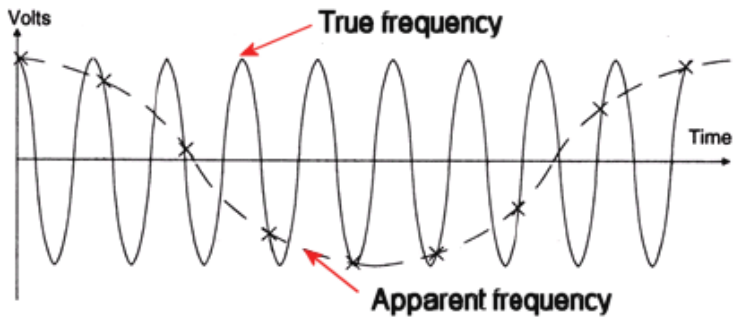

Figure 3.1: Aliasing effects in the time domain [115]

3.2 Techniques of Signal Processing

The signal is subjected to the processing techniques to identify and interpret sources within the digital signal and these techniques can be divided into three types:

1- Time domain
2- Frequency domain
3- Time-frequency domain

3.2.1 Analysis of Time Domain

Statistical analysis to extract features of interest is used mainly with time domain signals. Peak-to-peak amplitude, RMS, kurtosis, and crest factor are some examples of such statistical measures. In this section, statistical parameters are discussed, followed by a review of studies which used these parameters for the CM of bearings.

3.2.1.1 Root Mean Square

The most used measure of signal intensity is the root mean square (RMS), which is calculated according to Equation (3.1). A change in the dynamic behaviour of the machine or its integrity can result in a change in the signal RMS.

$$RMS = \sqrt{\frac{\int_{t_1}^{t_2} |s(t)|^2 dt}{t_2 - t_1}} \quad \text{(3.1)}$$

S(t): Signal in time domain

t: Time over which the average is taken

The RMS of the time domain signal is commonly used for CM. The RMS value observed when a defect is present in a machine's components, such as gear or bearings is expected to increase [19,47].

This approach difficulty determine incipient defects because, by definition, such defects are small and the energy generated makes little difference to the RMS value.

3.2.1.2 Kurtosis

Kurtosis represented the level of signal impulsiveness and defined in Equation (3.2) as the fourth statistical moment. Kurtosis has been successfully applied to detect incipient faults in bearings [116–118]. The advantage of this techniques is that a prior history is not essential for judging bearing condition. The value of kurtosis is evaluated with respect to the value 3, which is the value obtained for the Gaussian distribution (which is assumed to be the normal condition bearing). At its start, a small or incipient fault will increase the value of the kurtosis, but

when the fault is well-advanced, the value of kurtosis reduces to the level of an undamaged bearing [119].

The values of kurtosis as given in Equation (3.2) are calculated for time domain signals as:

$$Kurtosis = \frac{\sum_{i=1}^{N}(S_i-\mu)^4/N}{\sigma^4} \quad (3.2)$$

S_i: Signal data points

μ: Signal mean

σ: Standard deviation

N: Number of data points

3.2.1.3 Skewness

Skewness measures the lack of symmetry in distribution, or data set and calculated using Equation (3.3):

$$Skewness = \frac{\sum_{i=1}^{N}(S_i-\mu)^3/N}{\sigma^3} \quad (3.3)$$

Where the symbols have the meanings given above.

For a normal distribution, the skewness is zero. Positive skewness indicates data that are skewed to the left, and the opposite is true for the negative values. The main drawback of this parameter is that it is not sensitive to all conditions as load, speed, and defect deterioration [61]. Both kurtosis and skewness can be represented in histograms.

3.2.1.4 Energy Index

In order to overcome the shortcoming associated with RMS and kurtosis, the Energy Index (EI) can be used. The numerical value of the EI is obtained by squaring the value obtained by dividing the RMS value associated with a segment of a signal with the RMS value of the entire signal. The equation for the EI is:

$$Energy\ Index = (\frac{RMS_{segments}}{RMS_{total}})^2 \quad (3.4)$$

The application of EI to the CM of gears and bearings is gaining importance as it has been shown to detect symptoms of incipient faults, including spalling when the signal to noise ratio is as low as 0.25 [54].

EI analysis divides the signal into segments – the number of segments depends on the nature of the signal and is directly associated with EI sensitivity. In the case of a stationary and uniform signal having a sufficient length, the EI value for all segments is 1.0. The value of the EI will be more than unity if transient activities occur within that segment. That is, a high value of EI means a higher than expected energy activity in that segment, which could mean an abnormality such as a fault.

In the case of a gearbox, the number of segments is determined by the number of gear teeth. For bearings, and for convenience, the signals are initially split into 100 segments [54]. This technique has been applied successfully in monitoring bearing conditions and has demonstrated distinct advantages over other techniques. However, as mentioned previously, the selection of the number of sections depends on user experience.

3.2.1.5 Crest Factor (CF)

Crest factor (CF) is the ratio of the peak value to signal RMS, see Equation (3.5). It is a traditional method used for assessing the smoothness of a signal and is considered to be reliable only in the presence of significant impulses [114]. For healthy bearings, typical CF values are from about from 2.5 to 3.5, while for a bearing with an impulsive defect the CF could be as high as 11 [114].

$$Crestfactor = \frac{Peakvalue}{RMS} \quad (3.5)$$

Previous Work on Statistical Parameters

Al-Ghamdi and Mba [19,120] conducted a comparative study to identify bearing defects and to quantify outer race defects using statistical analysis of the AE and vibration signals. Four shaft speeds were employed in the range between 600 to 3000 rpm, under three load conditions ranging from 0.1 to 8.86 kN. The experiment was divided into two test programs; the first related to the detection

of defects with a change in load and speed using AE and vibration analysis. The second program investigated the correlation between AE activity and increasing defect size. It was concluded that AE RMS, peak amplitude, and kurtosis are more sensitive to the defect initiation and defect growth than vibration.

Furthermore, it was observed for both AE and vibration, that as the load increased, RMS and peak amplitude increased. The same was found with increasing speed. Additionally, a relationship was noted between defect length and AE burst duration. This allows the user to monitor defect propagation using AE, which is unachievable with vibration analysis.

To confirm the findings of Al-Ghamdi and Mba [19], Al-Dossary et al. [20] conducted an investigation to determine the relationship between AE burst duration and the actual dimensions of the defect on a roller bearing. Different bearings were tested at speeds ranging from 600 to 3000 rpm under loads between 2.7 and 8 kN with seeded faults of different dimensions and the AE waveform recorded. Several parameters were used for the fault detection, included AE maximum amplitude and energy.

A strong relationship was found between the actual defect size on the outer race and the AE burst duration. Also, the energy parameter was successfully used to identify the severity of the defect in both the inner and outer races of the bearing. However, AE maximum amplitude could be used only to monitor defects on the bearing outer race, as the signal was too strongly attenuated on the transmission path from the inner race to the AE sensor. This study agreed with [19], demonstrating that AE techniques can be effective in monitoring outer race conditions.

Tandon and Nakara [121] attempted to correlate AE statistical parameters such as counts and peak amplitude with outer race defects of different sizes for different speeds and loads but, surprisingly, found the AE count was independent of both. From this study, it was concluded that the diagnosis range of AE counts was limited because it was restricted to detecting defects of diameter 250 μm, or less. However, the ability of AE peak amplitude to detect outer race defects was not limited by defect size.

Later, Choudhury and Tandon [53] conducted a parallel experiment to monitor defective bearings, but with a wider range of speed, load, and defect size. They found that for a healthy bearing, the AE count was less than for a damaged bearing. According to Tandon and Nakara [121], the AE count for both damaged and undamaged cases should be independent of speed and load, but in this study, it was found that as speed increased, the AE count for both the undamaged and damaged bearings increased.

Tan [122] and Tan et al. [123] explored the dependability of AE count by varying operational conditions and attempting to identify the optimum AE count parameter and its threshold level. Tan posited that the AE count rate is dependent on factors such as the threshold level, pulse amplitude, and signal frequency.

Morhain and Mba [21] carried out an investigation into the application of AE statistical parameters for CM of a radially loaded bearing. A test rig was designed to allow seeded defects in both the inner and outer races of a split roller bearing. In the experiment, three rotational speeds were used (600, 1500, and 3000 rpm) at three loads between 0 and 4.8 kN. The results achieved showed that AE parameters such as RMS and counts are robust measures that can be used for detecting bearing deterioration. Furthermore, it was found that the relationship between AE counts and the mechanical integrity of the bearing was dependent on the selected threshold level. These results were in agreement with the published results of researchers [53,121,122] and has become the basis of studies on the effect of threshold levels on AE counts.

Miettinen and Andersson [124] conducted an experiment, in which they used AE to monitor bearing condition. Several types of grease were used in this experiment, which classified the AE signals according to the type and impurity level of four contaminants; quartz, iron, steel and iron oxide. The size of the contaminant grains was between 5 and 40 μm. AE counts and standard deviation were used to analyse the condition of the bearing lubrication. It was observed that both AE count and standard deviation increased when contaminated grease was added to the bearing. It was also noted that for contaminated grease, the AE count decreased with the size of the contaminant, while the harder the

contaminants, the greater the amplitude of the spikes in the AE signal. The dependence of the AE signal on the grain size can be reasoned by the agglomeration property of fine particles.

Miettinen and Andersson also explored replacing the grease in bearing lubrication. In this experiment, the bearing already lubricated with contaminated grease was cleaned and clean grease applied. As expected, a reduction in the level of the AE activity was observed to the half of the AE level with the contaminated grease. It was concluded that re-greasing could improve the lubrication of the bearing.

Another study based on analysis of the AE time domain signal for bearing fault detection was carried out by Elmaleeh and Saad [125]. They used AE peak amplitude, CF, standard deviation, and kurtosis. These parameters were used to distinguish between a healthy bearing, the same bearing with a defective inner race, and then with a defective outer race. It was found that the value of the standard deviation and peak amplitude for a healthy bearing did not exceed 0.5 and 1.5V, respectively. These values increased to as much as 12 when either inner race or outer race faults were present. It was concluded that standard deviation and peak amplitude were appropriate to differentiate between normal and defective bearings, but CF was not.

He et al. [23] conducted an experimental investigation using various AE parameters for bearing CM. In this study, it was proposed to extract the characteristic frequencies of the bearing fault based on the AE short-time RMS (STRMS) and autocorrelation functions. Additionally, several more traditional AE parameters such as amplitude, counts, energy and kurtosis were also measured for various speeds, loads, and defect sizes. It was concluded that rotating speed has a strong influence on the AE parameters. This conclusion was in agreement with the findings of several other researchers [19,21,126]. Moreover, it was observed that AE counts increase exponentially with increasing rotating speed and defect size which agreed with [122,126]

Kim et al. [78] conducted an experimental study of incipient fault detection in bearings at a speed of 140 rpm using AE. Statistical parameters as RMS, peak

value, skewness, kurtosis, and entropy were used to distinguish between the healthy and defective bearings. To find the best-suited frequency band, six band-pass filters ranges up to 100 kH were applied. To evaluate the effectiveness of these statistical parameters for incipient fault detection, a separation Index (SI) was introduced as calculated from Equation (3.6).

$$SI = \frac{Mean(P_{defective}) - Mean\,(P_{healthy})}{Std(P_{defective}) - Std\,(P_{healthy})} \quad (3.6)$$

Where, Mean and Std are the mean and standard deviations of $P_{healthy}$ and $P_{defective}$, which are the relevant parameters for the healthy and the defective bearings, respectively.

They concluded that RMS and entropy are the best suited statistical parameters to distinguish between normal operation and a faulty bearing. This finding was observed for bearings with faults on the inner race, outer race, and roller elements [45].

Additionally, Kim et al. [127] have demonstrated an online CM system for moderate-speed machinery using both AE and vibration analysis. This system includes noise removal techniques to improve the signal-to-noise ratio and peak-hold-down-sampling to reduce the massive data load. This method has been applied on a site machine and successfully detected an incipient bearing defect. This study also concluded AE was superior to vibration analysis in early stage fault detection.

Another attempt to monitor bearing degradation [52,128,129], investigated the effectiveness of AE parameters such as RMS, peak amplitude, and energy for defect deterioration. Speeds in the range 222-2980 rpm and loads in the range 0.3 to 2.2 kN were used with defects of several sizes on both inner and outer races.

The above studies confirm that statistical parameters are suitable for detecting incipient faults and bearing deterioration. However, while time domain analysis provides the time waveform, it lacks information on the frequency content of the signal which provides valuable information to specify the defective component.

3.2.2 Analysis of Frequency-Domain

Certain frequency bands are linked with various elements of the machine, such as gears, bearings, and shafts, and a distinctive rotational frequency is associated with each element of the machine. These frequencies can be obtained from analysis of recorded signals made during the CM of machines. If there is an increase in the energy of a frequency band associated with any particular element of the machine, this could indicate the presence of a fault in that bearing component.

Bearing Fundamental Frequency

The bearing in the presence of a surface anomaly on the raceway will generate an impulse every time it meets the fault, at a fundamental frequency often referred to as the fault frequency. The fault frequencies can be calculated knowing bearing geometry (the pitch and roller diameters), and the relative speed of the two raceways from Equations (3.7) to (3.12) [130]:

Possible fault frequencies of interest are listed below and may be used to indicate a likely source from the frequency of the captured signal.

$$\text{Ball/Roller (BSF)} = \frac{\text{Pd}}{2\text{Bd}} * \text{s} * \left(1 - \left(\frac{\text{Bd}}{\text{Pd}}\right)^2 (\cos\text{Ø})^2\right) \quad \text{(3.7)}$$

$$\text{Inner race (BPFI)} = \frac{\text{Nb}}{2} * \text{s} * \left(1 + \frac{\text{Bd}}{\text{Pd}}\cos\text{Ø}\right) \quad \text{(3.8)}$$

$$\text{Outer race (BPFO)} = \frac{\text{Nb}}{2} * \text{s} * \left(1 - \frac{\text{Bd}}{\text{Pd}}\cos\text{Ø}\right) \quad \text{(3.9)}$$

$$\text{Cage (FTF)} = \frac{\text{S}}{2}\left(1 - \frac{\text{Bd}}{\text{Pd}}\cos\text{Ø}\right) \quad \text{(3.10)}$$

$$\text{Shaft Frequency} = \text{S} * \text{Gear ratio} \quad \text{(3.11)}$$

$$\text{Gear Mesh Frequency (GMF)} = \text{S} * \text{Nb} \quad \text{(3.12)}$$

Where: Pd= Pitch diameter, Bd= Ball diameter, S =Rotational speed (Hz), Ø=Contact angle and Nb= Number of balls, see Figure 3.2.

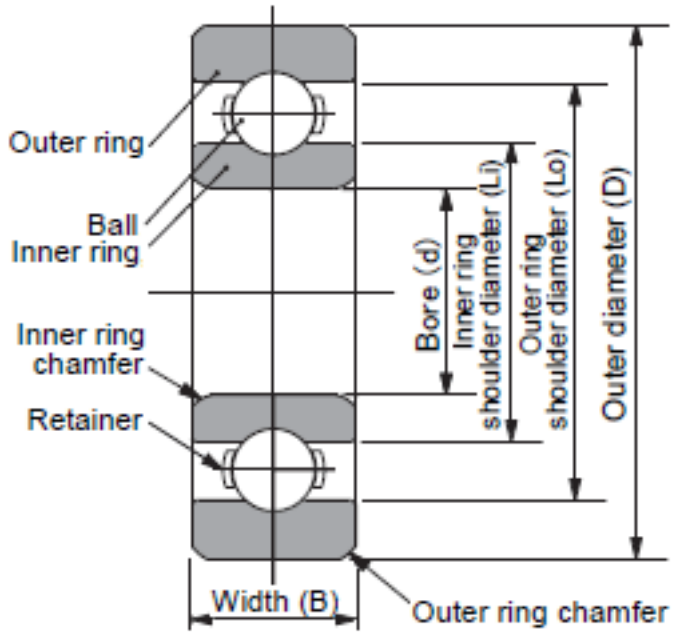

Figure 3.2: Bearing parts [131]

The frequency spectrum of the acquired signals is obtained using a Fast Fourier Transform (FFT). The FFT is extremely powerful in demonstrating the presence of a discontinuity in a signal but provides no information on the time-based localisation of the source. This means that, strictly, the FFT is not applicable for nonlinear and nonstationary signal [132].

The Fourier transform of signal S(t) and the signal's frequency spectrum is shown in Equation (3.13) [133].

$$S(\omega) = \int_{-\infty}^{+\infty} S(t) e^{-2\pi i t \omega} dt \qquad (3.13)$$

Where: ω: Frequency and S(ω): Signal in frequency domain

3.2.2.1 Envelope Analysis

Every time a rolling element passes over a localized bearing defect an impact occurs and a signal pulse is generated. The duration of the pulse is very short compared to the time between pulses. Being of short duration the energy spectrum of the pulse will be wide-band, across an extensive range of frequencies which may well include the resonant frequencies of elements of the surrounding structure, and which may well be excited. It should also be noted that

the signal being of very short duration, the FFT technique cannot be used to extract fault frequencies. However, envelope detection can be used with a bipolar to unipolar converter followed by a smoothing circuit to analyse the bearing frequencies using FFT [134].

Ho and Randall [135] described the using of the Hilbert Transform (HT) for envelope analysis but only for those frequency bands where the signal to noise ratio was a maximum. Rai and Mohanty [136] investigated the diagnosis of bearing faults using the Hilbert-Huang Transform (HHT) to obtain frequencies characteristic of specific defects. HHT delivers multi-resolution for the different frequency scales and takes into account the variation of the frequency content of the signal with time. However, it contains a subjective error in the calculation of defect frequencies characteristic of rolling element bearings. To improve HT resolution in the frequency domain Ho and Randall included FFT intrinsic mode functions (IMFs) from the HHT method.

Another way of applying enveloping analysis is to square the signal and apply the low pass filter (LPF) in order to remove the unwanted noise captured as done in [137].

3.2.3 Time- Frequency Domain Analysis

As mentioned previously, time domain analysis gives an idea of the time of occurrence of events and the corresponding amplitude but lacks information on the frequency of the signal. Conversely, frequency domain analysis gives an idea of the signal frequency content without the times at which those frequencies occur. To overcome these limitations, time-frequency domain analysis is advised, as it shows both time and frequency content.

3.2.3.1 Short-Time Fourier Transform (STFT)

Short-Time Fourier Transform (STFT) is a method that is adopted for the analysis of signals that are non-stationary. STFT helps in the extraction of a number of signal frames with the help of a window (often the Hanning window) that moves along the record of the signal in steps that overlap and carries out an FFT for each window. This identifies a relationship between frequency and time. In other

words, STFT is a form of FFT in which the signal is taken in segments, and FFT is applied to each, rather than as a whole. The equation for the STFT is [138]:

$$G[f](t,w) = \int_{-\infty}^{\infty} f(\tau)g(\tau - t)e^{-iw\tau}d\tau \quad (3.14)$$

Where: $f(\tau)$: Signal to be analysed, $g(\tau - t)$: Window function, τ: Centre or mean location of window function in time, w: The centre or mean location of the window function in frequency.

STFT can be represented in a spectrogram, which is a way of representing spectral information as it varies over time in one single plot, using colour-coding to represent magnitude. The main drawback of using an STFT is that the best resolutions of time and frequency cannot be achieved together; if there is a good resolution in time, the poor resolution will found in frequency and vice versa [139].

3.2.3.2 Spectral Kurtosis

Spectral Kurtosis (SK) is an effective technique for the detection of signals that are transient and non-stationary. In this procedure, firstly, the signal is analysed using an STFT, and the spectra obtained plotted sequentially in a 3-D array with time, frequency and amplitude as the three axes. A particular frequency is selected, and the kurtosis values are calculated [139]. A critical review of the SK and its application in monitoring bearing conditions is presented in [140].

3.2.3.3 Wavelet transform

To overcome the disadvantages inherent in the STFT, Wavelet transform (WT) techniques are advised.

In most cases, CM signals contain both high- and low-frequency components. Windowing techniques require a short time window adequate time resolution at high frequencies but a long window for adequate time resolution at low frequencies. These requirements appear to be contradictory. Fortunately, wavelet analysis allows for variable window lengths, and one such approach is Multi-Resolution Analysis (MRA).

This wavelet analysis process is based on the adoption of a prototype function which is known as the mother wavelet or, sometimes, the analysing wavelet. The

family of wavelets is composed of dilated and translated forms of the respective prototype function [138].

The dilation and translation of the mother wavelet along the time and space axes are determined by the scale and shift features of the wavelets. If the scale factor exceeds the value of one, then it represents the dilation of the mother wavelet along the horizontal axis, while the positive shift of the scale factor corresponds to the translation of the wavelet towards the right along the horizontal axis. The continuous wavelet transform is defined as (3.15) [138]:

$$CWT_x^{\varphi}(\tau, s) = \frac{1}{\sqrt{|s|}} \int x(t) \varphi^* \left(\frac{t-\tau}{s}\right) dt \quad (3.15)$$

Where φ(t) is the mother wavelet which is a transformation function. The translation, $\boldsymbol{\tau}$, is used in a similar way in both CWT and STFT analysis and refers mainly to the window location. There is a correspondence of this term with information about time consumed in the transform domain. There is no frequency parameter in the CWT; rather a scale, *s*, parameter is used, defined as 1/frequency. In the above equation, the transformation signal can be considered as comprised of two different variables, namely $\boldsymbol{\tau}$ and *s*.

3.3 Closing Remark

Several studies have been demonstrated the usefulness of statistical parameters obtained from both AE and vibration spectra, in both time and frequency domains, for the CM of bearings at medium and high speeds.

Furthermore, this chapter shows several advanced signal processing techniques in term of both time and frequency domains, used to monitor bearing degradation.

However, there is a severe lack of knowledge on the applicability of these statistical parameters to the CM of bearings at low speeds. Given the experience contained in the industry relating to AE techniques and the capital invested in instrumentation and training, it is highly desirable to demonstrate that it is possible to extend present technique to the monitoring of low-speed bearings. If such an approach were found to be acceptable, it would save industry considerable time and money.

To investigate these possibilities an experimental programme has been carried out, and details of the methodology are presented and discussed in Chapter Four.

Chapter Four

4 Research Methodology

This study aims to demonstrate the applicability of AE techniques to diagnose early degradation in bearings operating at low rotational speeds. The research methodology is based on experimental testing of a roller bearing under various loadings and speeds, see Figure 4.1. Experimental investigation of the failure modes of rolling element bearings has shown that the component that most frequently fail is the inner race followed by the outer race [141]. Thus, the monitoring of these elements has become the subject of considerable attention. In this experimental study, an electric engraver was used to simulate faults of several sizes on the inner and outer races, see Figure 4.1. Further details of bearing test rig design, seeded faults, experimental setups, and procedures are discussed later in this chapter.

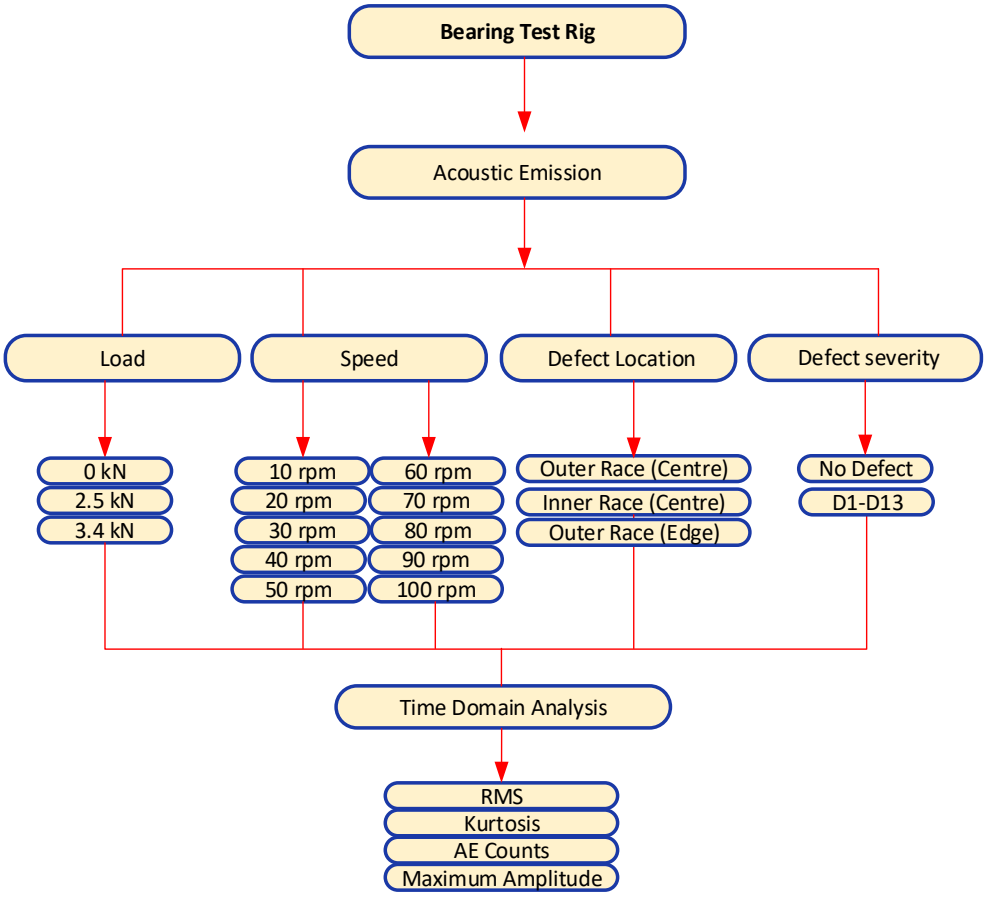

Figure 4.1: Bearing test rig conditions

4.1 Experimental Setups

To determine the applicability of AE techniques in detecting bearing degradation at low speeds, a series of experiments was carried out using the test rig shown in Figures 4.2 to 4.4. In this rig, a cylindrical roller bearing is assessed under static loads to test the likelihood of bearing failure. The test specimen (bearing) was mounted on the overhanging shaft, and the shaft supported by a pair of spherical roller bearings as shown in Figure 4.3. An air cylinder was positioned horizontally to exert a steady radial load on the specimen housing, see Figure 4.4. The rotating shaft was driven by an electric motor, connected to the shaft by a flexible coupling. A load cell was used for measuring the load and placed in front of the air cylinder. Two handheld tachometers were used to measure the shaft rotational speed.

The main components of the test rig are as follows:

- Specimen housing
- Specimen
- Shaft
- Support bearings and housing
- Air cylinder

Figure 4.5 shows a schematic of the test rig arrangement, with an air cylinder, load cell, and bearing housing assembly. It also shows a sectional view of the bearing housing.

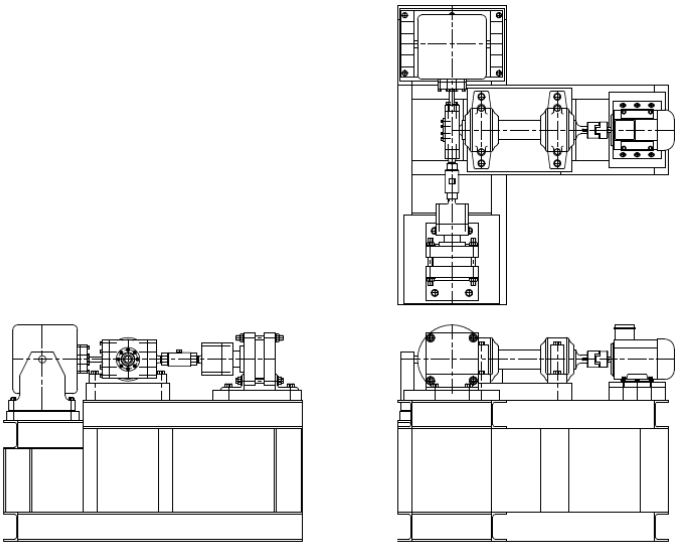

Figure 4.2: Different views of the bearing test-rig drawing [142]

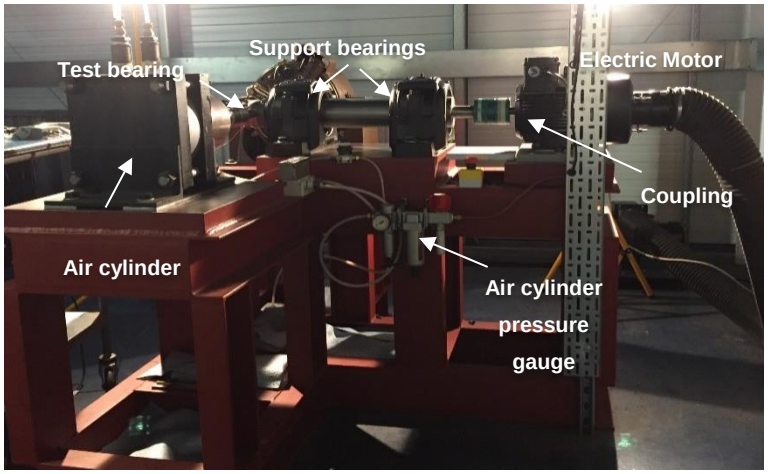

Figure 4.3: Front view of the bearing test rig

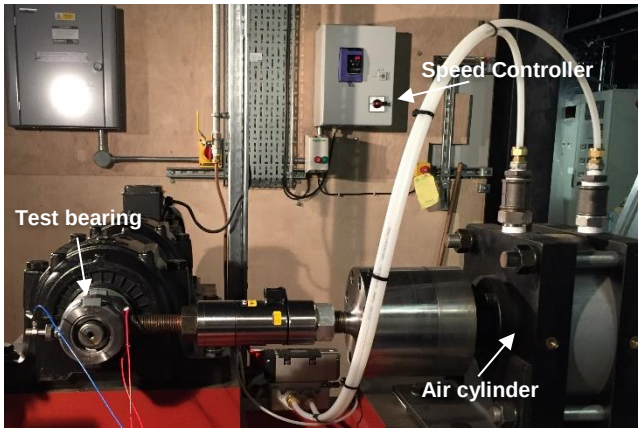

Figure 4.4: Side view of the bearing test rig

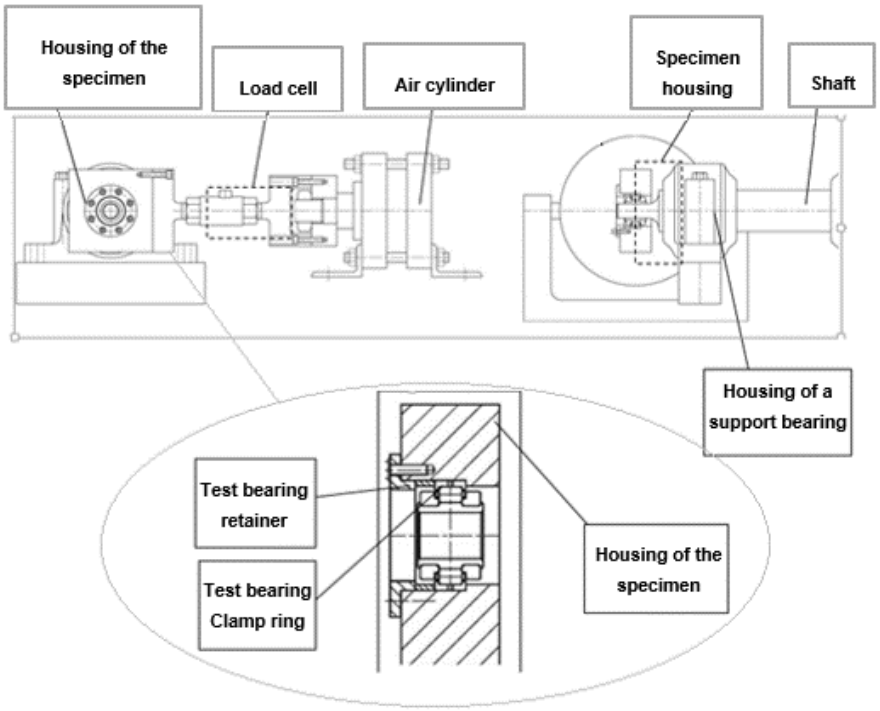

Figure 4.5: An overview of the bearing test rig arrangement

4.1.1 Specimen Housing

The bearing housing used was as advised by Cooper Bearings Ltd (see Figure 4.6). The connection of the air cylinder to the housing was considered to apply the load.

Figure 4.6: Specimen housing (01 BCP 35MM GR ATL)

4.1.2 Specimen

A Cooper split cylindrical roller bearing (type 01 B 35MM GR) was used in this experiment. This bearing was selected as it can be assembled and disassembled easily, thus allowing the test bearing to be regularly checked throughout the test programme with minimum disruption to the test rig during the introduction of defective components. All the elements of the test specimen were split into two, as shown in Figure 4.7, which illustrates (a) bearing parts and (b) their assembly. The dimensions of the specimen were:

- Bore (internal) diameter, 35.00 mm
- External diameter, 84.14 mm
- Roller diameter, 11.91 mm
- Pitch circle diameter, 62.71 mm
- Number of rollers, 10

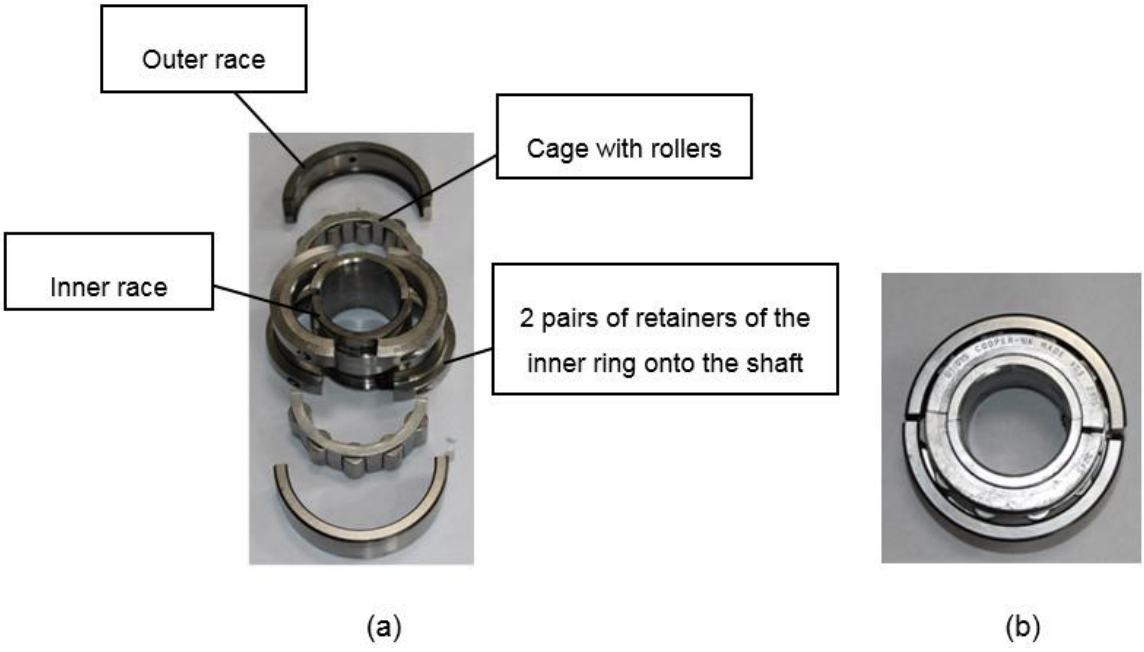

Figure 4.7: Specimen (a) in parts, and (b) assembled

4.1.3 Shaft

Given the dimensions of the specimen and the support bearings, the shaft had the dimensions presented in Figure 4.8. To ensure no misalignment, a flexible

coupling was used which linked the main shaft to the drive shaft that was supported by two spherical roller bearings.

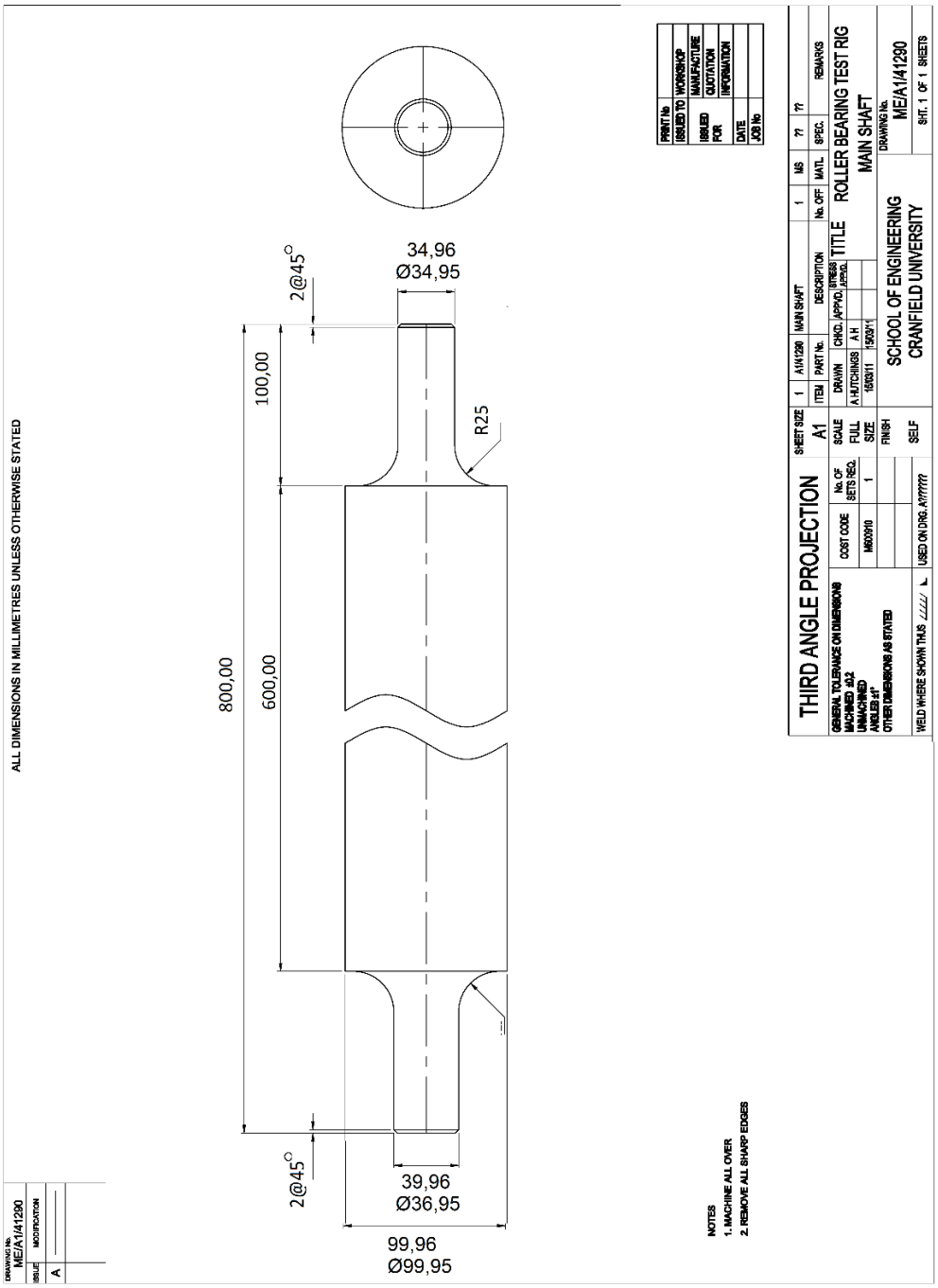

Figure 4.8: Drawing of shaft (bearing at "top") [143]

4.1.4 Air Cylinder

For applying the static load, an air cylinder (SMC, Type CS1LN250-25) was used. This is a single rod cylinder with a maximum pressure of 1 MPa, a bore size of 250 mm and maximum shaft travel of 25 mm. Foot style parts are used to support the cylinder on the rig.

Figure 4.9 shows a view of the cylinder, and its dimensions are as shown in Figure 4.10.

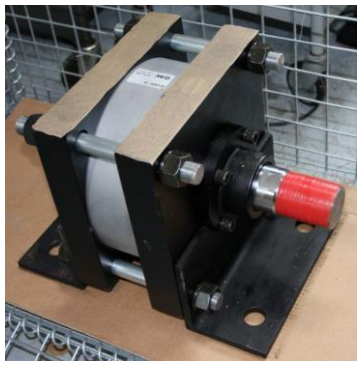

Figure 4.9: Air cylinder

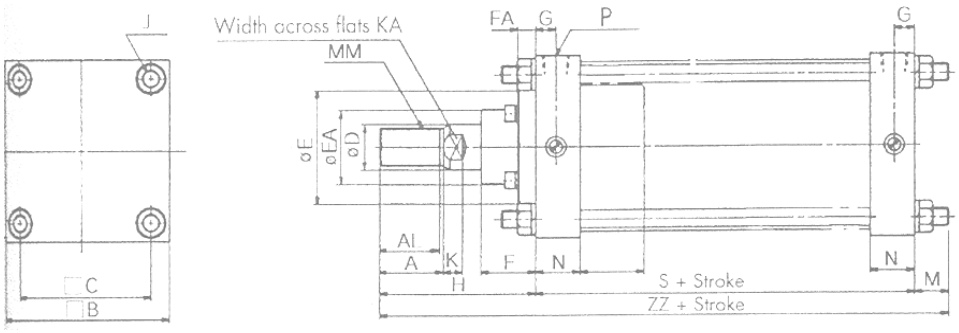

Product No.	Stroke range (mm)	A (mm)	AL (mm)	B (mm)	C (mm)	D (mm)	E (mm)	EA (mm)	F (mm)	FA (mm)	G (mm)
NT-25	Up to 1200	71	67	277	225	60	140	86	60	20	1823.5

Figure 4.10: Dimensions of the air cylinder [144]

4.2 Data Acquisition System

Two Physical Acoustics Nano-30 miniature AE sensors (Figure 4.11 (a)), having a frequency range from 125 to 750 kHz, were used for the AE tests. This sensor is ideal for applications where small size is important. This sensor features an integral of 1-meter coaxial cable, which exits from the side of the sensor (see Figure 4.11) terminating in a BNC connector.

(a)

Figure 4.11: A Nano-30 miniature AE sensor

The AE transducers were cemented with superglue onto the bearing housing, see Figure 4.12. To ensure even distribution of the couplant across the face of the sensor, a small amount of glue was placed in the centre of the sensor's intended position and the sensor carefully pressed onto the surface, spreading the couplant uniformly. To ensure obtaining a high amplitude signal, the AE sensors were positioned within the loading zone and close to the defect source to reduce signal attenuation. Whether the AE sensors were placed on a vertical or horizontal surface made no difference to the AE signal. This observation was confirmed, see Figure 4.13 which shows the AE RMS for the two channels for the same running conditions.

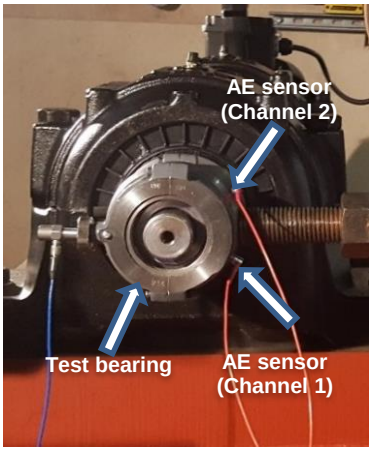

Figure 4.12: Close-up of test bearing

Figure 4.13 shows the RMS value of the AE signal for each of the two channels for a healthy bearing for an applied load of 3.4 kN and speeds from 10 to 100 rpm. From this chart, it was observed that the two AE sensors had the same response, though the signal from Channel 1 was of higher amplitude than for Channel 2 as it was closer to the source. This was also found to be the case for several defect severities. Therefore, in this research, the Channel 1 signal will be used for all analyses.

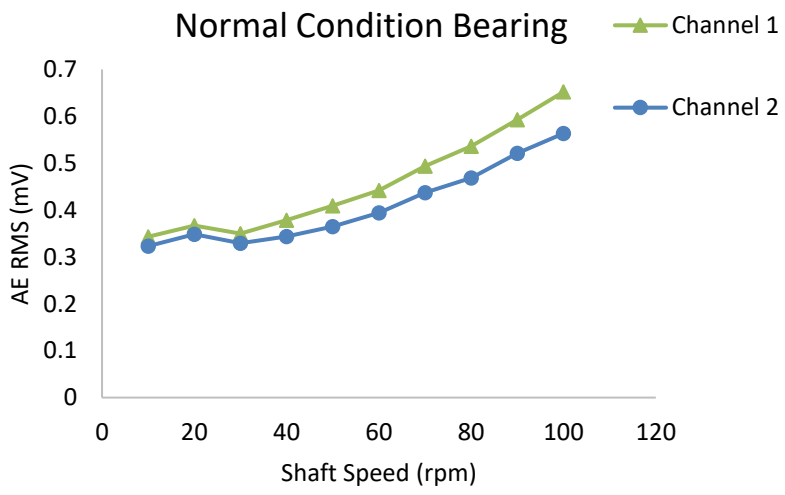

Figure 4.13: AE RMS for the two AE channels at applied load of 3.4 kN

Figure 4.14: Schematic diagram of acquisition system

With these sensors, the acquisition system was as shown in Figure 4.14. For the AE test, Physical Acoustics type 2/4/6 pre-amplifiers were used to provide initial amplification of the AE signal and reduce electromagnetic noise. These pre-amplifiers contain a plug-in analogue high-pass filter to eliminate low-frequency acoustic noise and show better temperature performance than could be achieved with an integral pre-amplifier. These pre-amplifiers have a selectable gain of 20, 40, or 60 dB, see Figure 4.15.

Figure 4.15: Pre-amplifier

For this particular experiment, the pre-amplifiers were set at a 40dB gain to get a suitable signal with low noise. Co-axial cables less than 1 m long were used to connect the AE sensors with the pre-amplifiers to avoid electromagnetic noise [69,91]. The pre-amplifiers were connected directly using coaxial cable to a commercial data acquisition card (DAQ) within a Pentium host PC (PCI-2 Based AE System with six channels) which provided a sampling rate of up to 10 MHz with 18-bit precision giving a dynamic range of more than 85 dB. The PCI-2 was selected because of its superior low noise system combined with low cost [145].

In the analogue-to-digital converter (ADC), the card has anti-aliasing filters that can be tuned (i.e. the band pass altered) by the software directly.

Each experiment was repeated three times for each condition to reduce the likelihood of anomalous results, and the data recorded for two minutes at each test. During the 2 minutes, several AE waveforms can be captured which gives more opportunity to ensure the accuracy of the results.

The sampling rate for the AE test was chosen as 2 MHz to get better data resolution according to the Nyquist Theorem [146,147] so that the aliasing effect, which causes different signals to become indistinguishable after sampling, would be avoided. For each case, the specific waveform recording length based on the rotational speed is listed in Tables A.1 and A.2 in Appendix A. The lower the speed, the longer the required recording time to observe the defect frequencies. For each speed, waveform recording length is calculated from bearing fault frequency equations shown in Section 3.2.2.

For the purpose of data acquisition, the longest recording time (for 10 rpm) was set to cover at least 4 pulses over the defect at each speed condition. Therefore, 5.94 and 4.04 seconds was set for the outer and inner races defective cases, respectively. Furthermore, for hit driven data, a trigger level was set as 38 dB to ensure that the captured signal is not sourced from the background noise, this setteing was achieved after running several experiments and analysis. The feature extraction and analysis for both AE and vibration was performed on MATLAB R2014a.

4.3 Experimental Procedures

Prior to the experiments, an attenuation test was carried out which will be described in Section 4.4. Furthermore, a series of experiments were conducted before any defects or faults being seeded into the system and baseline (normal bearing conditions) were recorded for each running condition. Before commencing each experiment, the test rig was run for at least 30 minutes to bring it to thermal equilibrium.

- The first test programme aimed to establish a correlation between AE activity and increasing speed and load conditions. This was accomplished by increasing the speed from 10 - 100 rpm, in steps of 10 rpm, at a constant radial load. This procedure was repeated three times with loads of 0, 2.5 and 3.4 kN, see Figure 4.1. These loads were chosen according to the limitations of the of the test rig and bearing. Moreover, this step was carried out for all the defectives from D1 to D5 as show in Table 4.1.
- The second test programme was intended to establish a correlation between AE activities and level of defect in the outer race (at the centre) by having incremental increases in the defect at a fixed speed and load. This involved starting a sequence on a bearing with a point defect (D1) at the centre of the outer race, followed by line defect (D2) and then increasing defect width and/or length (D3, D4, D5), see Table 4.1. The defect sequence is illustrated in Figure 4.16. All defects were of depth 0.03 mm.

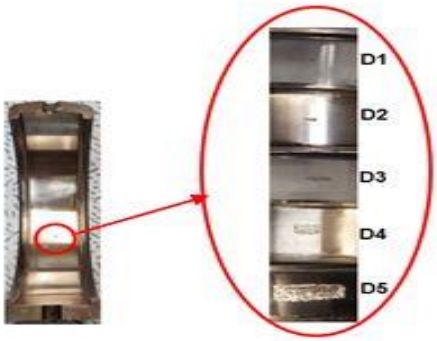

Figure 4.16: Outer race defect severities (at the centre)

It should be noted that the defect length is along the race in the rolling direction and the defect width is across the race. An engraving machining with a carbide tip was used for creating the defects shown in Figure 4.16.

- The third test program was a repeat of the first and second test programs, but for the inner race as presented in Figure 4.17. This step was to check the applicability of AE techniques to detect the defect on the inner race at such low speeds.

Figure 4.17: Inner race defect severities

- The final program was intended to establish a correlation between AE activity and increasing defect size at the edge of the outer race, see Figure 4.19. The size of the defect was increased incrementally at a fixed speed and load. This test sequence began with a line defect of given length (D6), followed by increasing the width with the same length (D7-D9), see Figure 4.18 (a). After that, beginning with the line defect of given width (D10) and increasing the length but retaining the same width (D11-D13). These defect sequences are illustrated in Figure 4.18 (b). Furthermore, to investigate the effect of fault location and the applicability of the measured parameter to monitor the defect at any location on the outer race. The measured parameters for two faults of the same dimensions (D4 and D12) at deferent locations were compared. As fault D4 was located at the centre of the outer race as shown in Figure 4.16 while D12 is at the edge, see Figure 4.18 (b).

Table 4.1: Defect sizes

Named as	Case	Defect Type (L x W) mm
ND	ND	Normal condition (free Defect)
D1	Point	Dent (D=0.5)
D2	L1XW1	2.5 X 0.9
D3	L2XW1	6.0 X 0.9
D4	L2XW2	6.0 X 3.0
D5	L3XW3	12.0 X 6.0
D6	L4XW4	3.0 X 5.0
D7	L4XW5	3.0 X 7.0
D8	L4XW6	3.0 X 10.0
D9	L4XW7	3.0 X 12.2
D10	L5XW2	2.0 X 3.0
D11	L6XW2	4.0 X 3.0
D12	L2XW2	6.0 X 3.0
D13	L7XW2	8.0 X 3.0

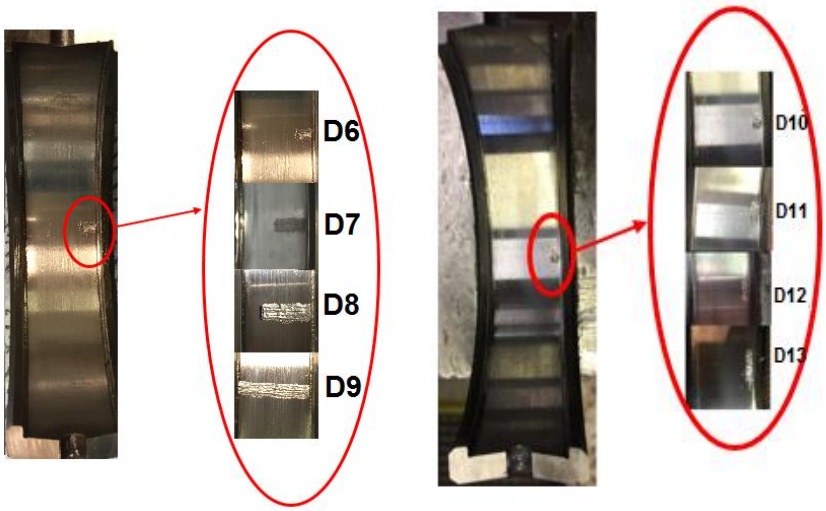

Figure 4.18: Outer race defects at the edge

4.4 Calibration and Attenuation Test

Calibration techniques can, typically, be categorised into two general groups namely, equipment testing and sensor calibration. AE tools are commonly designed to extract a set of parameters from the recorded AE signals and then store them. Thus, the characterizations of these signals rely mainly on the type of equipment commercially available and consequently comprehensively verifying the AE signal parameters recorded by these tools is essential.

However, before the full-scale AE tests, a performance verification test of the AE tools was undertaken and the results compared with the published performance criteria provided by the manufacturers. Prior to starting the experiments, the AE system was calibrated by the MISTRAS Group Limited Company. The manufacturer also provided calibration certificates for all the AE sensors. These certificates contain the characteristics and the technique used for calibration, see Figure 4.19. This calibration was performed according to ASTM Standard E976 [148], the standard guide for determining the reproducibility of AE sensor response.

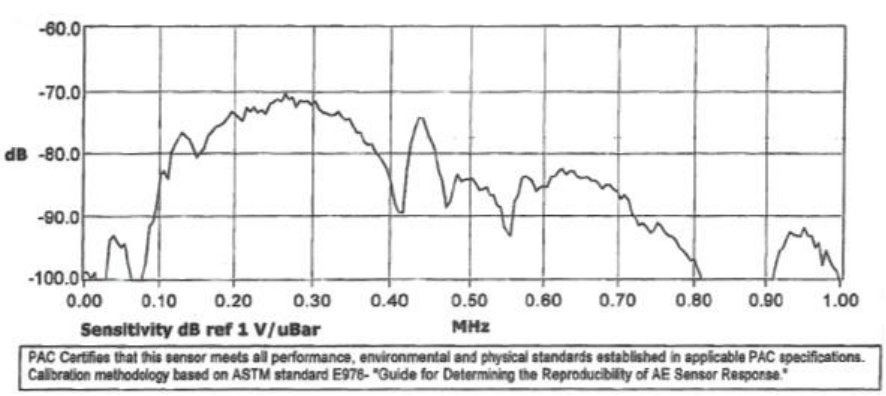

Figure 4.19: AE sensor calibration certificate [148]

Attenuation can be defined as any reduction in the AE signal strength in the form of amplitude or intensity occurring when the signals have travelled any distance through the medium. This is expressed in decibels (dB's). In AE applications, attenuation is critical as it rapidly reduces signal strength with the distance between source and sensor. Thus, it plays a significant role in determining AE sensor locations. Additionally, attenuation is directly affected by the thickness and type of the medium. For each type of medium, there is an attenuation coefficient (β) used to determine the decay rate of AE signal based on its frequency. Attenuation can be expressed as a function of transmission distance (*r*), the medium's attenuation coefficient (β), and the signal frequency (*f*).

$$Attenuation = \beta * r * f \quad \text{.....} \quad (4.1)$$

Thus, in practice, AE waves which propagate through a structure under test may be distorted and strongly attenuated, so AE sensor attenuation test was performed on a daily basis to check the quality of the sensor.

The attenuation between two different locations i.e. the signal source location and the sensor location can be calculated knowing the signal voltage and/or the signal power at each location. If Vs and Ps, respectively, are the signal voltage and the signal power at the signal source location, and Vd and Pd, respectively, are the signal voltage and the signal power at the sensor location, the attenuation between the two locations can be calculated by Equations (4.2)and (4.3)

$$Signal\ Voltage\ Attenuation(At_V) = 10\log_{10}\left(\frac{V_s}{V_d}\right)\ldots\ldots\ldots\ldots\ldots\ldots \quad (4.2)$$

Or:

$$Signal\ Power\ Attenuation\left(At_p\right) = 10\log_{10}\left(\frac{P_s}{P_d}\right)\ldots\ldots\ldots\ldots\ldots\ldots\ldots \quad (4.3)$$

An AE sensor attenuation test was carried out before any AE testing. The first step is to simulate an AE source, and this can be achieved by using a Hsu–Nielsen source, shown in the Figure 4.20, which based on the breaking of a pencil lead. This method is commonly used because of its simplicity and repeatability. It was used here to evaluate the AE attenuation across the bearing.

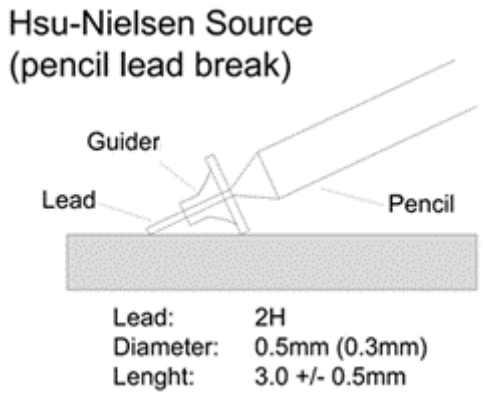

Figure 4.20: Hsu-Nielsen Source (pencil lead break) [149]

The test was carried out by breaking a pencil lead (Hsu Nielsen pin) of 0.3 mm diameter (2H) at several locations on the test rig, see Figure 4.21. As would be expected various levels of attenuation were observed depending on whether the “pin” was located on the roller, inner race, outer race, or the other locations as listed in Table 4.2.

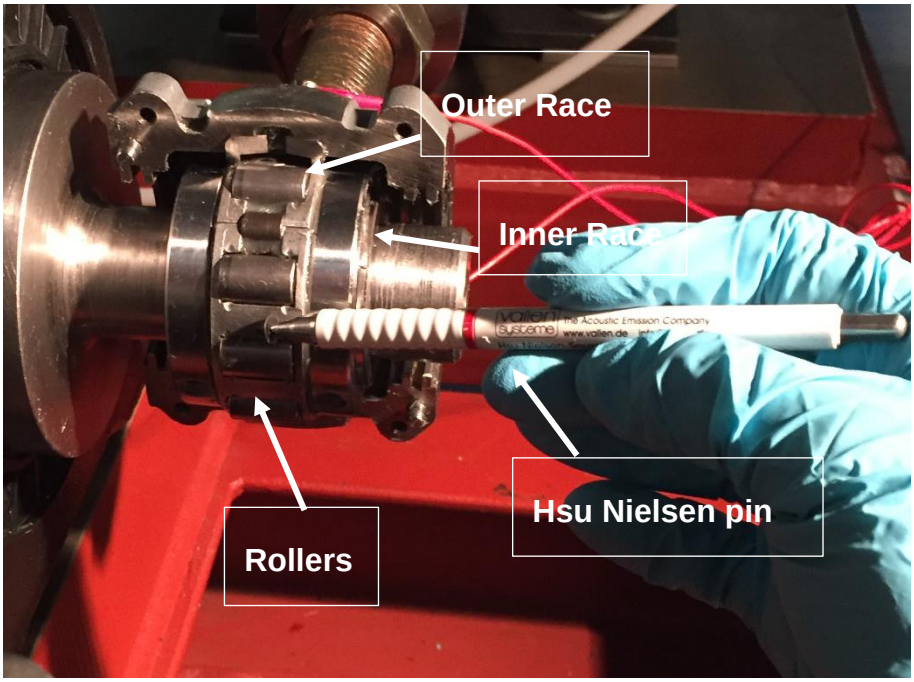

Figure 4.21: Determining attenuation characteristics across the bearing

The purpose of this test is to ensure that the sensors are in good acoustic contact with the part being monitored and to ensure direct contact between the outer race, inner race, roller and the bearing casing.This was accomplished by positioning a roller at right-dead-centre in a direct path with the load. Each calibration test was performed five times to check reliability and repeatability of sensor sensitivity.

Taking the reference level (Vd) as due to the pencil lead being broken on the casing between the two sensors and calculating the relative attenuation using Equation (18). It was found that the relative attenuation of the AE signatures in terms of maximum amplitude was 0.1 dB for the outer race, 1.8 dB for the inner race, and approximately 2.9 dB for the roller. These attenuations are explained as due to the different clearances present in the bearing. At each interface, the AE signal will be partially transmitted and partially reflected. The different paths from the sources to the sensor will include differing numbers of interfaces so that the attenuations will vary. As shown in Figure 4.21, at the left dead-centre of the roller, a clearance exists between the roller and the races and that is the reason for the substantial difference, irrespective of the loading [21].

On the other hand, it should be noted that for all locations other than the tested bearing, the signal attenuated totally before it reached to the sensor. Thus, it has been ensured that the captured signal was not from any source other than the bearing being tested.

Table 4.2: Description of the attenuation test

File Name	Location
S0L1	Motor, top middle casing
S0L2	Hydraulic support, on the top of the support
S0L3	Steel bed plate bottom side of the test bearing
S0L4	Rollers, the two support bearings
S0L5	Inner race, the two supports bearings
S0L6	Outer race, the two supports bearings
S0L7	Casing of the two support bearings
Shaft	
S0T1	Shaft before coupling, Top Dead Centre
S0T2	Shaft after coupling, Top Dead Centre
S0T3	Shaft before the tested bearing, Top Dead Centre
S0T4	Shaft after the tested bearing, Top Dead Centre
S0T5	Shaft between the two supported bearings, Top Dead Centre
Bearing	
S0B1	Right bearing casing, between the AE sensors
S0B2	Outer race of the test bearing at $90°$ from right dead centre to the top
S0B3	Inner race of the test bearing at $90°$ from right dead centre to the top
S0B4	Roller of the test bearing, left Dead Centre

Chapter Five

5 Outer Race Fault Diagnostics

5.1 Introduction

This chapter examines the applicability of AE to the CM of low-speed bearings. The chapter reviews the experimental monitoring of bearing conditions for both healthy bearings and bearings with a seeded defect on the outer race.

There is no single best measure for the CM of bearings, so this chapter presents and discusses the statistical parameters most commonly used to monitor bearing conditions: RMS, kurtosis, the maximum amplitude, and the number of counts. However, the temperature of the bearings at such low speed bearings is not a good indicator of the presence of a fault. This is because the low rotational speed allows the heat generated to be lost by convection and conduction and so this parameter is not used in this research investigation. Neither is it expected to affect the AE signal generated.

One major benefit of statistical parameters is their sensitivity to variation in speed and load of the item under test. Several investigations of this matter have been made, and some contradictory observations have been reported in the literature. For example, at moderate speeds, Al-Ghamdi et al. [19] observed that the RMS values of both AE and vibration signals are sensitive to both speed and load variation. Although, He et al. [23] agreed with these findings for changes in speed; they found no significant variation with load. Unfortunately, there is limited knowledge of the influence of load and/or speed within the low-speed range (10-100 rpm) of interest here.

Another key issue in bearing diagnostics is the detection of a developing fault at an early a stage as possible before it can develop into a catastrophic failure. Thus, this chapter also investigates the use of AE to detect fault initiation and propagation in the outer race of a roller bearing in the low-speed range by investigating the effect of the fault size on the outer race using several statistical parameters.

In summary, this chapter investigates two points:

1. The influence of speed and load on the statistical parameters for low speeds (10-100 rpm)
2. The applicability of the statistical parameters to detect defect initiation and propagation at the outer race (i.e. sensitivity to defect size).

This chapter present results of the first and second programs mentioned in Section 4.3 for a healthy bearing (ND) and five defective bearings at the outer race (D1 to D5) as described in Table 4.1 and shown in Figure 4.16.

The results demonstrate the usefulness of AE in the monitoring of both fault initiation and propagation in the bearing outer race at low speeds.

5.2 RMS Observations

RMS is a powerful statistical tool used for bearing CM. The RMS value of the AE signal is directly related to the mechanical deformation of the material when strain energy is released [23]. Thus, AE RMS is considered to be a suitable parameter for evaluating the presence of a defect and likely bearing failure.

The RMS values of AE signals under various loads and speeds are shown in Figure 5.1.

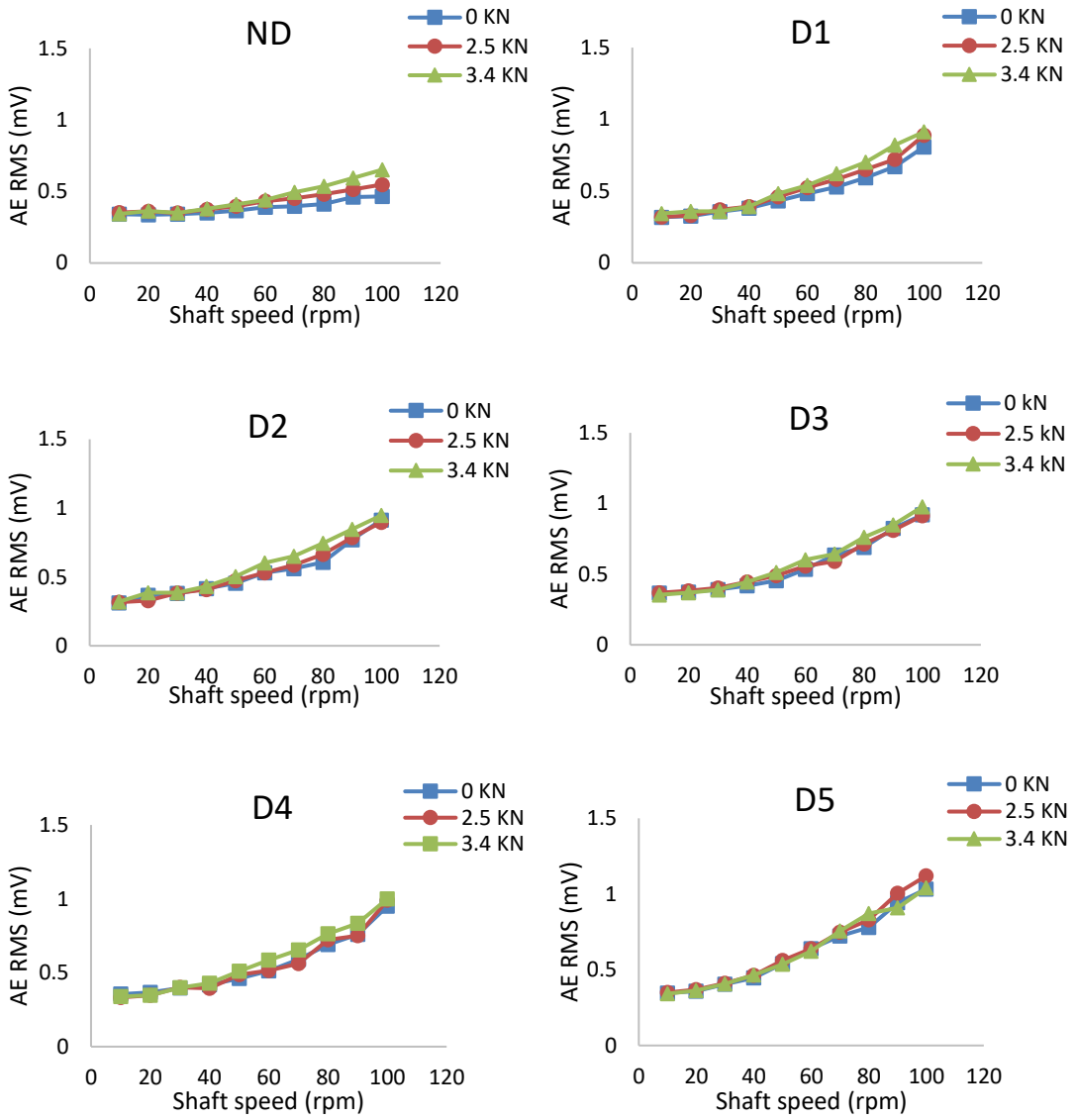

Figure 5.1: AE RMS as a function of shaft speed with three loads for a healthy bearing and five bearings with various faults on the outer race

Generally, for all the bearings tested, the AE RMS value increased with increasing speed of rotation, see Figure 5.1. This agrees with the data published by Graney and Starry [130] and indicates that the excitation energy supplied by the bearing's speed excites resonant frequencies (usually in the bearing itself) and hence generates the continuous emission that is characteristic of the raw signal profiles. This suggests a credible explanation for the increase in the value of the AE RMS with an increase in speed.

The rate of increase in the AE RMS appears to accelerate once the speed reaches 30 rpm. Furthermore, it was noticed that for the defect-free bearing (ND), the rotational speed has less influence on the AE RMS than for the defective cases. This because for the latter cases, the transient elastic waves (AE) are generated by the interaction of the bearing rollers with the inner and outer races, and also from the impingement of the rollers on the seeded defect in the outer race. While in the ND case, AE is generated only from the first source.

However, the AE RMS value appears to increase only very slightly with an increase in load, save for the no-fault case (ND) and fault D1. Nevertheless, even here the increase was not shown to be statistically significant.

The change in RMS values of the AE signals with a gradual increase in the size of the outer race defect at 80 rpm for three load conditions is presented in Figure 5.2. The increase of the defect size started with a point defect (D1), followed by line defect (D2) and then the defect width and length were increased (D3, D4, D5), see Table 4.1. The incremental values (IR - the ratio of the measured value relative to that measured for ND, using Equation (5.1)) for the measured AE RMS values for each of the five defective cases was calculated at 80 rpm and presented in Table 5.1. This incremental value is used to clarify the influence of the defect existence and the defect size, in each case, on the measured parameter.

Furthermore, Figure 5.2 and

Table 5.1 were repeated at 30, 50, and 100 rpm and are presented in Appendix B. This was done to demonstrate that the same trends existed for other low speeds.

$$\text{Incremental value, IR} = \frac{P_{D_i}}{P_R} \qquad (5.1)$$

Where:

D_i: is defective case *i*, (= 1, 2 ... 5)

P_{D_i}: Parameter value for the D_i case

P_R: Parameter value for the ND case (healthy condition)

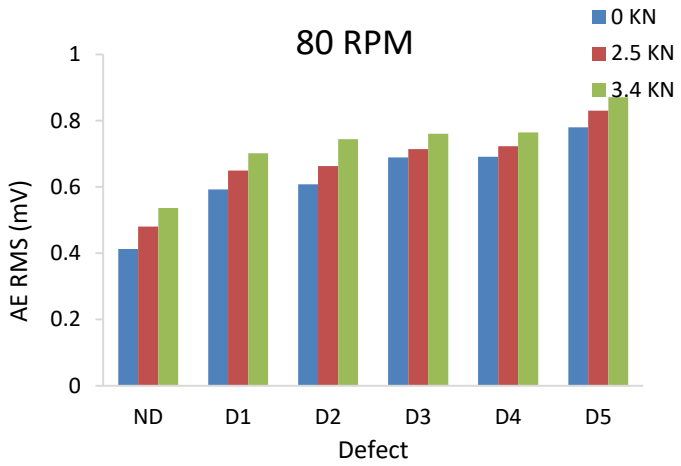

Figure 5.2: AE RMS for outer bearing race for healthy and five fault conditions, at 80 rpm for three loads

From Figure 5.2, it can be seen that the AE RMS for fault D1 was significantly higher than the AE RMS for the healthy condition and that the AE RMS increases with increase in defect size and for all defective cases.

Table 5.1: RMS IR values for five bearings with five fault conditions on the outer race, at 80 rpm for three loads

Fault	Defect Dimensions (mm)	0 kN	2.5 kN	3.4 kN
D1	Dent (D = 0.5)	1.43	1.35	1.31
D2	2.5 X 0.9	1.47	1.38	1.39
D3	6.0 X 0.9	1.67	1.49	1.42
D4	6.0 X 3.0	1.67	1.50	1.43
D5	12.0 X 6.0	1.89	1.73	1.62

The increases in the IR for AE RMS are not uniform because the increase in size when going from one fault to the next was not uniform, see

Table 5.1. However, between D3 and D4 it did remain almost constant, probably because of the defect length, in these two cases, was the same while the width is increased. These remarks also hold true for the other low speeds tested, see Appendix B.

In summary: These observations confirmed a strong correlation between AE RMS and shaft speed but failed to show any significant relation between AE RMS and load. This confirms the results of He et al. [23] and others [21,53,128,129], however Al-Ghamdi et al. [19] did mention a significant influence of the load on the AE RMS value. This could due to different load conditions.

Physically, AE signals are released due to deformation or damage within or on the surface of the material affected, and a constant load (once applied) has very little influence on the deformation mechanism of material and AE generation [23]. Hence, a constant load has a little influence on AE RMS. However, increasing rotational speed will increase the impact frequency and strength of the impact at the defect point, causing the AE RMS to increase.

It is concluded that AE RMS could be a good indicator to detect the initiation and propagation of outer race defects, which agrees with [19,22]. An explanation for this is that when the defect size is tiny the rolling element can roll easily over the defect with little obstruction or disturbance to its rolling motion. However, as the defect size increases, there comes a moment when the edge of the defect interferes with the motion of the rolling element to the extent that there is a sufficient change in momentum to register as an impact that can be detected by the AE sensor.

5.3 Kurtosis Observations

Another parameter commonly used for diagnosis of bearing defects is kurtosis [119]. A fault present in a bearing casing causes a shock pulse to be generated every time the roller passes over the fault. Consequently, the fault will produce a

periodical impulse which can be detected, and which can excite structural resonances in the bearing or the machine [150,151].

Hence, kurtosis - which is a measure of the peakiness of a signal - can be used as an indicator for defect existence, at least in its early stages. At high-speed applications, it has been observed that kurtosis is not sensitive to variations in speed and load [114]. However, it is essential to investigate if this measure can be useful at low speeds. The variation of AE kurtosis with speed and load for all six test runs (one healthy and five with faults at the outer race, and for three loads) is shown in Figure 5.3.

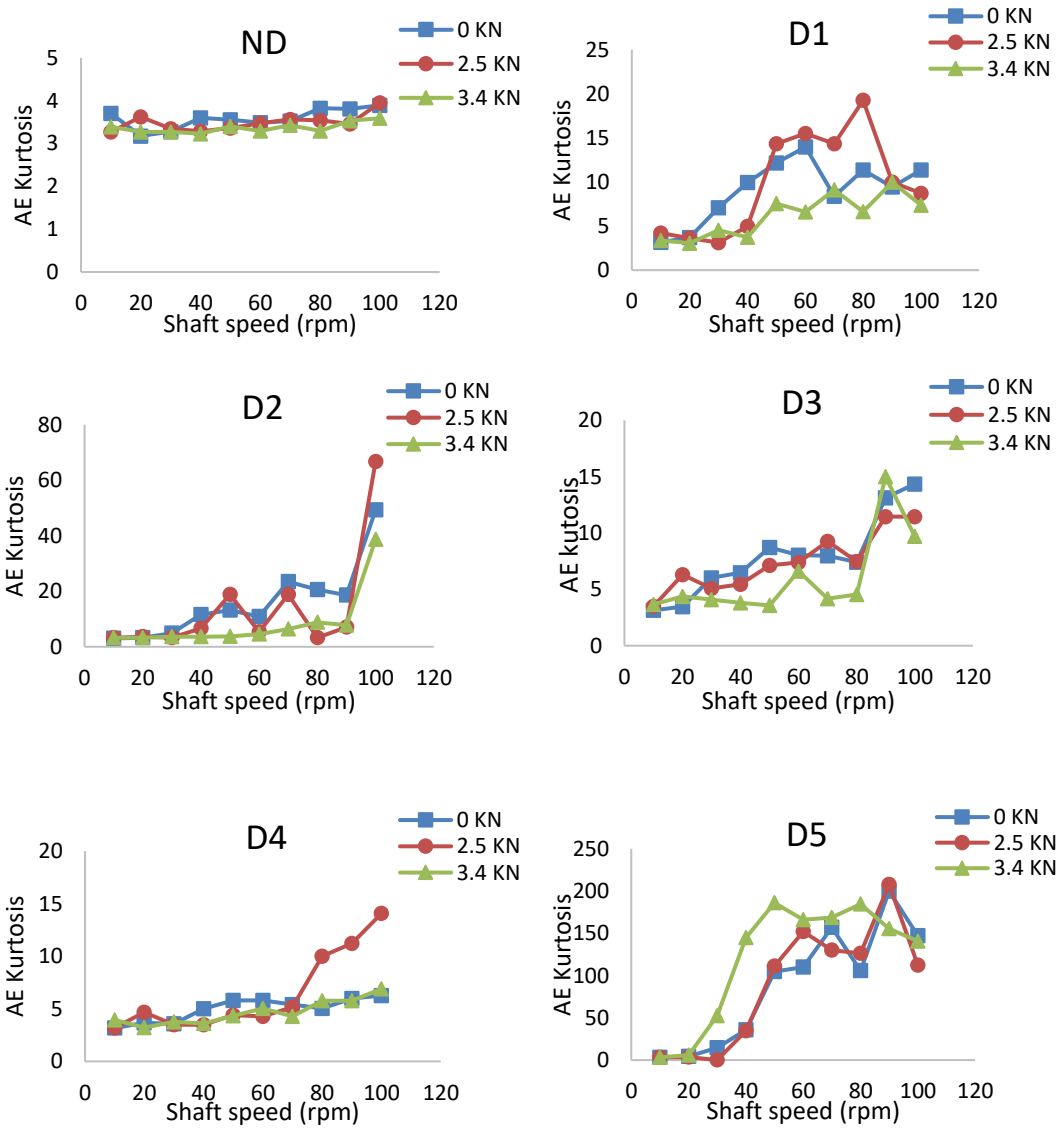

Figure 5.3: AE kurtosis as a function of shaft speed with three loads for a healthy bearing and five bearings with faults on the outer race

Figure 5.3 shows that AE RMS from the bearing without defects (ND) has a kurtosis value of close to 3 (as would be found for a Gaussian distribution) or slightly higher due to the presence of noise. This observation is in agreement with many other studies [19,114,119]

However, once the defect exists, and especially above about 30 rpm, the number of periodic impulses with larger amplitude increases and the AE kurtosis increases greatly. Nevertheless, in Figure 5.3, D5, for instance, with the 3.4 kN load and about 80 rpm, it can be seen that with further increases in shaft rotational speed the AE kurtosis ceases to increase as the system transfers from one Gaussian distribution to another and kurtosis starts to decrease. While, at low speeds (lower than 30 rpm) of all faulty cases, kurtosis value is relatively close to the Gaussian distribution value. However, no obvious influence of the load on the AE kurtosis can be noticed in Figure 5.3. Thus applying a constant load does not change the system's state.

Figure 5.4 present the change in the AE kurtosis with a change in the size of the outer race defect for the three load conditions, at 80 rpm. The incremental value of each defective condition related to the ND was calculated using Equation (5.1) and listed in Table 5.2.

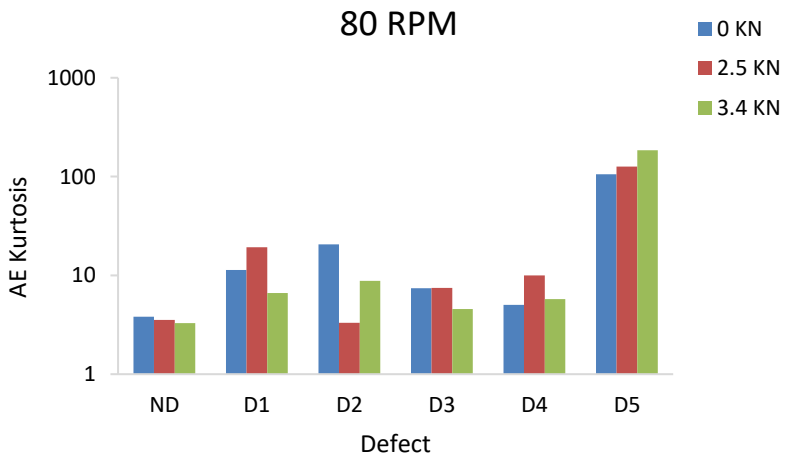

Figure 5.4: AE Kurtosis for outer bearing race for healthy and five fault conditions, at 80 rpm for three loads

From Figure 5.4, the AE kurtosis for ND was between 3.3 and 4 for all loads which indicated the Gaussian nature of the AE signal. Although once the defect exists, the AE kurtosis increases then it decreases again till D4 which after the AE kurtosis rose again.

From Table 5.2, for 80 rpm, for fault D1 at all three loads, the IR for the kurtosis increased to between 2.02 and 5.44 which indicates that the signal became very much peakier. For fault D2, the kurtosis IR increased (except at 2.5 kN), while for faults D3 and D4, even as the fault size increased, the kurtosis IR generally (with two obvious exceptions) fell, that is their peakedness reduced. However, a further increase in defect size (D5) led to a substantial increase in kurtosis IR. These observations also hold true for the other low speeds (30, 50, and 100 rpm) tested see Figure B.2 and Table B.2 in Appendix B.

Table 5.2: Kurtosis IR values for five bearings with five fault conditions on the outer race, at 80 rpm for three loads

Fault	Defect Dimensions (mm)	0 kN	2.5 kN	3.4 kN
D1	Dent (D = 0.5)	2.96	5.44	2.02
D2	2.5 X 0.9	5.38	0.93	2.66
D3	6.0 X 0.9	1.94	2.12	1.38
D4	6.0 X 3.0	1.32	2.83	1.75
D5	12.0 X 6.0	27.64	35.73	56.10

Given that the AE kurtosis value for fault D1 (minimum size fault) is significantly larger than for ND (except at 10 and 20 rpm). It can be stated that for shaft speeds of 30 rpm AE kurtosis is a good indicator of the first stage of a defect. However,

it is not sensitive to the subsequent defect growth as it produces a continuous, not impulsive, signal as the first impulse does not terminate before the second one is produced which cause kurtosis to decrease again. This is consistent with observations made at moderate speeds [23,119].

To summarise: once the defect exists in the bearing, the AE kurtosis is strongly related to rotational speed but is widely independent of load.

By using a physical description of Kurtosis, some insight can be drawn from Figure 5.4. When the defect first emerges, periodic impulses will be generated, increasing the AE kurtosis level. However, it is accepted that if the fault is severe enough and increases sufficiently in size, the signal will lose its peakiness, and the value of the kurtosis will decrease and eventually stop being useful as a measure of the presence of a fault [152].

5.4 Amplitude Observations

As defined in Section 2.4.6.1, the amplitude of the AE pulse is the largest peak voltage achieved by the waveform of a signal from an emission event. It is expressed in decibels (dB), see Equation (5.2). The amplitude will depend on the particular mechanism generating the AE signal, the transmission path, and the test conditions including the response characteristics of the sensor [23].

$$dB = 20\log\left(\frac{V_{max}}{1\mu - volt}\right) \qquad (5.2)$$

Figure 5.5, presents the measured AE amplitude as a function of shaft speed for the three loads, for a healthy bearing and five bearings with faults on the outer race.

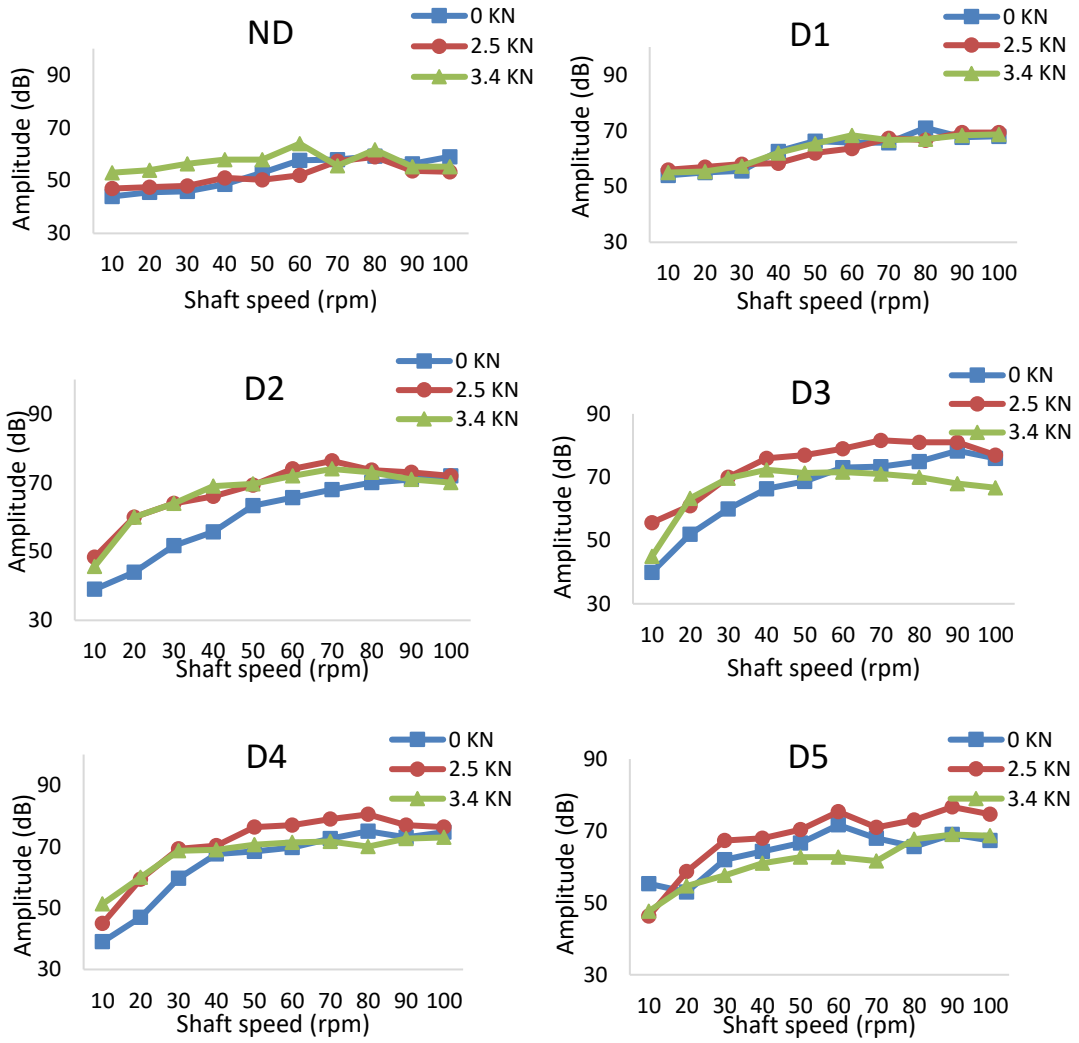

Figure 5.5: AE Amplitude as a function of shaft speed with three loads for a healthy bearing and five bearings with faults on the outer race

Figure 5.5, shows a strong correlation between AE amplitude and shaft rotational speed when a defect exists in the bearing. However, for the defect-free bearing (ND), the shaft rotational speed has little effect on the AE amplitude, even when a load is applied.

From Figure 5.5 it is noticeable that AE amplitude not influenced by the load increasing at ND and D1. However, for the other cases, AE amplitude increases with increasing the load from zero load to the 2.5 kN and then decreased at 3.4 kN. Therefore, it can state that AE amplitude has no apparent trend with load.

The effect of changing the size of the outer race defect on AE amplitude is shown in Figure 5.6, at a shaft speed of 80 rpm. The IR values, calculated using Equation (5.1), are shown in Table 5.3.

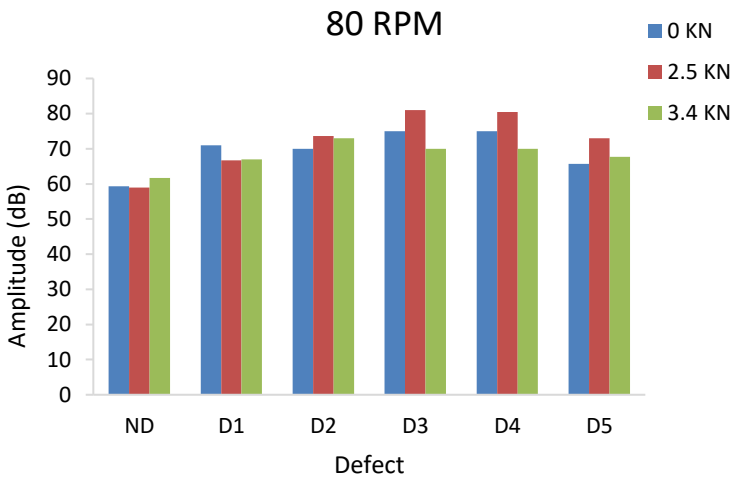

Figure 5.6: AE Amplitude at shaft speed of 80 rpm with three loads for a healthy bearing and five bearings with faults on the outer race

From Figure 5.6 and Table 5.3, it is seen that the AE amplitude, at a given load, initially increases with defect size, reaches a maximum at D2 (3.4 kN) or D3 (0 and 2.5 kN), after which it decreases. These results mean that AE amplitude will increase noticeably when a defect emerges in the outer race of the bearing. However, once the defect already exists, the AE amplitude might even decrease as defect size increases and so cannot be used to identify the size and extent of the defect. This remark also holds true for the other low speeds tested, see Section Appendix B.

Furthermore, from Table 5.3, it is observed that AE amplitude remain almost constant between D3 and D4, which again probably because of the defect length. To better relate defect size with AE amplitude and RMS further experiments will be reported in Chapter 8 regarding fixed width and variable length and vice versa.

Table 5.3: AE amplitude IR value at shaft speed of 80 rpm with three loads for five bearings with several fault conditions on the outer race

Fault	Defect Dimensions (mm)	0 kN	2.5 kN	3.4 kN
D1	Dent (D = 0.5)	1.20	1.13	1.09
D2	2.5 X 0.9	1.18	1.25	1.18
D3	6.0 X 0.9	1.26	1.37	1.14
D4	6.0 X 3.0	1.26	1.36	1.14
D5	12.0 X 6.0	1.11	1.24	1.10

In summary: If there is no defect in the bearing, then the AE amplitude is not influenced obviously by varying shaft rotational speed and/or load. Once a defect has been seeded into the bearing, the AE amplitude is affected by rotational speed, but not by the applied load. These remarks support the observations of [23,53,128,129].

This again suggests that as the applied load has little influence on the deformation mechanism generating the AE signal, then it will have little influence on the AE amplitude. However, increasing shaft rotational speed will increase the impact strength and the impact frequency at the defect point, thus causing an increase in the AE signal amplitude. Furthermore, defect generation changes the deformation mechanism in the defect area. However, such deformation of the defect area is not influenced by the defect size obviously. This explains the reason of the insensitivity of the AE amplitude to the defect size.

5.5 AE Counts Observations

As shown in Figure 2.5 in section 2.4.6.1, the AE counts is the number of times the amplitude of the signal exceeds a pre-set threshold level. Thus the AE counts reflects the AE activity level. Unfortunately, AE counts are easily influenced by the test conditions, such as the geometrical shape of the specimen, the characteristics and mounting condition of the transducer, and the performance of the amplifier and the filter, so care must be taken to maintain these as constant as possible. Figure 5.7 shows the comparison of AE counts for the healthy bearing and five faulty bearings for three applied loads as a function of shaft rotational speed.

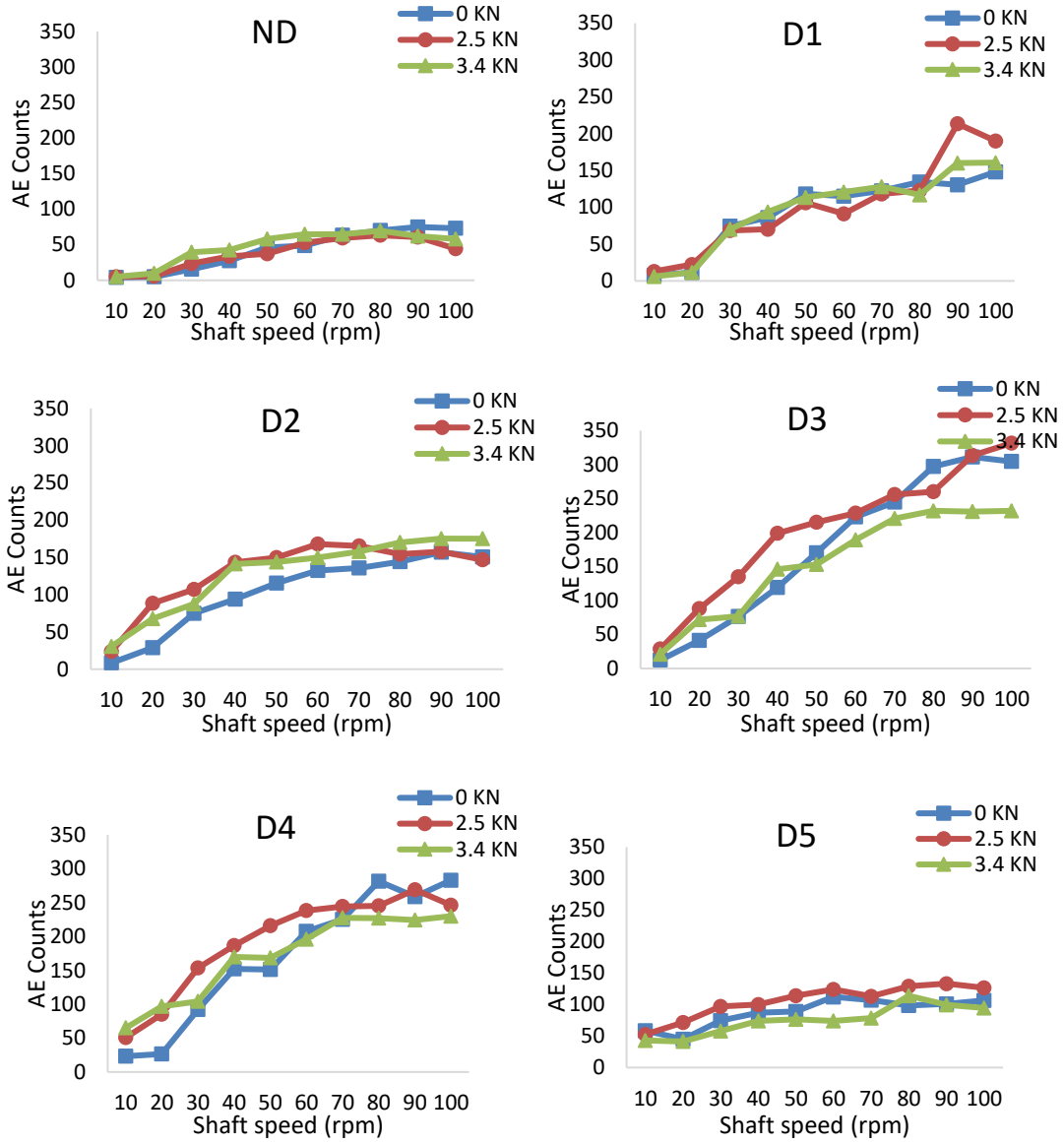

Figure 5.7: AE counts as a function of shaft speed with three loads for a healthy bearing and five bearings with faults on the outer race

In Figure 5.7, it is shown that for ND, the rotational speed had a small but considerable influence on AE counts. However, once a defect was seeded into the outer race, then, generally, the AE counts increased substantially with shaft rotational speed.

Furthermore, Figure 5.7 shows that, for ND and D1, the AE count is not influenced by the increasing load. However, with D2, it is noticeable that as the load

increased, the AE counts increased. The same phenomenon was observed with D3, D4 and D5 when the load was increased from zero to 2.5 kN, however, at 3.4 kN, the AE count decreased to a value lower than for the other load conditions. Thus, AE count does not have an obvious trend with the load.

The number of AE counts for the five outer race defects and three load conditions at 80 rpm is presented in Figure 5.8, and the IR values are listed in Table 5.4. The figure shows that at 80 rpm, the AE counts increased with the defect size from D1 to D3, after which the AE counts decreased. From the table, it is seen that the AE IR values for all defective cases were greater than one, which means greater than for the healthy bearing. However, these IR values do not have any noticeable trend with increasing defect sizes.

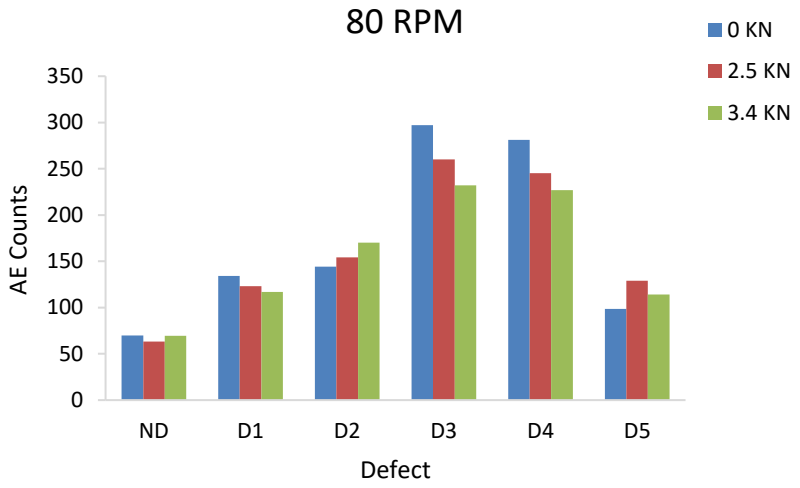

Figure 5.8: AE counts at shaft speed of 80 rpm with three loads for a healthy bearing and five bearings with faults on the outer race

Table 5.4: AE counts IR value at shaft speed of 80 rpm with three loads for five bearings with several fault conditions on the outer race

Fault	Defect Dimensions (mm)	0 kN	2.5 kN	3.4 kN
D1	Dent (D = 0.5)	1.92	1.94	1.68
D2	2.5 X 0.9	2.06	2.44	2.44
D3	6.0 X 0.9	4.24	4.11	3.33
D4	6.0 X 3.0	4.02	3.87	3.26
D5	12.0 X 6.0	1.41	2.04	1.64

In summary: AE counts are not sensitive to varying load applied to the bearing, but generally increase with rotational speed. This generally agrees with the findings of [23,114], though other studies have found that AE counts are sensitive to the load [19,153].

Furthermore, from above observations, it can be said that the AE counts is sensitive to the defect's existence but do not provide a clear and consistent trend with defect size. This finding is in agreement with Mba [153], of non-sensitivity of the AE counts to the defect size at moderate speeds. Although in [23], it was found that at moderate speeds, AE counts were not effective in identifying incipient defects. Likewise, the same AE counts observations found for the other low speeds, are presented in Figure B.4 and Table B.4 in Appendix B.

An explanation for these observations may be that AE counts reflect the activity level of the AE source, and the activity is mainly determined by the properties of the material, the defect condition, and the manner of excitation. The load does not directly affect these factors, especially at low speeds and so does not significantly affect AE source activity. However, increasing shaft rotational speed

will increase the frequency of excitation and strength of the impact between the rollers and the defect and, hence, will meaningfully increase the AE counts. Furthermore, the defect generation changes the deformation mechanism of the defect area, but this deformation was not influenced by the visible defect size at low speeds.

5.6 Closing Remark

The results show the applicability of AE techniques to detect defect initiation and propagation on the bearing outer race at low speeds. Table 5.5 summarises the relation and sensitivity of the parameters to the various conditions (load, shaft speed, and defect size) within low speeds range.

Table 5.5: Summary of AE parameter sensitivity to various conditions at outer race of low-speed bearing

Condition	RMS	Kurtosis	Amplitude	Counts
Speed ↑	↑(greatly)	↑(when defect exists) then ↓	↑(when defect exists)	↑ (greatly)
Load ↑	-	-	-	-
Defect size ↑	↑(greatly)	↑(when defect emerges) then ↓	↑(when defect emerges) then ↓	↑(when defect emerges) then ↓

From the outer race outcomes, it is concluded that the shaft rotational speed has a strong influence on the listed AE parameters. However, they are entirely independent of the load. Moreover, the defect size has some impact on the AE parameters, but of the parameters examined only RMS is sensitive to defect size. Nevertheless, all the mentioned parameter are sensitive to the defect existence on the outer race.

To demonstrate the applicability of AE for monitoring bearing conditions, a parallel investigation for the inner race will be described in Chapter 6.

Chapter Six

6 Inner Race Fault Diagnostics

6.1 Introduction

In the literature, it is reported that around 37.5% of bearings failure is due to inner race deterioration [141]. Thus, it is necessary to examine the applicability of AE time domain analysis to monitor the conditions of the inner race. This chapter does that for low speeds.

As in Chapter 5, this chapter investigates the two points:

1. The influence of speed and load on the statistical parameters for low speeds (10-100 rpm)
2. The applicability of the statistical parameters to detect defect initiation and propagation at the inner race (i.e. sensitivity to defect size).

Again, as in Chapter 5, the results demonstrate the usefulness of AE to monitor fault initiation and propagation in the inner race of bearing rotates at low speeds.

6.2 RMS Observations

Figure 6.1 shows AE RMS as a function of shaft speed and three loads for a healthy bearing (ND) and bearings with five defects of increasing size at the inner race, from D1 to D5 as described in Table 4.1 and Figure 4.17.

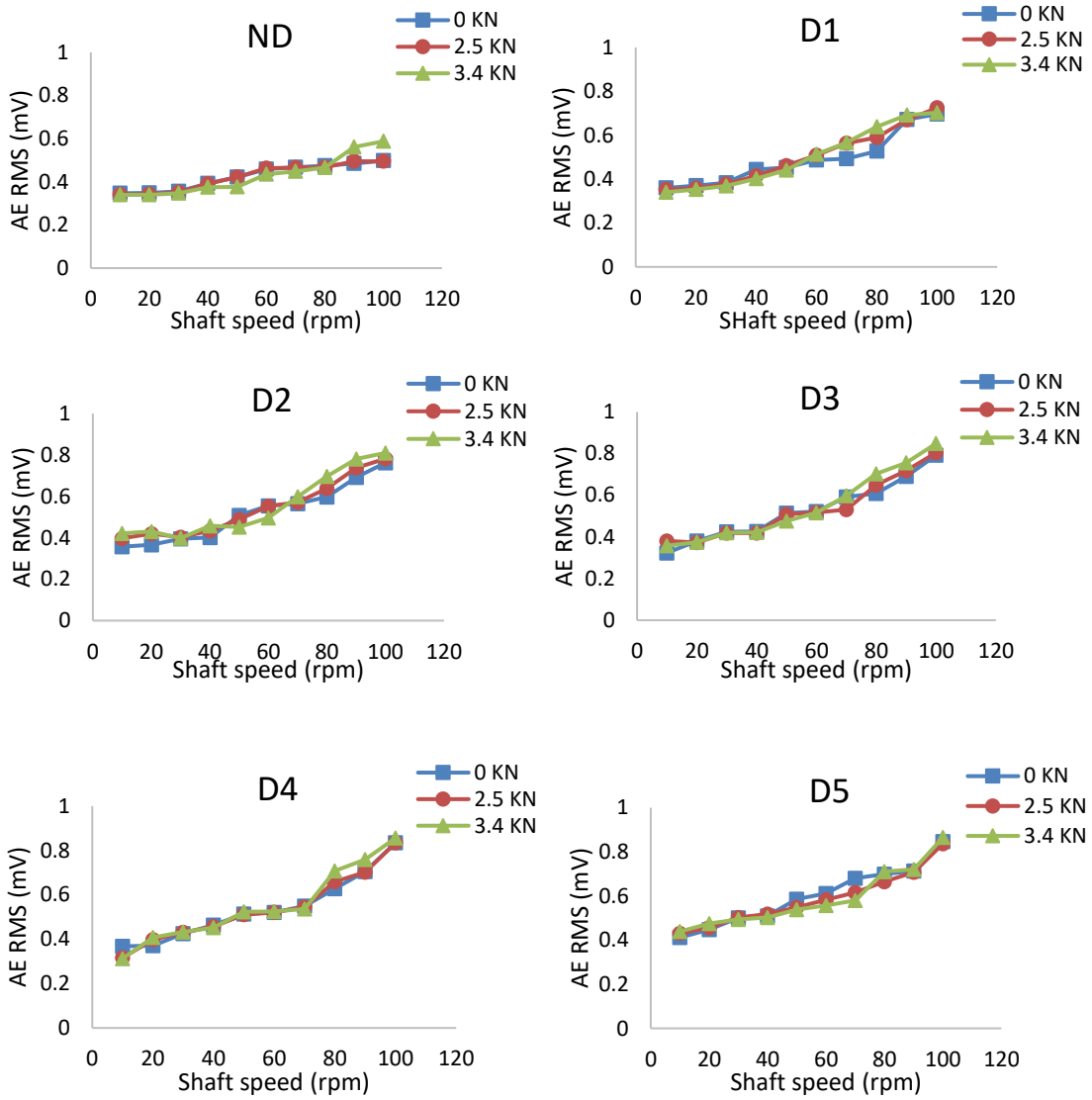

Figure 6.1: AE RMS as a function of shaft speed with three loads for a healthy bearing and five bearings with faults on the inner race

From Figure 6.1, for all test conditions, it is clear that the AE RMS value increases with increasing shaft rotational speed in all cases. However, it can state that the load has no obvious influence on the AE RMS which is in agreement with the finding of Section 5.2.

Figure 6.2 shows AE RMS for the normal condition (ND) bearing and bearings with five defects of varying size on the inner race at 80 rpm. The increase of the defect size started with a point defect (D1), followed by line defect (D2) and then the defect width and length (D3, D4, D5) were increased as done in Chapter 5 for

the outer race, see Table 4.1. The IR value of the AE RMS values for the five defective cases relative to that measured for ND is presented in Table 6.1.

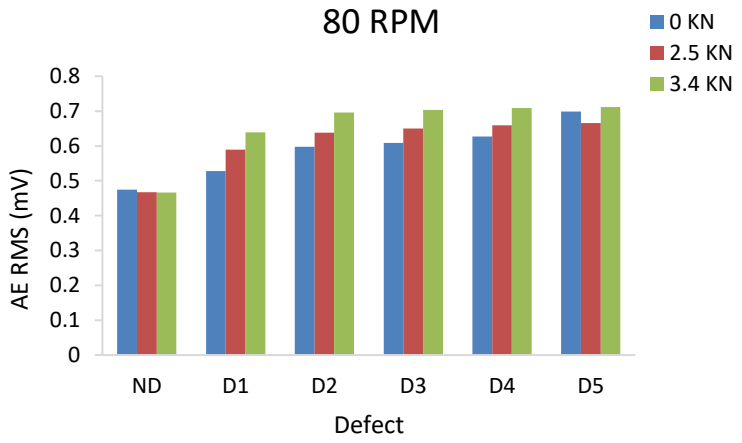

Figure 6.2: AE RMS for inner bearing race for healthy and five fault conditions, at 80 rpm for three loads

From Figure 6.2 it is seen that at 80 rpm for all defective cases, the AE RMS was higher than the value obtained for ND. The same observation found for the other test speeds as presented in Figure C.1 in Appendix C. It also appears from Figure 6.2 that at this speed the AE RMS level increased with a load for all the defective cases except for ND and D5. However, this observation does not hold true for the other low speeds tested, see Figure C.1. Hence, it can state that AE RMS does not have a clear trend with load varying.

Furthermore, Table 6.1 shows that, as the defect size increased, the IR for AE RMS increased but not uniformly as the increase in size when going from one fault to the next was not uniform. However, between D3 and D4 it did remain almost constant, probably because of the defect length, as mentioned previously in Section 5.2.

Table 6.1: RMS IR values for five bearings with five fault conditions at the inner race, at 80 rpm for three loads

Fault	Defect Dimensions (mm)	0 kN	2.5 kN	3.4 kN
D1	Dent (D = 0.5)	1.11	1.26	1.37
D2	2.5 X 0.9	1.26	1.36	1.49
D3	6.0 X 0.9	1.28	1.39	1.51
D4	6.0 X 3.0	1.32	1.41	1.52
D5	12.0 X 6.0	1.47	1.42	1.53

To summarise the RMS outcomes, there is a strong correlation between the shaft speed and AE RMS, which is entirely independent of the load. This statement supports the observations of [12] for inner race defects for bearings rotating in the moderate speed range. It is concluded that AE RMS is a good indicator of defect initiation and propagation of the inner race.

6.3 Kurtosis Observations

Figure 6.3 presents kurtosis values of AE signals under various conditions (speed and load) for a defect free bearing (ND) and five inner race defective bearings with increasing size of the defect.

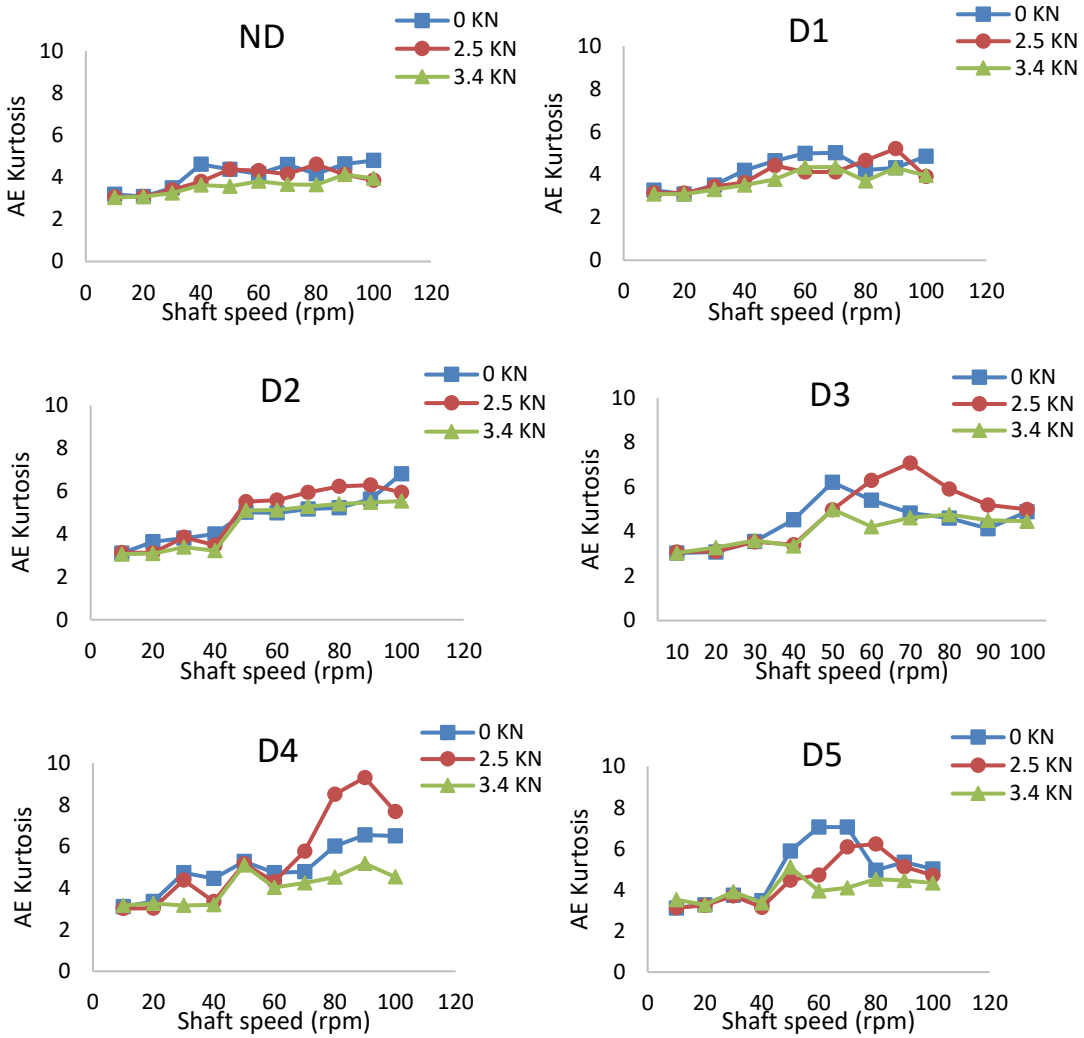

Figure 6.3: AE kurtosis as a function of shaft speed with three loads for a healthy bearing and five bearings with faults on the inner race

Figure 6.3 shows that AE kurtosis at both ND and D1 is close to 3 (or slightly higher due to the presence of some noise) which indicates the Gaussian nature of the signal captured. Also for ND and D1 bearing speed has little influence on the AE kurtosis, which is the same as found for all fault cases below about 30 rpm. Above 30 rpm there is an increase in the AE kurtosis indicating the presence of periodic pulses within the AE signal. However, with further increases in rotating speed, more and more periodic impulse are produced within the captured AE signal, and the AE kurtosis decreases as shown in D3 to D5.

Conversely, the load has little influence on the AE kurtosis for ND, D1, and D2. The same observation was correct for all the remaining cases for speeds lower

than 40 rpm. However, above 40 rpm, this behaviour changed for D3 and D4 the AE kurtosis increased with increasing load from zero to 2.5 kN and decreased again at 3.4 kN. The reverse observation was found for D5. Hence, AE kurtosis has no apparent trend with load, and thus, for inner race defects, AE kurtosis is not sensitive to load.

The kurtosis for the AE signals with defect size at 80 rpm and three loads are compared in Figure 6.4. The IR values of the AE and vibration kurtosis are presented in Table 6.2.

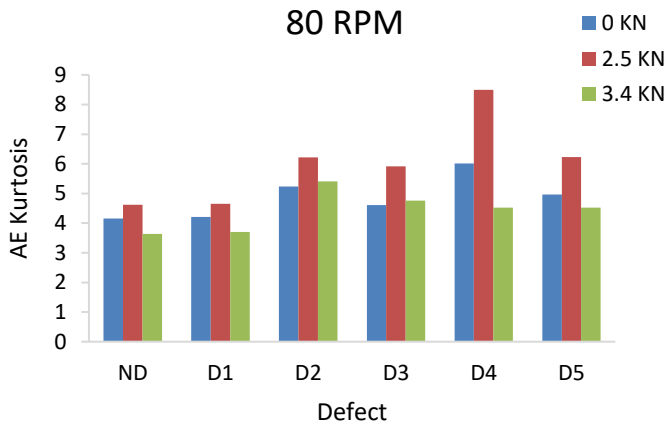

Figure 6.4: AE Kurtosis for inner bearing race for healthy and five fault conditions, at 80 rpm for three loads

It can be observed from Figure 6.4 and Table 6.2 that for D1 there is no obvious increase in the AE kurtosis with respect to the healthy case, and the value was close to 3 and 4 which indicated the Gaussian nature of the signal. Once the defect had grown to the size of D2, AE kurtosis increased significantly, indicating the existence of a defect. The AE kurtosis decreased again for D3 after which it generally increased at D4 followed by a reduction at D5.

Table 6.2: Kurtosis IR values for five bearings with five fault conditions at the inner race, at 80 rpm for three loads

Fault	Defect Dimensions (mm)	0 kN	2.5 kN	3.4 kN
D1	Dent (D = 0.5)	1.01	1.01	1.02
D2	2.5 X 0.9	1.26	1.35	1.48
D3	6.0 X 0.9	1.11	1.28	1.31
D4	6.0 X 3.0	1.45	1.84	1.24
D5	12.0 X 6.0	1.19	1.35	1.24

To summarise kurtosis outcomes of the bearing, there is no significant increase in AE kurtosis going from ND to D1, though once the defect reaches the size of D2, the AE kurtosis increases with increase in shaft rotational speed, regardless of the load. Thus, it can be stated that AE kurtosis is sensitive to the existence of a fault on the inner race once it reaches a specific size but not at the incipient stage.

6.4 Amplitude Observations

Figure 6.5 shows measured AE amplitude as a function of shaft speed with three loads for a healthy bearing and five bearings with faults on the inner race.

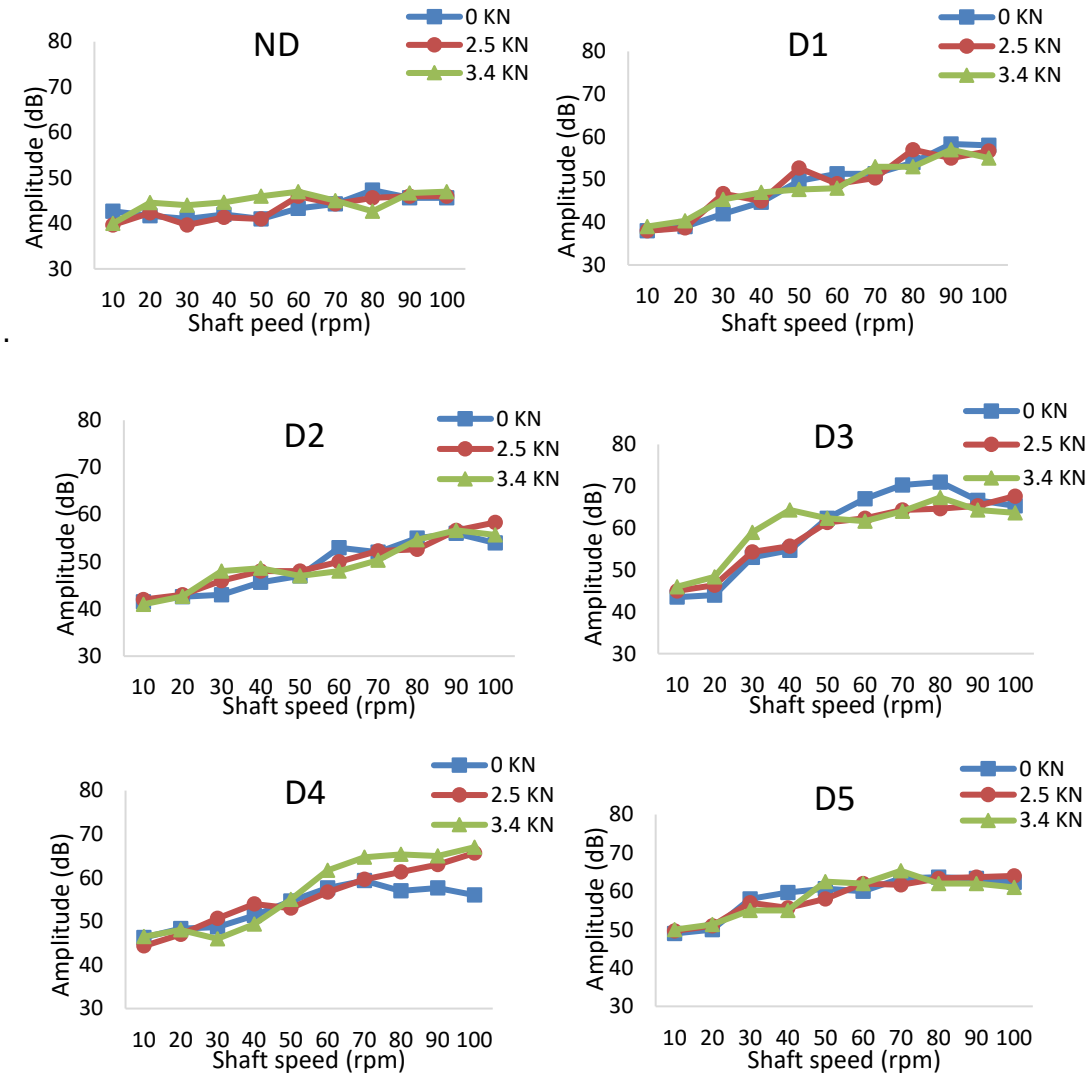

Figure 6.5: AE Amplitude as a function of shaft speed with three loads for a healthy bearing and five bearings with faults on the inner race

Figure 6.5, shows that for the ND, healthy bearing, the rotational speed has no significant influence on AE amplitude. However, once a defect was seeded into the inner race, the AE amplitude increased with increase in rotating speed.

Furthermore, Figure 6.5 shows that the load, has no significant influence on the AE amplitude, except in some conditions for D3 and D4 where there are slight differences. Thus, there is no reason to regard these as due to increasing load alone.

The influence of changing inner race defect size on AE amplitude is shown in Figure 6.6, and the incremental values are given in Table 6.3.

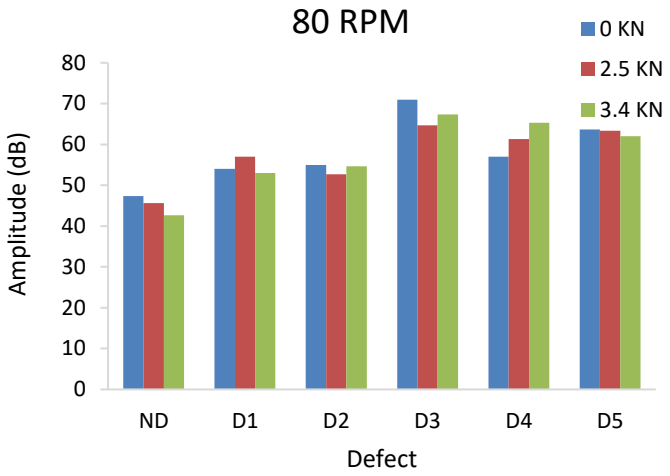

Figure 6.6: AE Amplitude at shaft speed of 80 rpm with three loads for a healthy bearing and five bearings with faults on the inner race

Table 6.3: AE amplitude IR values for five bearings with five fault conditions at the inner race, at 80 rpm for three loads

Fault	Defect Dimensions (mm)	0 kN	2.5 kN	3.4 kN
D1	Dent (D = 0.5)	1.14	1.25	1.24
D2	2.5 X 0.9	1.16	1.15	1.28
D3	6.0 X 0.9	1.50	1.42	1.58
D4	6.0 X 3.0	1.20	1.34	1.53
D5	12.0 X 6.0	1.35	1.39	1.45

From Figure 6.6 and Table 6.3, it is seen that the AE amplitude initially increases with the initiation of the defect and continues to increase with defect size till it reaches D3 after which it decreases and then reverts to increasing above that (save for D2 at 2.5 kN load). These results strongly suggest that the AE amplitude increases noticeably with the emergence of a defect in the inner race of the bearing but, that once a defect exists, AE amplitude could decrease with increase in defect size and so cannot be used to identify the extent of a defect. The same observations found for other low speeds as presented in Figure C.3 and Table C.3.

In summary, for the no defect case, the AE amplitude is not significantly influenced by either increase in shaft speed or load. However, once a defect exists in the bearing inner race, the AE amplitude increases with rotational speed, irrespective of the investigated load. Moreover, AE amplitude increased noticeably when the defect first emerges in the bearing inner race, but when the defect already exists, the AE amplitude is not sensitive to defect size. Thus, AE amplitude may be used to detect an incipient fault but not the size and extent of an established defect on the inner race.

6.5 AE Counts Observations

Figure 6.7 illustrates measured AE counts as a function of shaft speed with three loads for a healthy bearing and five bearings with faults on the inner race.

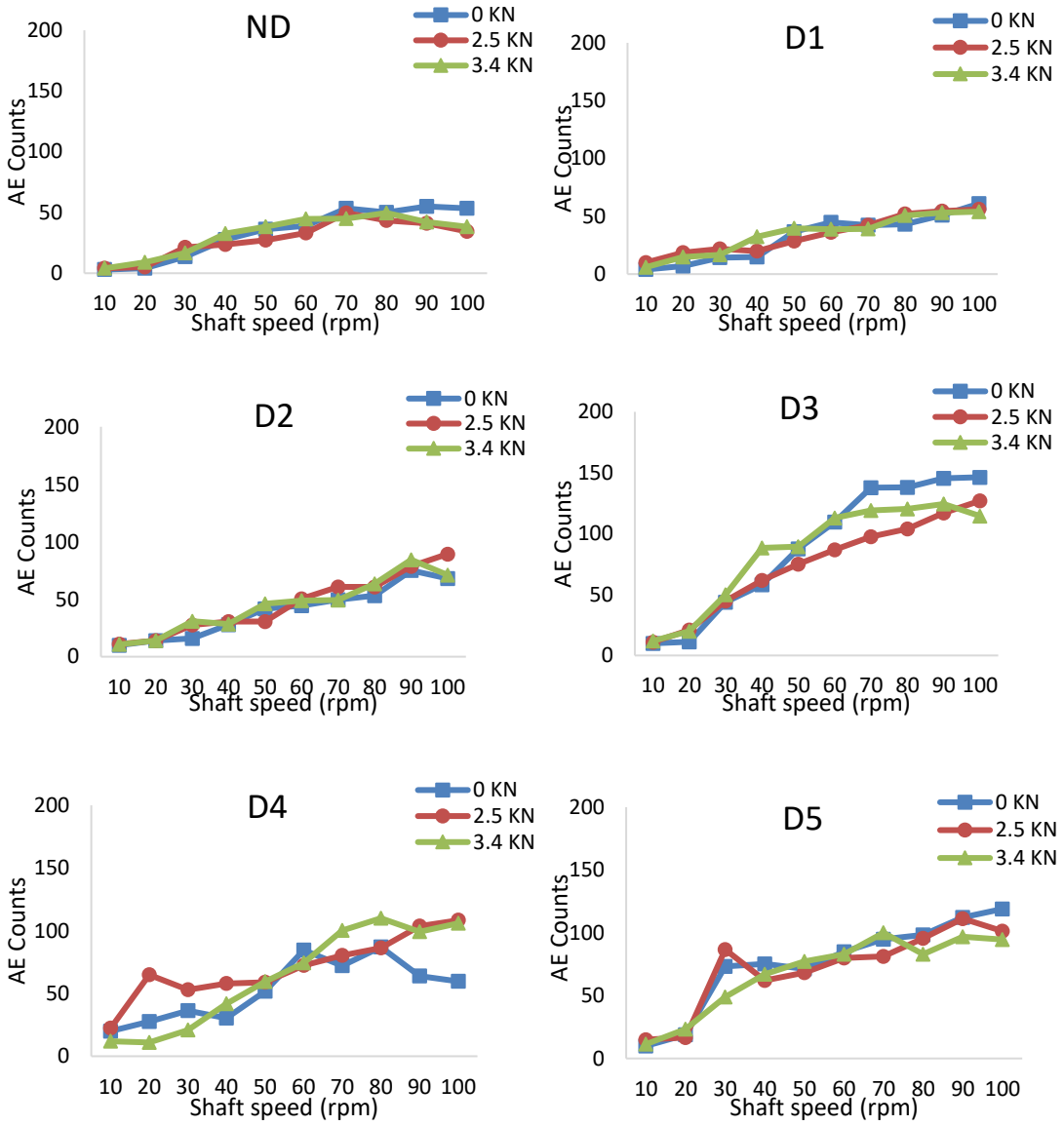

Figure 6.7: AE counts as a function of shaft speed with three loads for a healthy bearing and five bearings with faults on the inner race

From Figure 6.7 it can be seen that for ND, D1, and D2, the AE counts increased with increasing rotational speed. However, this increase was slightly less noticeable than for the other defective cases.

Furthermore, for plots ND, D1, and D2 there is no clearly discernible and consistent trend for AE counts against the load. Despite the apparently wide variety of AE counts with the load for D3, D4 and D5, no clear trend was discerned.

The influence of the inner race defect size on the AE counts is shown in Figure 6.8, for a shaft speed of 80 rpm. The corresponding IR values are listed in Table 6.4.

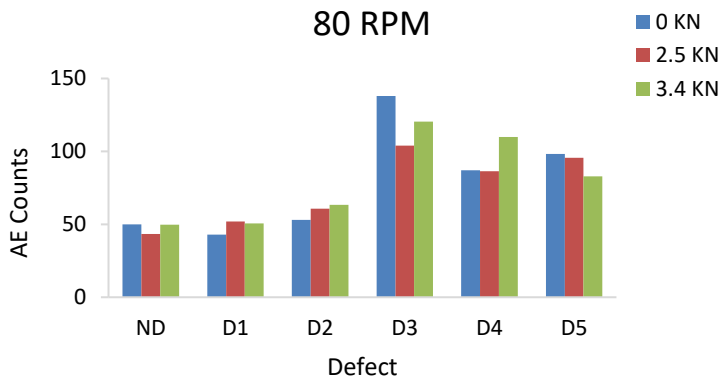

Figure 6.8: AE counts AE counts at shaft speed of 80 rpm with three loads for a healthy bearing and five bearings with faults on the inner race

Table 6.4: AE counts IR value at shaft speed of 80 rpm with three loads for five bearings with several fault conditions on the inner race

Fault	Defect Dimensions (mm)	0 kN	2.5 kN	3.4 kN
D1	Dent (D = 0.5)	0.99	1.07	1.02
D2	2.5 X 0.9	1.06	1.53	1.28
D3	6.0 X 0.9	2.76	2.40	2.42
D4	6.0 X 3.0	1.74	1.99	2.21
D5	12.0 X 6.0	1.97	2.21	1.67

From Figure 6.8 and Table 6.4, it is noted that the AE counts do not differ sufficiently from ND to capture defect initiation in the inner race until it reaches the size of the D2 fault when the AE count increases significantly for loads of 2.5 and 3.4 kN. It then increased further as the defect raised to D3, after which it fell back and then increased. These observations also hold true for the other tested speeds as presented in Appendix C.

In summary, the AE counts increased with shaft speed for ND and all defects. However, only for defects of the size of D2, or bigger, were the AE counts substantially influenced by the rotation speed. Thus, it can be stated that AE counts were susceptible to the existence of the defect when the defect reached the D2 size but not for D1, which represents fault initiation. Therefore, it can conclude that AE counts was not sufficiently sensitive or consistent to defect initiation and propagation at the inner race. This could be linked to the signal attenuation as it travels from the inner race to the AE sensor. Besides, for all cases, AE count was not sensitive to changes in the load applied to the bearing.

6.6 Closing Remark

This chapter assessed the applicability of AE techniques to monitor defect initiation and propagation on the inner race of a bearing rotating at low speeds. Table 6.5 presents the findings that AE measurement can detect a fault when it first emerges, but there are limitations on the sensitivity to the fault size.

Table 6.5: Summary of AE parameter sensitivity to various conditions at inner race of a low-speed bearing

Condition	RMS	Kurtosis	Amplitude	Counts
Speed ↑	↑(greatly)	↑(when defect propagated to D2) then ↓	↑(when defect exists)	↑ (greatly)
Load ↑	-	-	-	-
Defect size ↑	↑(slightly)	↑ (when defect propagated to D2) then ↓	↑(when defect emerges) then ↓	↑(when defect propagated to D2) then ↓

For faults on the inner race, the shaft rotational speed has a strong influence on the listed AE parameters. However, they are entirely independent of the load. Moreover, while AE kurtosis and counts cannot detect the existence of an inner race fault in its early stages, AE amplitude and RMS can detect the inner race faults at early stages. However, once established only AE RMS is sensitive to defect size.

The next chapter will compare the sensitivity of the AE parameters for monitoring the conditions of the outer and inner races of low speed bearings.

Chapter Seven

7 Outer and Inner Race Comparison

7.1 Introduction

Chapters 5 and 6 have demonstrated the ability of AE to monitor the condition of bearings rotating at low speeds. This chapter compares the outcomes reported from Chapters 5 and 6 to find the most suitable technique to monitor both races simultaneously. Furthermore, because Chapters 5 and 6 showed that the statistical parameters used were not sensitive to the load, this chapter will only compare:

1. The influence of speed on the statistical parameters for low speeds (10-100 rpm).
2. The sensitivity of the statistical parameters to detect defect initiation and propagation (i.e. defect size).

This chapter confirms that AE measures are suitable for the CM of both outer and inner races of bearing rotates at low speeds.

7.2 RMS Observations

Figure 7.1 shows the AE RMS values for three identical bearings; one healthy, the second with the D1 fault (which represents fault initiation) seeded on the inner race, and the third bearing with the D1 fault seeded on the outer race. AE RMS values as a function of speed for speeds in the range 10 to 100 rpm and a load of 3.4 kN and the other tested loads shown in Appendix D.

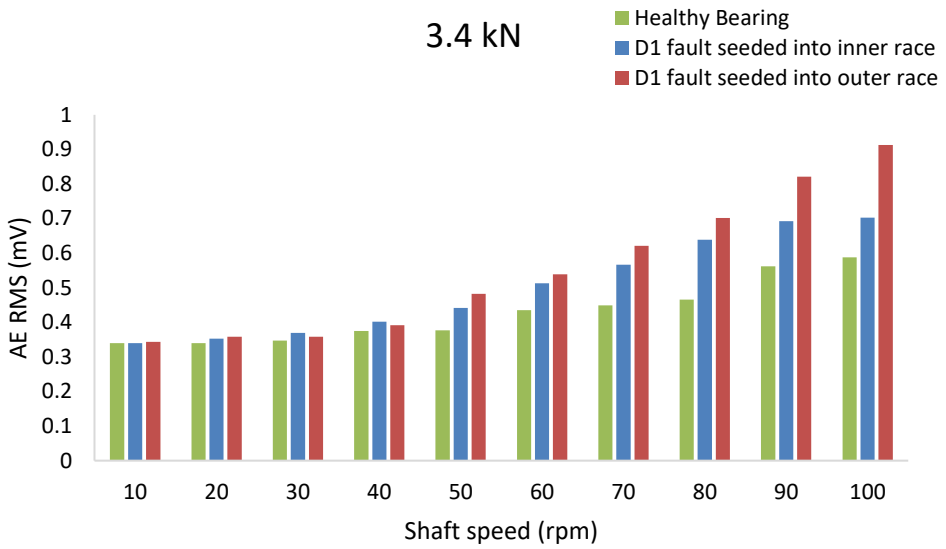

Figure 7.1: Comparison of AE RMS as a function of shaft speed at 3.4 kN load, for a healthy bearing and two bearings with D1 fault on the inner and outer races

Figure 7.1 shows that for all running speeds the AE RMS for the defective bearings is greater than for the healthy bearing. Also, the AE RMS for the outer race defect is higher than for the inner race defect. This is attributed to the shorter transmission path of the AE signal from the outer race to the AE sensor, and less signal interference.

For all cases, the AE RMS increased with the increase in shaft speed which confirmed the sensitivity of the AE RMS to the speed variation.

The consequence of changing defect size on inner and outer races on the AE RMS, for a shaft speed of 80 rpm and load 3.4 kN, is shown in Figure 7.2 and listed in Table 7.1 for the three load conditions.

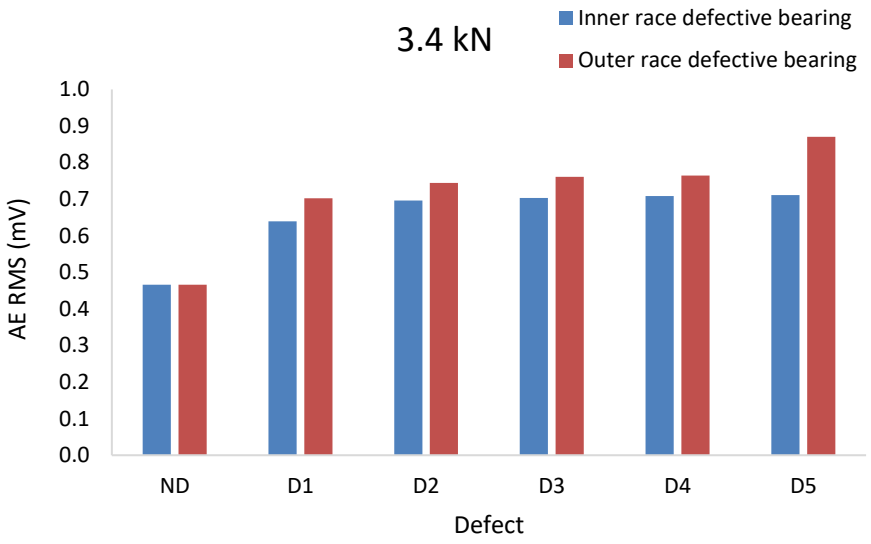

Figure 7.2: AE RMS for six inner and outer races bearing conditions, at 80 rpm and 3.4 kN load

It can be observed from Figure 7.2 and Table 7.1 that for both defective bearings, the AE RMS increased as the defect is grown. However, the incremental increase was more evident for the defect in the outer race. These observations also hold true for the other loads tested, see Appendix D.

Table 7.1: AE RMS value for five fault conditions at both inner and outer races, at 80 rpm and for three loads

Fault	Defect Dimensions (mm)	Inner Race			Outer Race		
		0 kN	2.5 kN	3.4 kN	0 kN	2.5 kN	3.4 kN
D1	Dent (D = 0.5)	0.474	0.468	0.466	0.474	0.468	0.466
D2	2.5 X 0.9	0.528	0.589	0.639	0.592	0.650	0.702
D3	6.0 X 0.9	0.598	0.638	0.696	0.608	0.663	0.745
D4	6.0 X 3.0	0.609	0.650	0.703	0.689	0.714	0.761
D5	12.0 X 6.0	0.627	0.659	0.708	0.691	0.723	0.765

Thus, AE RMS is a suitable parameter for monitoring the faults on both inner and outer races of a bearing rotating at low speed, but that the AE RMS for the outer race may be more reliable than for the inner race due to the lower attenuation of the signal.

7.3 Kurtosis Observations

Figure 7.3 shows the AE kurtosis values for three identical bearings; one healthy bearing, the second bearing with the D1 fault seeded on the inner race, and the third bearing with the D1 fault seeded on the outer race. These kurtosis values are presented as a function of speed for speeds in the range 10 to 100 rpm and a load of 3.4 kN, other loads are shown in Figures D.5 and D.6.

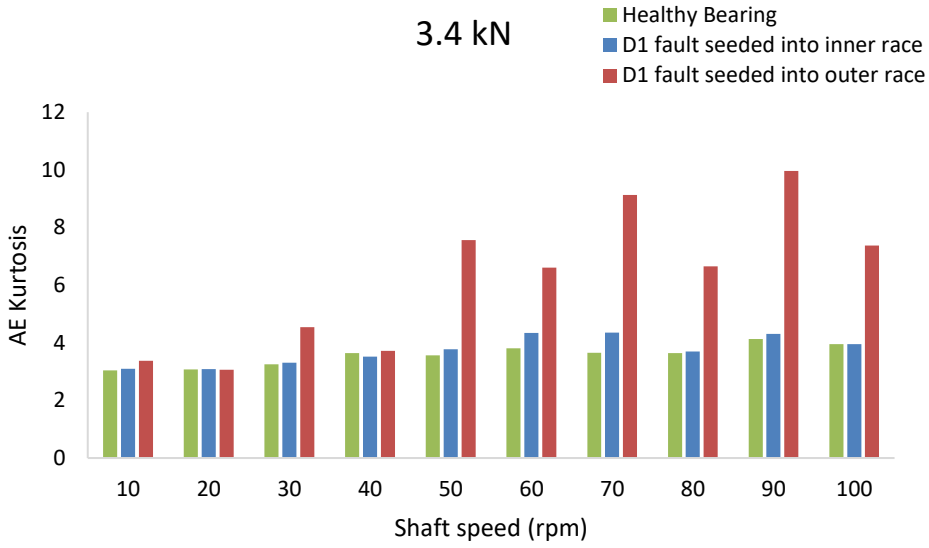

Figure 7.3: Comparison of AE kurtosis as a function of shaft speed at 3.4 kN load, for a healthy bearing and two bearings with D1 fault on the inner and outer races

From Figure 7.3, for the outer race defective bearing, the AE kurtosis increases with rotational speed over the range of speeds tested. However, it can be seen that with an increase in shaft rotational speed above about 80/90 rpm the AE kurtosis starts to decrease. This latter phenomenon was likely due to the transferring the system from one normal distribution to another normal distribution as discussed in Section 5.3. For the inner race defective bearing, the AE kurtosis remained close to the healthy bearing values. Thus, it can be said that generally

for the outer race, AE kurtosis was obviously influenced by the rotational speed from 30 rpm, while not for the inner race case at D1.

Figure 7.4 shows the sensitivity of the AE kurtosis with an increase in defect size at both inner and outer races for shaft speed of 80 rpm and a load of 3.4 kN.

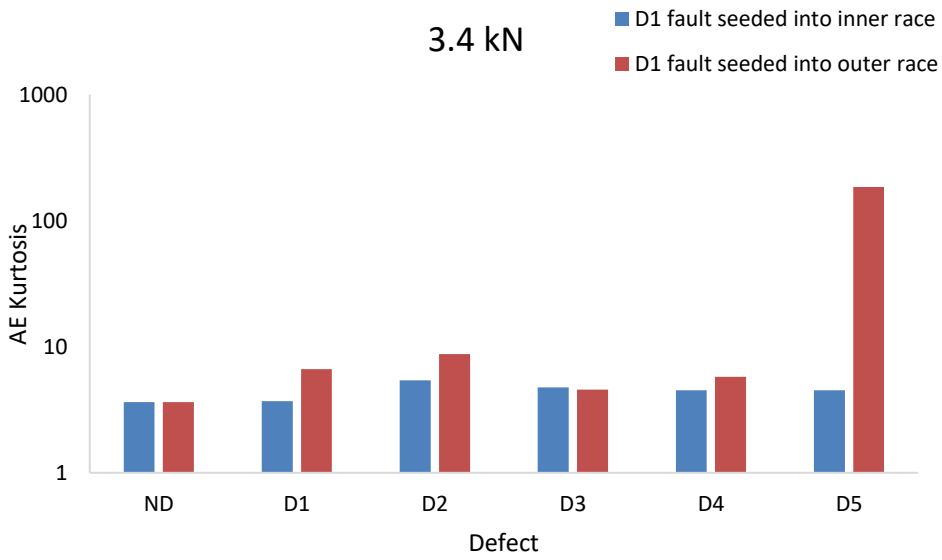

Figure 7.4: AE kurtosis for six inner and outer races bearing conditions, at 80 rpm and 3.4 kN load

Figure 7.4, shows that AE kurtosis was able to detect the defect on the outer race at the early stage (D1), but did not detect the defect on the inner race until it reached the stage of D2. The histogram is fully consistent with the argument that AE kurtosis increases in the early stages of a fault, but as the defect developed it became less sensitive, decreases then increased again. The same observations found for the other loads as presented in Figures E.7 and E.8.

7.4 Amplitude Observations

Figure 7.5 shows the AE amplitude as a function of shaft speed for three bearings; healthy bearing, bearing with the D1 fault on the inner race, and bearing with the D1 fault on the outer race. These amplitude values are for speeds in the range 10 to 100 rpm and a load of 3.4 kN.

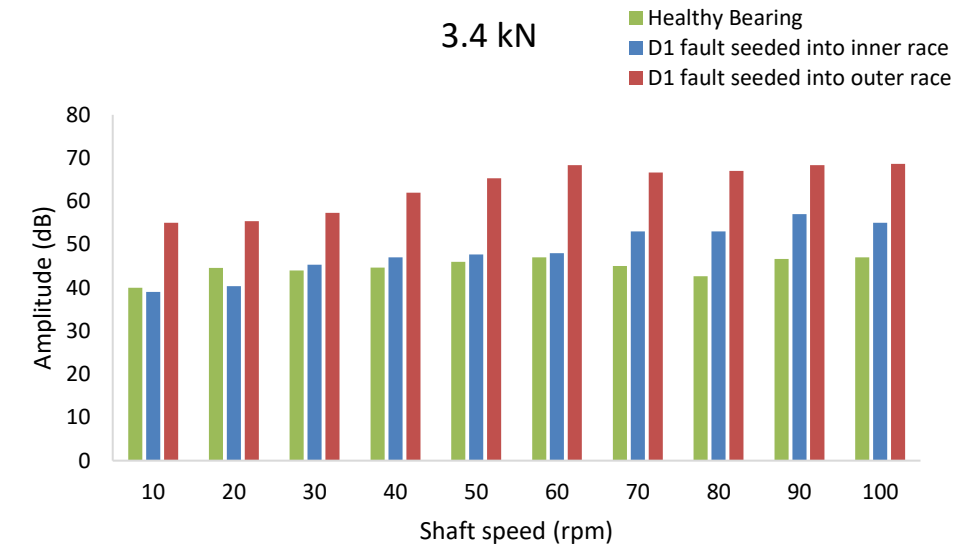

.

Figure 7.5: Comparison of AE amplitude as a function of shaft speed at 3.4 kN load, for a healthy bearing and two bearings with D1 fault on the inner and outer races

Figure 7.5 clearly shows the differences in the AE amplitude between the two defective bearings and the healthy bearing. Furthermore, the variation in the AE amplitude between the two faulty bearings at each speed is noticeable and is believed to be due to attenuation, as described above. Also, it is evident that rotational speed has a strong influence on the AE amplitude for both defective bearings, while for the healthy bearing, the rotational speed has no significant influence on AE amplitude.These observations also hold true for the other loads tested as shown in Appendix D.

The consequence of changing defect size on inner and outer races on the AE amplitude, for a shaft speed of 80 rpm and load 3.4 kN, is shown in Figure 7.6.

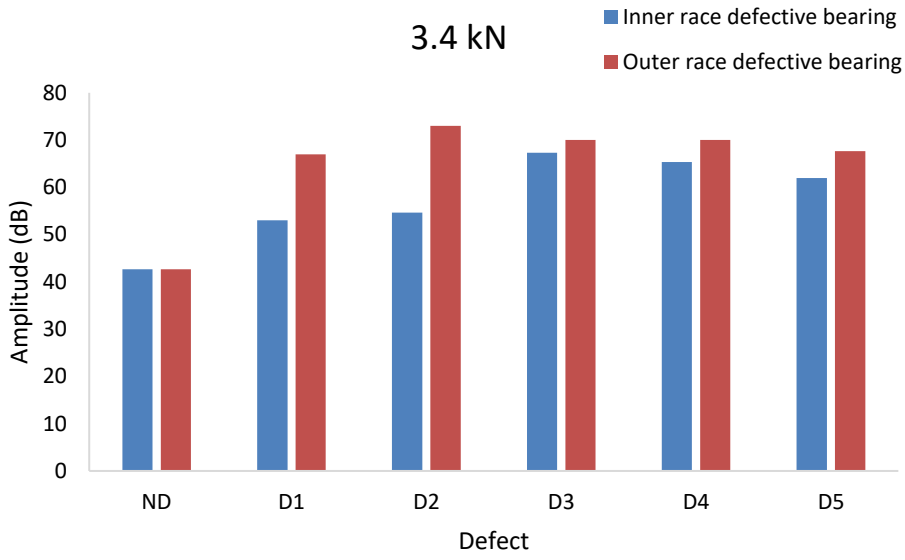

Figure 7.6: AE amplitude for six inner and outer races bearing conditions, at 80 rpm and 3.4 kN load

As it indicated in Figure 7.6 that the AE amplitude increased significantly for both bearings at fault D1, which shows the applicability of AE amplitude to detect defect initiation at both races. For both bearings, AE amplitude increased with defect size to a maximum and then decreased. However, for the other tested loads, as the defect developed, AE amplitude gives a fluctuating response as shown in Figures E.11 and E.12. Hence, this parameter not consistently influenced by the defect sizes for either race.

7.5 AE Counts Observations

Figure 7.7 shows the AE counts for three identical bearings; healthy bearing, bearing with the D1 fault seeded on the inner race, and bearing with the D1 fault seeded on the outer race. These AE counts are presented as a function of speed for the range 10 to 100 rpm and a load of 3.4 kN.

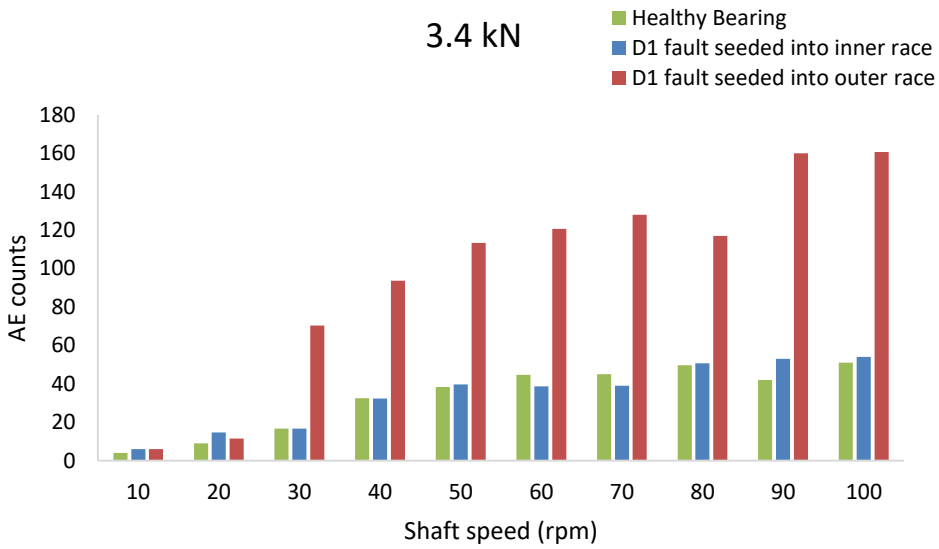

Figure 7.7: Comparison of AE counts as a function of shaft speed at 3.4 kN load, for a healthy bearing and two bearings with D1 fault on the inner and outer races

Figure 7.7 shows a higher number of AE counts for the outer race defective bearing than the other two bearings at all speeds. However, for the healthy and inner race defective bearing, the number of AE counts were relatively close to each other. Furthermore, from Figure 7.7 it can observe that for the three bearings, the AE count was significantly influenced by the rotational speed. Thus, it is concluded that the AE count is sensitive to the speed variations.

The consequence of changing defect size on inner and outer races on the AE counts, for a shaft speed of 80 rpm and load 3.4 kN, is shown in Figure 7.8 and for the other loads in Appendix D.

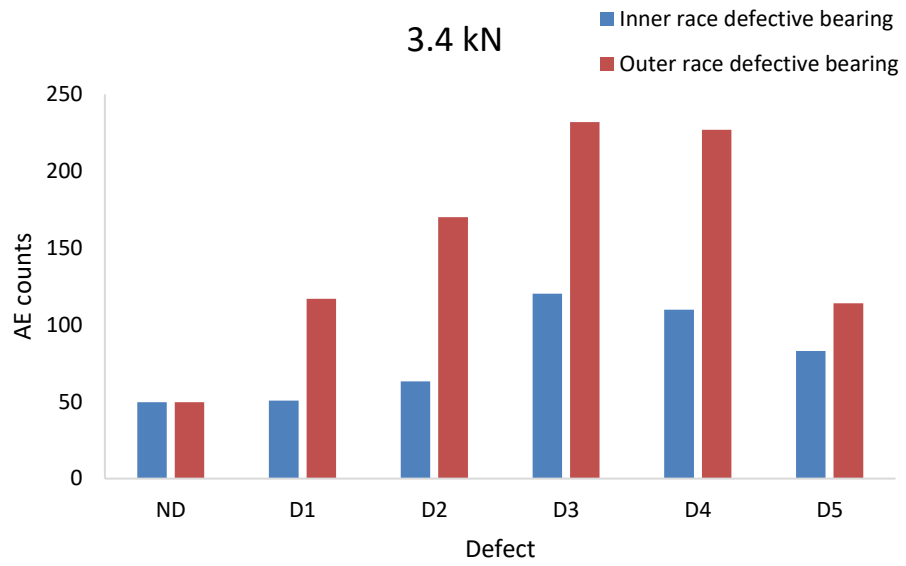

Figure 7.8: AE counts for six inner and outer races bearing conditions, at 80 rpm and 3.4 kN load

From Figure 7.8 it can be seen that, at 80 rpm, the number of AE counts for D1 in the outer race is significantly different from the value for ND, and the AE counts increased with the defect size from D1 to D3, after which the AE count decreased. However, the number of AE counts for D1 in the inner race is close to the value of ND, then increases from D2 to D3 before decreasing again. The AE counts produced by the inner race defective bearing, when tested for other loads, did not produce a consistent response; it first decreased and then increased with increase in defect size, see Figures E.15 and E.16. Again it is noted, for all defect cases, the AE counts at the outer race was greater than the inner race due to signal attenuation.

It is concluded that AE counts is a suitable parameter for the detection of incipient faults in the outer race, but not in the case of the inner race as it detects the defect only once it has reached the stage of D2.

7.6 Closing Remark

It can be concluded that statistical measures of the AE signal are able to monitor both inner and outer races of a bearing rotating at low speeds. Furthermore, the rotational speed has a strong influence on the AE parameters. Once the defect

has been initiated, only AE RMS is sensitive to defect size for both races. Possibly more important, the AE parameters successfully detected faults on the outer race at the incipient stage, but only AE RMS and AE Amplitude did so with the inner race. Table 7.2 sums up the conclusions of this chapter.

Table 7.2: Summary of the AE parameter sensitivity to the incipient fault and fault size

	SENSITIVITY TO THE INCIPIENT FAULT	SENSITIVITY TO THE FAULT SIZE
AE RMS INNER	YES	YES
AE RMS OUTER	YES	YES
KURTOSIS INNER	NO (Until it reaches D2)	NO
KURTOSIS OUTER	YES	NO
AMPLITUDE INNER	YES	NO
AMPLITUDE OUTER	YES	NO
AE COUNTS INNER	NO (Until it reaches D2)	NO
AE COUNTS OUTER	YES	NO

Next chapter will examine the applicability of the measured AE parameters to detect the defect at different locations on the outer race of bearing rotates at low speeds.

Chapter Eight

8 Comparison of Defect Location and size

8.1 Introduction

This chapter investigates the applicability of AE measurements to detect and monitor defects located at different locations on the outer race of low-speed bearings and to compare the sensitivity of the AE parameters to speed and load variation at these locations.

Another key issue in bearing diagnostics is to be able to monitor bearing deterioration. Here this was achieved by increasing the size of the seeded faults in a uniform manner.

This chapter presents the results of the final programme described in Section 4.3 for a healthy bearing (ND) and eight defective bearings with faults D6 to D13, as described in Table 4.1 and shown in Figure 4.18, seeded into the outer race.

The results demonstrate the usefulness of AE in monitoring faults at any location, in the sense of the fault being in the middle or at the edge of the bearing's outer race. Furthermore, it shows the sensitivity of the AE RMS to defect size, which the other measures were not.

8.2 Defect Location Comparison

This section reports the experimental monitoring of the condition of three bearings. These bearings are one healthy bearing and two bearings each with a seeded defect of size 6x3 mm, one with the defect in the centre (D4) and the other with the defect on the edge (D12) of the outer race, as shown in Figures 4.17 and 4.19 (b).

8.2.1 RMS Observations

The RMS values of the AE signal under various speeds at zero applied load, and for speeds in the range, 30 to 100 rpm are shown in Figure 8.1. These values are for a healthy and two defective bearings each with a seeded defect on the outer

race; one in the centre (D4) and the other at the edge (D12), as described in Section 4.3.

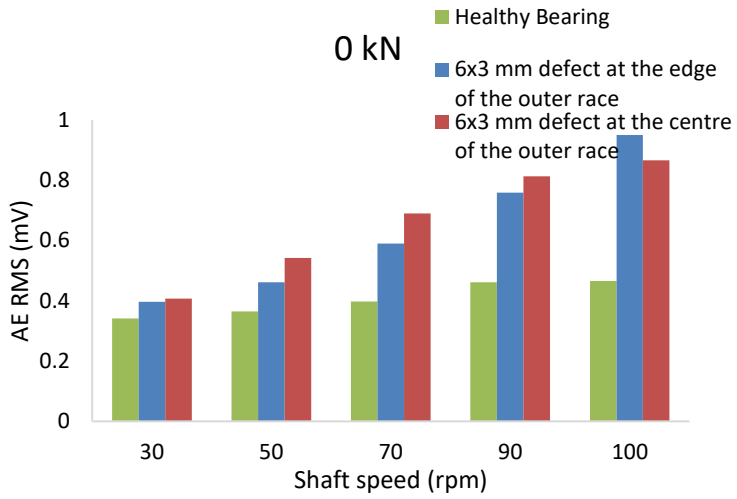

Figure 8.1: AE RMS as a function of shaft speed at zero applied load, for healthy and two defective bearings (D4 and D12)

Figure 8.1 shows that for all running speeds the AE RMS for all bearings increases with increasing rotational speed. However, for the healthy bearing, the increment in the AE RMS was lower than the other bearings. Also, the AE RMS level of the bearing with the D4 fault (seeded at its centre) is greater than for the D12 fault (seeded at the edge), save at 100 rpm. This is attributed to the transmission path of the AE signal being greater for the D12 defect. Hence the attenuation will be greater. The same trends were found in tests performed under 2.5 kN and 3.4 kN loads, see Figures F.1 and F.2.

Figure 8.2 shows the AE RMS values for the three bearings at 90 rpm, for three load conditions. The incremental value of each defective condition related to the ND was calculated using Equation (5.1) and is listed in Table 8.1.

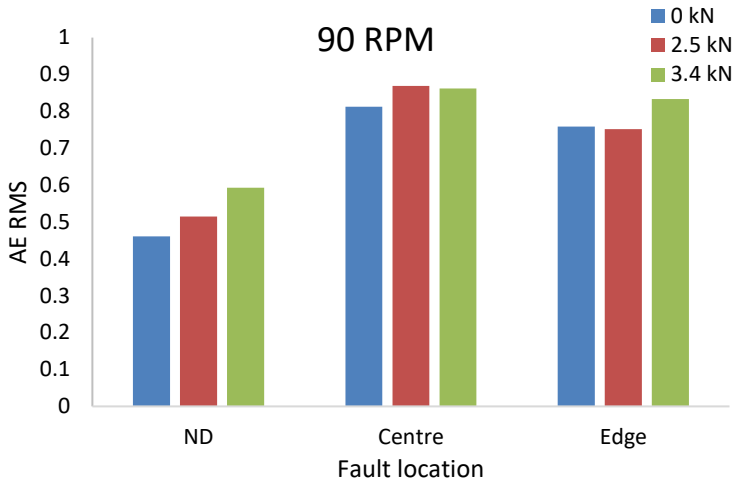

Figure 8.2: AE RMS for a healthy bearing and two defective bearings (D4 and D12), at 90 rpm under three loads

Table 8.1: AE RMS IR value for two defective bearings (D4 and D12), for three loads

Speed (rpm)	D4 Fault (at the centre)			D12 Fault (at the edge)		
	0 kN	2.5 kN	3.4 kN	0 kN	2.5 kN	3.4 kN
30	1.19	1.17	1.19	1.16	1.15	1.14
50	1.48	1.29	1.29	1.26	1.23	1.25
70	1.74	1.46	1.36	1.49	1.24	1.32
90	1.76	1.69	1.45	1.65	1.46	1.41
100	1.86	1.71	1.44	2.04	1.81	1.53

From Figure 8.2 and Table 8.1, it is noticeable that for all conditions, the AE RMS value for both defective bearings was greater than for the healthy bearing. Hence, it can be stated that AE RMS is able to detect the presence of a $6X3\ mm^2$ defect at both locations, which confirms the applicability of this parameter to monitor the bearing condition.

On the other hand, it is observable from Table 8.1 that load variation does not provide any obvious trend on the RMS which confirmed the conclusion in Section 5.2.

8.2.2 Kurtosis Observations

Figure 8.3 shows the kurtosis values for a healthy bearing and two bearings with faults D4 and D12 as a function of speed for speeds in the range 30 to 100 rpm, under zero applied load. The corresponding results obtained for loads of 2.5 kN and 3.4 kN are presented in Appendix F.

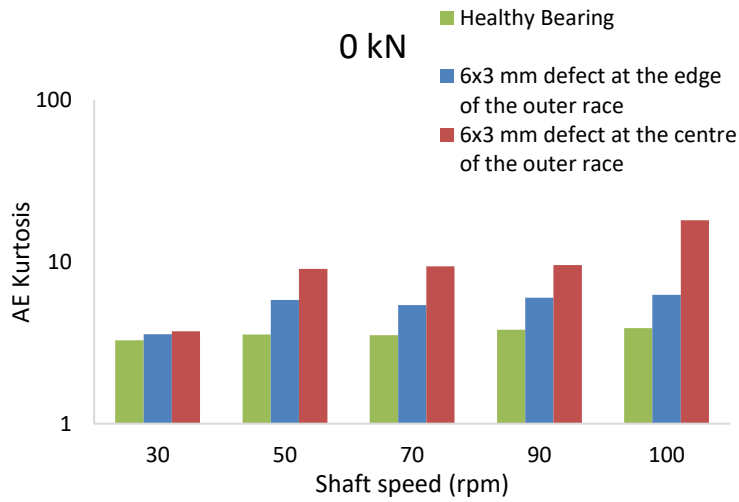

Figure 8.3: AE kurtosis as a function of shaft speed at zero applied load, for a healthy and two defective bearings (D4 and D12)

For both defective bearings, the AE kurtosis increased as the rotating speed increased (save for D4 at 70 rpm), see Figure 8.3, which confirms the outcomes of Section 5.3. Furthermore, for all speeds, the AE kurtosis for the fault at the centre of the outer race had the highest value. This observation also holds true for the other tested loads tested, see Figures F.3 and F.4.

Figure 8.4 shows the ability of the AE kurtosis to defect existence of a fault at both locations (centre and edge of the outer race) by comparing them with a healthy bearing at a shaft speed of 90 rpm for three load conditions. Furthermore, the IR value of each defected bearing related to the healthy bearing was calculated using Equation (5.1) and is listed in Table 8.2.

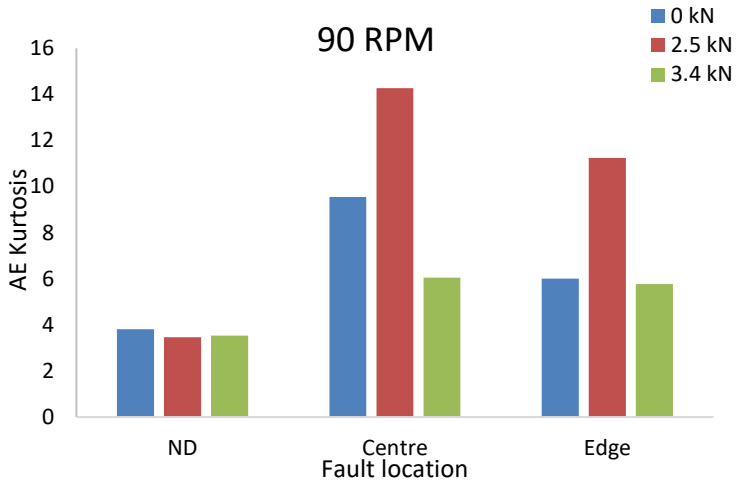

Figure 8.4: AE kurtosis for a healthy bearing and two defective bearings (D4 and D12), at 90 rpm under three loads

Table 8.2: AE kurtosis IR value for two defective bearings (D4 and D12), for three loads

Speed (rpm)	D4 Fault (at the centre)			D12 Fault (at the edge)		
	0 kN	2.5 kN	3.4 kN	0 kN	2.5 kN	3.4 kN
30	1.14	1.20	1.10	1.09	1.04	1.15
50	2.54	2.06	1.57	1.63	1.31	1.28
70	2.67	1.91	1.68	1.54	1.45	1.25
90	2.51	4.13	1.71	1.57	3.25	1.63
100	4.66	18.32	1.92	1.61	3.56	1.92

From Figure 8.4 and Table 8.2, it is shown, for all load conditions, the AE kurtosis for the defective bearings was higher than in ND case, which indicated the existence of the D4 and D12 defects. However, the AE kurtosis value for the D4

bearing defect at the centre of the outer race was greater than for the D12 bearing at all conditions.

From Table 8.2, it is clear that load variation did effect the kurtosis, but no clear trends were discernible. For the D4 fault, the IR fell when increasing the load for the speeds 50 and 70 rpm, but increased for the three speeds 30, 90, and 100 rpm at 2.5 kN, and decreased again in 3.4 kN. For the D12 fault, the same variation was observed.

In summary: it can be stated that AE kurtosis is able to detect the presence of a defect at both locations, which confirms the applicability of this parameter to detect defects at any locations within the outer race. Furthermore, as confirmation of the earlier conclusion in Chapters 5 and 6, AE kurtosis is strongly related to rotational speed but is independent of load.

8.2.3 Amplitude Observations

Figure 8.5 illustrates the measured AE amplitude as a function of shaft speed with zero applied load for a healthy and two defective bearings D4 (at the centre of the outer race) and D12 (at the edge).

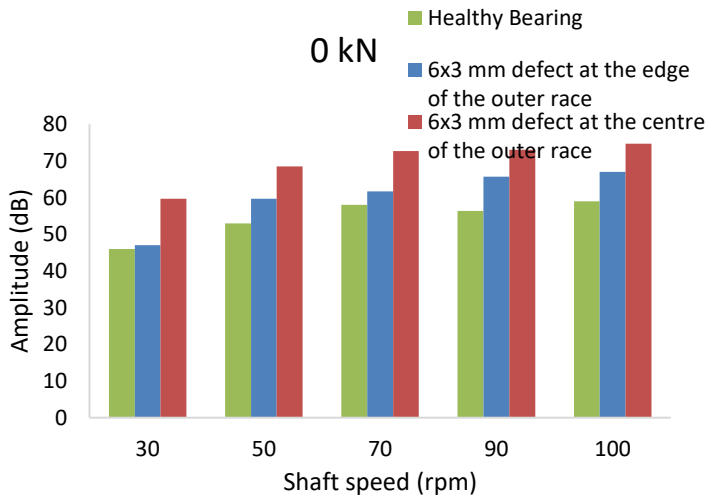

Figure 8.5: AE Amplitude as a function of shaft speed at zero applied load, for a healthy and two defective bearings (D4 and D12)

From Figure 8.5, it is noticeable that for all bearings the AE amplitude increased as the rotational speed increased, while the incremental increase for the healthy bearing was less than the defective bearings, and this shows agreement with the results reported in Section 5.4. This assessment also holds true for the other loads tested, see Appendix E.

Figure 8.6 shows the maximum amplitude values for the three bearings at 90 rpm for three load conditions and the IR value listed in Table 8.3.

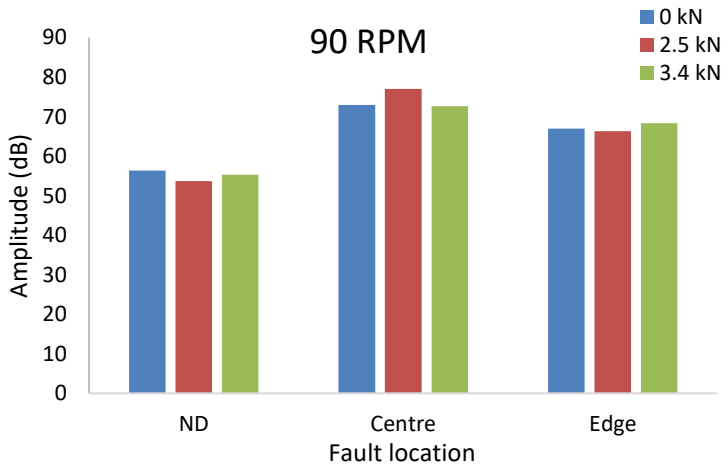

Figure 8.6: AE Amplitude for a healthy bearing and two defective bearings (D4 and D12), at 90 rpm under three loads

Table 8.3: AE amplitude IR value for two defective bearings (D4 and D12), for three loads

Speed (rpm)	D4 Fault (at the centre)			D12 Fault (at the edge)		
	0 kN	2.5 kN	3.4 kN	0 kN	2.5 kN	3.4 kN
30	1.30	1.44	1.22	1.02	1.03	1.01
50	1.29	1.52	1.22	1.13	1.16	1.13
70	1.25	1.38	1.29	1.06	1.11	1.13
90	1.30	1.43	1.31	1.17	1.24	1.23
100	1.27	1.43	1.32	1.14	1.26	1.21

From Figure 8.6 and Table 8.3, it is clear that the amplitude for both defective bearings was greater than for the healthy bearing, which is an indicator of the existence of a defect. This was the case for all the load conditions. Furthermore, it is shown that at 90 rpm the amplitude for the bearing with a seeded defect at the centre of the outer race (D4) is higher than for the D12 defect. This is attributed to the transmission path of the AE signal being greater for the D12 defect, hence it has lower amplitude due to the attenuation.

On the other hand, from Table 8.3, it can observe that the AE amplitude increased as the load increased from zero loads to 2.5 kN. However, it decreased again in 3.4 kN. This again agreed with the finding of the previous chapters regards the non-sensitivity of the amplitude to the load variation at low speeds.

8.2.4 AE Counts Observations

The number of counts for the AE signals under various speeds at zero applied load is shown in Figure 8.7 for a healthy bearing and two bearings seeded with the same size fault; one in the centre (D4) and the other at the edge (D12) of the outer race.

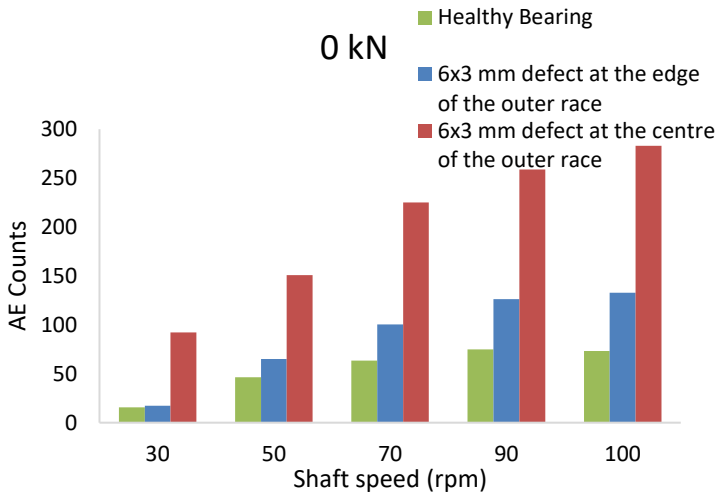

Figure 8.7: AE counts as a function of shaft speed at zero applied load, for a healthy and two defective bearings (D4 and D12)

Figure 8.7 clearly shows the differences in the AE counts between a healthy and two defective bearings for all speeds used. Moreover, it is obviously shown that

the bearing with a defect at the centre (D4) of the outer race has a higher value than the other. This difference is ascribed to the attenuation suffered by the signal generated by the D12 fault. However, for all bearings, the number of AE counts increased with increase in rotational speed which also confirms the outcomes reported in Section 5.5.

Figure 8.8 shows the ability of AE counts to detect the fault at either middle or edge of the outer race, at a shaft speed of 90 rpm and under three load conditions. The IR value for each defective bearing was calculated using Equation (5.1) and listed in Table 8.4.

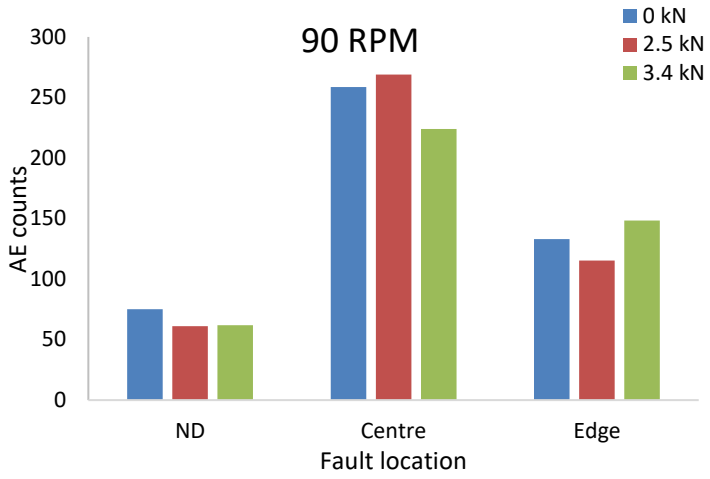

Figure 8.8: AE counts for a healthy bearing and two defective bearings (D4 and D12), at 90 rpm under three loads

Table 8.4: AE counts IR value for two defective bearings (D4 and D12), for three loads

Speed (rpm)	D4 Fault (at the centre)			D12 Fault (at the edge)		
	0 kN	2.5 kN	3.4 kN	0 kN	2.5 kN	3.4 kN
30	5.89	6.59	2.65	1.11	0.96	1.34
50	3.26	5.78	2.89	1.40	2.26	1.73
70	3.55	4.09	3.50	1.58	1.89	1.51
90	3.45	4.41	3.61	1.68	1.89	2.39
100	3.86	5.55	3.94	1.81	3.04	2.72

For both defects and all three loads, the AE count was higher than for the healthy bearing save for D12 at 30 rpm and 2.5 kN. Hence, it can be stated that AE counts were able to detect the given fault at both locations which mean this parameter can detect faults in any location on the outer race.

However, the load variation does not show any clear trend with the AE counts as it increased in some cases with increasing load, and the reverse in other cases. Hence, this observation confirmed that load variation did not affect the AE counts.

8.3 Defect Size Sensitivity

This section examines the influence of defect size on the AE parameters. This was achieved by successively seeding faults of uniformly increasing size. This process has been carried out to confirm the outcomes reported Sections in 5.2 and 5.4.

The test sequence began by inserting a line defect of given width, 5.0 mm, and length, 3.0 mm (D6), on the edge of the outer race. This was followed by incrementally increasing the defect width while maintaining the length constant at 3.0 mm, see D7-D9 in Table 4.1 and Figure 4.18 (a). Next, a line defect on the

edge of the outer race of given width 3.0 mm had its length incrementally increased, see D10-D13 in Table 4.1 and Figure 4.18 (b).

Figure 8.9 shows the measured AE RMS values for a healthy bearing and bearings with various defect sizes on the outer race at 100 rpm, for three load conditions. The IR values, calculated using Equation (5.1), are shown in Table 8.5.

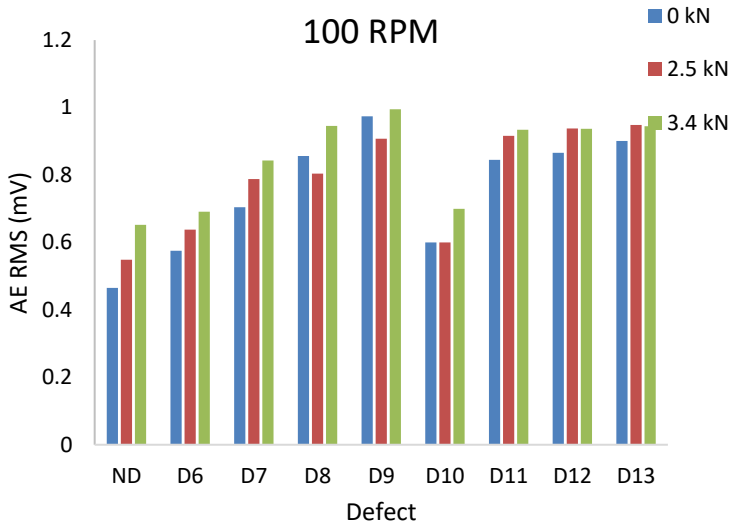

Figure 8.9: AE RMS for healthy bearing and eight bearings with various fault conditions at the outer race, at 100 rpm for three loads

Table 8.5: AE RMS IR values for a healthy bearing and eight bearings with various fault conditions on the outer race, at 100 rpm for three loads

Fault	Defect (L X W) mm	0 kN	2.5 kN	3.4 kN
D6	3.0 X 5.0	1.24	1.16	1.06
D7	3.0 X 7.0	1.51	1.44	1.29
D8	3.0 X 10.0	1.84	1.47	1.45
D9	3.0 X 12.2	2.09	1.66	1.53
D10	2.0 X 3.0	1.29	1.09	1.07
D11	4.0 X 3.0	1.81	1.67	1.43
D12	6.0 X 3.0	1.86	1.71	1.44
D13	8.0 X 3.0	1.94	1.73	1.45

From Figure 8.9 and Table 8.5 it can be seen that the AE RMS for all defective bearings was higher than for the healthy bearing. For all defective cases where the width of the defect was increased with fixed length, the AE RMS clearly increased as the defect width increased, see cases D6 to D9. The same general trend was found for defects D10 to D13, where the defect width was fixed at 3.0 mm, and the length increased.

However, the incremental increase is more obvious in the first four cases in which the defect width increased at a fixed length. This suggests that defect width has a greater influence on the AE RMS than defect length.

Figures 8.10 and 8.11, respectively reveal the sensitivity of AE kurtosis and AE counts to various defects for a rotational speed of 100 rpm under three load conditions.

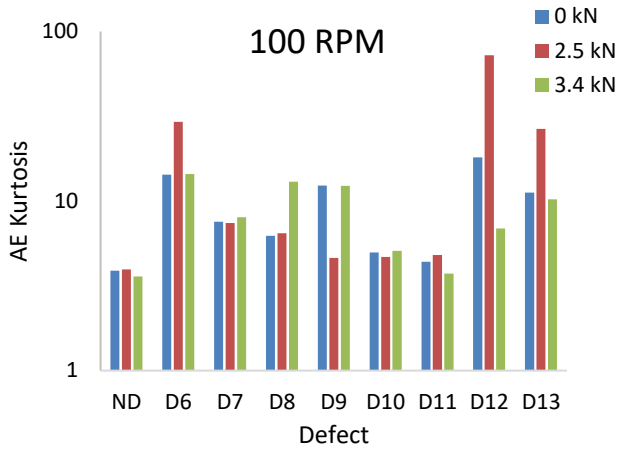

Figure 8.10: AE kurtosis for healthy bearing and eight bearings with different fault conditions at the outer race, at 100 rpm for three loads

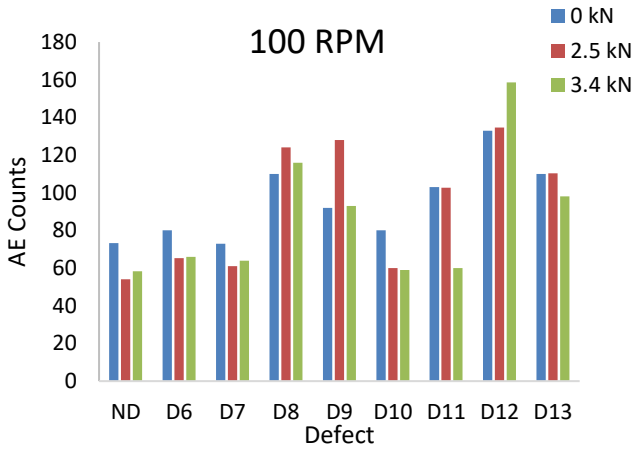

Figure 8.11: AE counts for healthy bearing and eight bearings with various fault conditions at the outer race, at 100 rpm for three loads

Figure 8.10 shows that the kurtosis value for all defective bearings was higher than for the healthy bearings. With an increasing defect width at fixed length (D6-D9), the AE kurtosis increased then decreased again, the same was true for the increasing defect length at a fixed width (D10-D13).

The same observations can be made of Figure 8.11 for the AE counts. Thus, from these two sets of observations, it can be said that both kurtosis and AE counts are not sensitive to the defect size. This again confirms the outcomes of Chapters 5 and 6 of the insensitivity of kurtosis and AE counts to the defect size.

Figure 8.12, presents the variation in AE amplitude for three loads at 100 rpm, for a healthy bearing and eight bearings with faults of different sizes in the outer race. The IR values, calculated using Equation (5.1), are shown in Table 8.6.

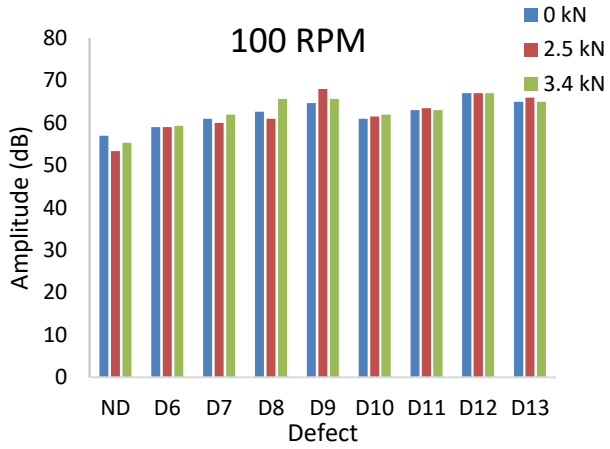

Figure 8.12: AE Amplitude for healthy bearing and eight bearings with various fault conditions at the outer race, at 100 rpm for three loads

Table 8.6: AE Amplitude IR values for a healthy bearing and several fault conditions on the outer race, at 100 rpm for three loads

Fault	Defect Type (L X W) mm	0 kN	2.5 kN	3.4 kN
D6	3.0 X 5.0	1.04	1.11	1.07
D7	3.0 X 7.0	1.07	1.13	1.12
D8	3.0 X 10.0	1.10	1.14	1.19
D9	3.0 X 12.2	1.13	1.28	1.19
D10	2.0 X 3.0	1.07	1.15	1.12
D11	4.0 X 3.0	1.11	1.19	1.14
D12	6.0 X 3.0	1.18	1.26	1.21
D13	8.0 X 3.0	1.14	1.24	1.17

From Figure 8.12 and Table 8.6, it is shown that for all defective bearings, AE amplitude was higher than for the healthy bearing. Furthermore, for the cases of fixed length (D6–D9), the AE amplitude increased as the width increased. The same observation was true for the cases of fixed width and increasing the length. Hence, it can state that the AE amplitude, for the defect sizes used here, generally increased with both defect length and width. However, when the defect width reaches 8.0 mm (D13), the AE amplitude did decrease slightly, and this last observation is taken as confirmation of the conclusion of Chapter 5, of non-sensitivity of the amplitude to the defect size.

8.4 Closing Remark

It can conclude that statistical measures of the AE signal are able to monitor defects at both locations (middle and edge) on the outer race of a bearing rotating at low speeds, and hence AE is applicable for monitoring the condition of the bearing's outer race.

Additionally, the measured AE parameters had higher values when the defect was seeded in the centre of the outer race, possibly due to the shorter path traversed by the signal between source and sensor which gave a lower attenuation than when the defect was on the edge of the outer race.

The defect size did have some impact on the AE parameters investigated, but only RMS was sensitive to defect size. This confirms the outcomes of Chapters 5 and 6. However, RMS is more sensitive to the defect width than length.

Chapter Nine

9 Conclusions and Recommendations for Future Work

This chapter explains how well this research has met its specified aim and objectives, as set out in Section 1.3, and the contributions to knowledge that it has made. The major achievements of this research are described briefly and related to the original aim and objectives.

This research project has investigated the use of AE as a viable monitoring technique to be used with low speed rotating machinery for defect detection. This has included investigating the use of statistical parameters to effectively detect incipient faults using AE signals. A series of test were conducted in which different defects were seeded into a bearing, and the AE signals monitored. These tests were for rotational speeds of between 10 to 100 rpm and three load conditions: zero applied load, 2.5 kN and 3.4 kN.

Chapter 2 reviewed the literature relevant to bearing failure and CM techniques for bearings, followed by a review of the application of vibration and AE techniques to the monitoring of a bearing's condition. Chapter 3 critically reviewed signal processing techniques and Chapter 4 described the research methodology, test rig design, construction and instrumentation, experimental procedure, instrument calibration, and data acquisition. With this new test rig, Cranfield University expects to be able to study low-speed bearings and develop diagnostic techniques. Section 4.3, detailed the faults to be seeded into the bearings.

One objective of the research was to compare the measurements obtained from both inner and outer races under similar conditions to check the applicability of AE techniques in detecting faults in these parts. This was achieved in Chapters 5 and 6.

In Chapter 5, an investigation was made of AE techniques to determine their relative efficacy in monitoring bearing conditions. A healthy bearing and bearings with defects seeded into the outer race were monitored under set test conditions.

It was concluded that the shaft rotational speed has a strong influence on the measured AE parameters (AE kurtosis, amplitude, counts and RMS). Nevertheless, they were entirely independent of the load which agrees with the results of He et al. [23] and others [53,128,129]. However, Al-Ghamdi et al. [19] has stated another observation as he mentioned that the load had a significant influence on some of the AE parameters such as the RMS.

All the AE parameters were sensitive to the existence of a defect on the outer race. Moreover, the defect size had some impact on the AE parameters, but only RMS was consistently sensitive to defect size.

A parallel investigation for the inner race was carried out in Chapter 6. It was concluded that AE techniques are able to monitor defect initiation and propagation on the inner race of a bearing rotating at low speeds. This chapter showed that as for the outer race the listed AE parameters were strongly influenced by the shaft rotational speed, but were entirely independent of the load. Furthermore, from the inner race results, it was concluded that AE amplitude and RMS, were able to detect the inner race faults at an early stage, while AE kurtosis and counts did not. However, once the fault was established only AE RMS was consistently sensitive to defect size.

Chapter 7 analysed the outcomes of Chapters 5 and 6 to find the most suitable technique to monitor both races simultaneously. First, Chapter 7 compared only AE measures to detect defect existence and, since Chapters 5 and 6 revealed that the statistical parameters used were not sensitive to load, this chapter investigated only the sensitivity of the AE measures to variation in rotational speed. It was concluded that statistical measures of the AE signal are able to detect a fault in both inner and outer races of a bearing rotating at low speeds. Importantly the AE parameters successfully detected the presence of a fault in both outer and inner races at an early stage, except for kurtosis and AE counts used with the inner race. However, once the defect had been initiated, only AE RMS was sensitive to defect size for both races. Moreover, with increasing shaft rotational speed, the AE parameters increased which showed the sensitivity of the parameters to the speed variation.

Chapter 8 reported the results of two investigations, the first with a healthy bearing and two defective bearings at different locations (centre and edge) on the outer race. The objective of this investigation was to check the applicability of the AE to monitor defect at both locations on bearing rotates at low speeds, ≤100 rpm.

The second program was a set of experiments investigating the effects of different defect sizes at the outer race of a roller bearing at low speeds. The objective of the program was to re-assess and extend the findings of Chapter 5 by increasing the size of the seeded faults in a uniform manner on the outer race. The size of the defects was changed in two ways, in the first the length was held constant at 3 mm and the width increased, and in the second the width was held constant, and the length increased. The sizes of the defects and the positions on the bearing are shown in Table 4.1 and Figure 4.18.

It was concluded that statistical measures of the AE signal (RMS, kurotsis, amplitude, and counts) could detect defects at any location on the outer race of a bearing rotating at low speeds. The term " any location" is used since moving the defect from the centre to the edge of the race covers - in principle - all points on the outer race. Hence AE is suitable for monitoring the condition of the outer race.

On the other hand, from the second programme it was concluded that the defect size has an impact on the AE parameters but, of the parameters examined (AE kurtosis, amplitude, counts and RMS), only RMS was sensitive to defect size, confirming the results of Chapter 5. However, the RMS value was more susceptible to fault width than length.

In conclusion, this research has investigated several aspects of condition monitoring of bearing rotating at low speeds (10 -100 rpm). This research shows that the AE technique could be part of an early fault detection system for machines whose bearings operate in the low speed range.

To conclude the first and most important task of this research program was to demonstrate a correlation between AE and defect initiation and propagation in low-speed bearings which has been achieved.

Recommendations for Future Work

The results of the investigation into the use of AE techniques for monitoring of bearing at low speeds were encouraging, and it is hoped that future researchers will explore its full potential as it is a wide area.

1. Advanced signal processing techniques

Advanced signal processing techniques need to be used to analyse the captured AE signals to detect a fault more readily in its early stages for bearings rotating at low speeds. Furthermore, the application of neural networks should be encouraged, and to this end, statistical analysis could be used to provide a database to train neural networks for diagnosing bearing condition at low speeds and detecting incipient faults under various conditions.

2. Heavily loaded bearings

The work could be extended to more heavily loaded bearings as this research only covered lightly loaded bearing. Then a comparison between of a heavily and lightly loaded bearing could be carried out.

3. Dynamic speed and load conditions

Future work could be made more useful by simulating industrial conditions, by running the bearing under dynamic speed and load conditions. This would have the advantage of providing a reasonable opportunity to show the applicability of AE in real life monitoring of bearing conditions.

4. Bearing roller monitoring

A similar study could be performed on the AE measurements to improve the effectiveness of AE as a means of detecting defects in the rollers of bearing rotating at low speeds.

5. Natural bearing degradation

Future work could demonstrate the use of AE measurements to detect, monitor, and locate natural degradation, and defect initiation and propagation in bearings rotating at low speeds.

6. Fault prognostics and life estimation at such low speeds range is a critical area for future work.

REFERENCES

1. Donnell PO., Heising C., Singh C., Wells SJ. Report of large motor reliability survey of industrial and commercial installations: Part 2. IEEE Transactions on Industry Applications. 1985; IA-21(4): 865–872. Available at: DOI:10.1109/TIA.1987.4504880

2. Mba D. Condition monitoring of slow speed rotating machinery using stress waves. PhD Thesis. Cranfield University; 1998.

3. Kuboyama K. Development of low speed bearing diagnosis technique. Detection, Diagnosis and Prognosis of Rotating Machinery to Improve Reliability, Maintainability, and Readiness Through the Application of New and Innovative Techniques: 28-30 October. Maryland; 1986. pp. 178–185.

4. Mechefske CK., Mathew J. Fault detection and diagnosis in low speed rolling element bearings Part II: The use of nearest neighbour classification. Mechanical Systems and Signal Processing. 1992; 6(4): 309–316. Available at: DOI:10.1016/0888-3270(92)90033-F

5. Elforjani MA. Condition monitoring of slow speed rotating machinery using acoustic emission technology. PhD Thesis. Cranfield University; 2010. Available at: http://dspace.lib.cranfield.ac.uk/handle/1826/4568 (Accessed: 27 January 2017)

6. Jamaludin N., Mba D. Monitoring extremely slow rolling element bearings: Part I. NDT and E International. 2002; 35: 349–358. Available at: DOI:10.1016/S0963-8695(02)00006-3

7. Jamaludin N., Mba D. Monitoring extremely slow rolling element bearings: Part II. NDT and E International. 2002; 35: 359–366. Available at: DOI:10.1016/S0963-8695(02)00006-3

8. Mba D., Rao RBKN. Development of acoustic emission technology for condition monitoring and diagnosis of rotating machines; bearings, pumps, gearboxes, engines and rotating structures. The Shock and Vibration Digest. 2006; 38(1): 3–16. Available at: DOI:10.1177/0583102405059054

9. The Barden Corporation. Bearing failure: causes and cures. Danbury, CT: The Barden Corporation; 2007. Available at: http://www.schaeffler.com/remotemedien/media/_shared_media/08_media_library/01_publications/barden/brochure_2/downloads_24/barden_bearing_failures_us_en.pdf (Accessed: 26 January 2017)

10. Kurfess TR., Billington S., Liang SY. Advanced diagnostic and prognostic techniques for rolling element bearings. Condition Monitoring and Control for Intelligent Manufacturing. London: Springer; 2006. pp. 137–165.

11. Tandon N., Choudhury A. A review of vibration and acoustic measurement methods for the detection of defects in rolling element bearings. Tribology International. 1999; 32(8): 469–480. Available at: DOI:10.1016/S0301-679X(99)00077-8

12. Hemmati F. Rolling element bearing condition monitoring using acoustic emission technique and advanced signal processing. MSc Thesis. The University of British Columbia; 2012.

13. Elforjani M., Mba D. Accelerated natural fault diagnosis in slow speed bearings with acoustic emission. Engineering Fracture Mechanics. 2010; 77(1): 112–127. Available at: DOI:10.1016/j.engfracmech.2009.09.016

14. Elforjani M., Mba D. Natural mechanical degradation measurements in slow speed bearings. Engineering Failure Analysis. 2009; 16(1): 521–532. Available at: DOI:10.1016/j.engfailanal.2008.06.005

15. Elforjani M., Mba D. Detecting natural crack initiation and growth in slow speed shafts with the acoustic emission technology. Engineering Failure Analysis. 2009; 16(7): 2121–2129. Available at: DOI:10.1016/j.engfailanal.2009.02.005

16. Elforjani M., Mba D. Observations and location of acoustic emissions for a naturally degrading rolling element thrust bearing. Journal of Failure Analysis and Prevention. 2008; 8(4): 370–385. Available at: DOI:10.1007/s11668-008-9141-x

17. Elforjani M., Mba D. Monitoring the onset and propagation of natural degradation process in a slow speed rolling element bearing with acoustic emission. Journal of Vibration and Acoustics. 2008; 130: 41013. Available at: DOI:10.1115/1.2948413

18. Williams T., Ribadeneira X., Billington S., Kurfess T. Rolling element bearing diagnostics in run-to-failure lifetime testing. Mechanical Systems and Signal Processing. 2001; 15(5): 979–993. Available at: DOI:10.1006/mssp.2001.1418

19. Al-Ghamd AM., Mba D. A comparative experimental study on the use of acoustic emission and vibration analysis for bearing defect identification and estimation of defect size. Mechanical Systems and Signal Processing. 2006; 20(7): 1537–1571. Available at: DOI:10.1016/j.ymssp.2004.10.013

20. Al-Dossary S., Hamzah RIR., Mba D. Observations of changes in acoustic emission waveform for varying seeded defect sizes in a rolling element bearing. Applied Acoustics. 2009; 70(1): 58–81. Available at: DOI:10.1016/j.apacoust.2008.01.005

21. Morhain A., Mba D. Bearing defect diagnosis and acoustic emission. Journal of Engineering Tribology. 2003; 217(4): 272–275. Available at: DOI:10.1243/135065003768618614

22. Rao V V., Ratnam C. A comparative experimental study on identification of defect severity in rolling element bearings using acoustic emission and vibration analysis. Tribology in Industry. 2015; 37(2): 176–185.

23. He Y., Zhang X., Friswell MI. Defect diagnosis for rolling element bearings using acoustic emission. Journal of Vibration and Acoustics. 2009; 131(6): 61012. Available at: DOI:10.1115/1.4000480

24. Márquez FP., Tobias AM., Pérez JM., Papaelias M. Condition monitoring of wind turbines: Techniques and methods. Renewable Energy. 2012; 46(0): 169–178. Available at: DOI:http://dx.doi.org/10.1016/j.renene.2012.03.003

25. Koulocheris D., Gyparakis G., Stathis A., Costopoulos T., Al ET. Vibration signals and condition monitoring for wind turbines. Engineering. 2013; 5: 948–955. Available at: http://dx.doi.org/10.4236/eng.2013.512116

26. Shakya P., Darpe AK., Kulkarni MS. Vibration-based fault diagnosis in rolling element bearings : ranking of various time, frequency and time-frequency domain data-based damage identification parameters. The International Journal of Condition Monitoring. 2013; 3(2): 1–10.

27. Elasha F. Condition monitoring and prognosis of tidal turbines gearboxes. PhD Thesis. Cranfield University; 2015.

28. Miller R.K. MP. Nondestructive testing handbook. McIntire P (ed.) American Society for Nondestructive Testing. ASM International; 1987.

29. Mauntz MR., Gegner J., Kuipers U., Klingau S. A sensor system for online oil condition monitoring of operating components. In: Gegner J (ed.) Tribology - fundamentals and advancements. 2013. pp. 305–321. Available at: http://www.intechopen.com/books/tribology-fundamentals-and-advancements/a-sensor-system-for-online-oil-condition-monitoring-of-operating-components (Accessed: 27 January 2017)

30. Nagata M., Fujita M., Yamada M., Kitahara T. Evaluation of tribological properties of bearing materials for marine diesel engines utilizing acoustic emission technique. Tribology International. 2012; 46(1): 183–189. Available at: DOI:10.1016/j.triboint.2011.05.026

31. Mba D. Applicability of acoustic emissions to monitoring the mechanical integrity of bolted structures in low speed rotating machinery: Case study. NDT and E International. 2002; 35(5): 293–300. Available at: DOI:10.1016/S0963-8695(01)00053-6

32. Miettinen J., Pataniitty P. Acoustic emission in monitoring extremely slowly rotating rolling bearing. Proceedings of COMADEM ´99: 6-9 July. England: Coxmoor Publishing Company; 1999. pp. 289–297. Available at: http://cur.g.andritz.com/c/www/00/05/37/-

396127963/53745/1/1/0/paper_c.pdf

33. Parizi HA., Kafil M., Ghayour M., Rad SZ. Fault diagnosis of slow-speed rolling element bearings with the use of acoustic emission and wavelet packet. The 21st International Congress on Sound and Vibration: 13-17 July. Beijing, China: International Institute of Acoustics and Vibration; 2014. pp. 1–8.

34. Law L-S., Kim JH., Liew WYH., Lee S-K. An approach based on wavelet packet decomposition and hilbert–huang transform (WPD–HHT) for spindle bearings condition monitoring. Mechanical Systems and Signal Processing. 2012; 33: 197–211. Available at: DOI:10.1016/j.ymssp.2012.06.004

35. Tandon N., Ramakrishna KM., Yadava GS. Condition monitoring of electric motor ball bearings for the detection of grease contaminants. Tribology International. 2007; 40(1): 29–36. Available at: DOI:10.1016/j.triboint.2006.01.024

36. Lees AW., Quiney Z., Ganji A., Murray B. The use of acoustic emission for bearing condition monitoring. Journal of Physics: Conference Series. 2011; 305: 12074. Available at: DOI:10.1088/1742-6596/305/1/012074

37. Eftekharnejad B., Carrasco MR., Charnley B., Mba D. The application of spectral kurtosis on acoustic emission and vibrations from a defective bearing. Mechanical Systems and Signal Processing. 2011; 25(1): 266–284. Available at: DOI:10.1016/j.ymssp.2010.06.010

38. Yoshioka T., Shimizu S. Monitoring of ball bearing operation under grease lubrication using a new compound diagnostic system detecting vibration and acoustic emission. Tribology Transactions. 2009; 52(6): 725–730. Available at: DOI:10.1080/10402000902913345

39. Mirhadizadeh SA., Moncholi EP., Mba D. Influence of operational variables in a hydrodynamic bearing on the generation of acoustic emission. Tribology International. 2010; 43(9): 1760–1767. Available at:

DOI:10.1016/j.triboint.2010.03.003

40. Rahman Z., Ohba H., Yoshioka T., Yamamoto T. Incipient damage detection and its propagation monitoring of rolling contact fatigue by acoustic emission. Tribology International. 2009; 42(6): 807–815. Available at: DOI:10.1016/j.triboint.2008.10.014

41. Yoshioka T., Fujiwara T. A new acoustic emission source locating system for the study of rolling contact fatigue. Wear. 1982; 81: 183–186. Available at: DOI:10.1016/0043-1648(82)90314-3

42. Wu Z., Shen G., Zhang J. Characteristics of acoustic emission signals in the rolling bearing on giant wheel. 30th European Conference on Acoustic Emission Testing & 7th International Conference on Acoustic Emission: 12-15 September. Beijing, China; 2012.

43. Sako T., Yoshie O. Diagnostic method of low speed rolling element bearing using AE envelope waveform. IEEE Region 10 Annual International Conference, Proceedings/TENCON: Nov 23. Singapore; 2010. pp. 724–729. Available at: DOI:10.1109/TENCON.2010.5686610

44. Jamaludin N., Mba D., Bannister RH. Condition monitoring of slow-speed rolling element bearings using stress waves. Proceedings of the Institution of Mechanical Engineers, Part E: Journal of Process Mechanical Engineering. 2001; 215(4): 245–271. Available at: DOI:10.1243/0954408011530488

45. Kim EY., Tan a. CC., Mathew J., Yang BS. Condition monitoring of low speed bearings: A comparative study of the ultrasound technique versus vibration measurements. Australian Journal of Mechanical Engineering. 2008; 5(2): 177–189.

46. Tavakoli MS. Review of bearing condition monitoring — Application of acoustic emission method. 1st International conference on Acoustic Emission in Manufacturing: 16-19 September. Boston, MA; 1991. pp. 453–460. Available at: DOI:10.1016/0963-8695(94)90489-8

47. Hawman MW., Galinaitis WS. Acoustic emission monitoring of rolling element bearings. IEEE 1988 Ultrasonics Symposium Proceedings: 2-5 October. Chicago, IL: IEEE; 1988. pp. 885–889. Available at: DOI:10.1109/ULTSYM.1988.49503

48. Lin TR., Kim E., Tan ACC. A practical signal processing approach for condition monitoring of low speed machinery using peak-hold-down-sample algorithm. Mechanical Systems and Signal Processing. 2013; 36(2): 256–270. Available at: DOI:10.1016/j.ymssp.2012.11.003

49. Liu X., Wu X., Liu C. A comparison of acoustic emission and vibration on bearing fault detection. 2011 International Conference on Transportation, Mechanical, and Electrical Engineering (TMEE): 16-18 December. Changchun, China: IEEE; 2011. pp. 922–926. Available at: DOI:10.1109/TMEE.2011.6199353

50. Kilundu B., Chiementin X., Duez J., Mba D. Cyclostationarity of acoustic emissions (AE) for monitoring bearing defects. Mechanical Systems and Signal Processing. 2011; 25(6): 2061–2072. Available at: DOI:10.1016/j.ymssp.2011.01.020

51. Tandon N., Yadava GS., Ramakrishna KM. A comparison of some condition monitoring techniques for the detection of defect in induction motor ball bearings. Mechanical Systems and Signal Processing. 2007; 21(1): 244–256. Available at: DOI:10.1016/j.ymssp.2005.08.005

52. Kim YH., Tan ACC., Yang BS. Parameter comparison of acoustic emission signals for condition monitoring of low-speed bearings. Australian Journal of Mechanical Engineering. 2008; 6(1): 45–52. Available at: DOI:10.1080/14484846.2008.11464556

53. Choudhury A., Tandon N. Application of acoustic emission technique for the detection of defects in rolling element bearings. Tribology International. 2000; 33(1): 39–45. Available at: DOI:10.1016/S0301-679X(00)00012-8

54. Al-Balushi KR., Addali A., Charnley B., Mba D. Energy index technique for

detection of acoustic emissions associated with incipient bearing failures. Applied Acoustics. 2010; 71(9): 812–821. Available at: DOI:10.1016/j.apacoust.2010.04.006

55. Rogers LM. The application of vibration signature analysis and acoustic emission source location to on-line condition monitoring of anti-friction bearings. Tribology International. 1979; 12(2): 51–58. Available at: DOI:10.1016/0301-679X(79)90001-X

56. Niknam SA., Thomas T., Hines JW., Sawhney R. Analysis of acoustic emission data for bearings subject to unbalance. International Journal of Prognostics and Health Management. 2013; 69(9–12): 2679–2689.

57. Chiementin X., Mba D., Charnley B., Lignon S., Dron JP. Effect of the denoising on acoustic emission signals. Journal of Vibration and Acoustics. 2010; 132(3): 031009–9. Available at: DOI:10.1115/1.4000789

58. Gu DS., Choi BK. Machinery faults detection using acoustic emission signal. Acoustic Waves - From Microdevices to Helioseismology. InTech; 2011. pp. 171–190. Available at: DOI:10.5772/22892

59. Kakishima H., Nagatomo T., Ikeda H., Yoshioka T., Korenaga A. Measurement of acoustic emission and vibration of rolling bearings with an artificial defect. Quarterly Report of RTRI. 2000; 41(3): 127–130. Available at: DOI:10.2219/rtriqr.41.127

60. Price ED., Lees a W., Friswell MI. Detection of severe sliding and pitting fatigue wear regimes through the use of broadband acoustic emission. Journal of Engineering Tribology. 2005; 219(Part J): 85–98. Available at: DOI:10.1243/135065005X9817

61. Niknam SA., Songmene V., Au YHJ. The use of acoustic emission information to distinguish between dry and lubricated rolling element bearings in low-speed rotating machines. International Journal of Advanced Manufacturing Technology. 2013; 69(9–12): 2679–2689. Available at: DOI:10.1007/s00170-013-5222-4

62. Towsyfyan, H., Raharjo, P., Gu, F., & Ball A. Characterization of acoustic emissions from journal bearings for fault detection. NDT 2013: 10-13 September. Telford; 2013.

63. Ruiz-Cárcel C., Hernani-Ros E., Cao Y., Mba D. Use of spectral kurtosis for improving signal to noise ratio of acoustic emission signal from defective bearings. Journal of Failure Analysis and Prevention. 2014; 14(3): 363–371. Available at: DOI:10.1007/s11668-014-9805-7

64. Hemmati F., Orfali W., Gadala MS. Rolling element bearing condition monitoring using acoustic emission technique. International Conference on Noise and Vibration Engineering 2012, ISMA 2012, including USD 2012: International Conference on Uncertainty in Structure Dynamics. 2012; 1: 699–713. Available at: http://www.scopus.com/inward/record.url?eid=2-s2.0-84906346145&partnerID=tZOtx3y1

65. McFadden P. Condition monitoring or rolling element bearings by vibration analysis. Machine Condition Monitoring: Papers presented at a seminar. London: Professional Engineering Publishing; 1990. pp. 49–54.

66. Radcliff G. Condition monitoring of rolling element bearings using the enveloping technique. Machine Condition Monitoring. 1990; 23: 55–67.

67. Setford GAW. Bearings-condition monitoring,condition measurement and condition control. Profitable Condition Monitoring. 1993. pp. 231–240.

68. Murphy TJ. The development of a data collector for low-speed machinery. Profitable Condition Monitoring. 1993. pp. 251–258. Available at: DOI:10.1007/978-94-011-1616-9_23

69. Robinson, J.C, Canada RG. Vibration measurments on slow speed machinery. Predictive Maintenance Technology National Conference (P/PM Technology). Indianapolis, Indiana.; 1995. pp. 33–37.

70. National Instruments. Vibration Signals and Transducers (Sound and Vibration Measurement Suite) - Sound and Vibration Measurement Suite 6.0 Help. Available at: http://zone.ni.com/reference/en-XX/help/372416A-

01/svtconcepts/vbr_sig/ (Accessed: 4 March 2017)

71. Robinson, J.C, Canada, R.G. and Piety RG. Vibration monitoring on slow speed machinery: New methodologies covering machinery from 0.5 to 600rpm. Proc. 5th International Conference on Profitable Condition Monitoring - Fluids and Machinery Performance Monitoring: 3-4 December. Harrogate, UK: Mechanical Engineering Publications; 1996. pp. 169–182.

72. Mechefske CK., Mathew J. Fault detection and diagnosis in low speed rolling element bearings Part I: The use of parametric spectra. Mechanical Systems and Signal Processing. 1992; 6(4): 297–307. Available at: DOI:10.1016/0888-3270(92)90032-E

73. Patidar S., Soni PK. An overview on vibration analysis techniques for the diagnosis of rolling element bearing faults. International Journal of Engineering Trends and Technology (IJETT). 2013; 4(5): 1804–1809.

74. Liu TI., Singonahalli JH., Iyer NR. Detection of roller bearing defects using expert system and fuzzy logic. Mechanical Systems and Signal Processing. 1996; 10(5): 595–614. Available at: DOI:10.1006/mssp.1996.0041

75. Samanta B., Al-Balushi KR. Artificial neural network based fault diagnostics of rolling element bearings using time-domain features. Mechanical Systems and Signal Processing. 2003; 17(2): 317–328. Available at: DOI:10.1006/mssp.2001.1462

76. Subrahmanyam M., Sujatha C. Using neural networks for the diagnosis of localized defects in ball bearings. Tribology International. 1997; 30(10): 739–752. Available at: DOI:10.1016/S0301-679X(97)00056-X

77. Shull JP. Nondestructive evaluation: Theory, techniques, and applications. New York: Marcel Dekker; 2002.

78. Kim EY., Tan ACC., Yang B-S., Kosse V. Experimental study on condition monitoring of low speed bearings: Time domain analysis. 5th Australasian Congress on Applied Mechanics (ACAM): 10-12 December. Brisbane, Australia; 2007.

79. Zhou J. A study of acoustic emission technique for concrete damage detection. MSc Thesis. Michigan Technological University; 2011.

80. Roberts TM., Talebzadeh M. Fatigue life prediction based on crack propagation and acoustic emission count rates. Journal of Constructional Steel Research. 2003; 59(6): 679–694. Available at: DOI:10.1016/S0143-974X(02)00065-2

81. Dunegan HL. Location of leaks in pipes by use of acoustic emission modal. 2004.

82. Sun L., Li Y. Active defects detection and localization using acoustic emission method. Proceedings of the 8th World Congress on Intelligent Control and Automation: July 6-9. Jinan, China; 2010. pp. 5348–5351.

83. Ai Q., Liu CX., Chen XR., He P., Wang Y. Acoustic emission of fatigue crack in pressure pipe under cyclic pressure. Nuclear Engineering and Design. 2010; 240(10): 3616–3620. Available at: DOI:10.1016/j.nucengdes.2010.05.022

84. Yu J., Ziehl P., Zarate B., Caicedo J., Yu L., Giurgiutiu V., et al. Quantification of fatigue cracking in CT specimens with passive and active piezoelectric sensing. Proc. of SPIE. 2010; 7649: 76490R–1–76490R–12. Available at: DOI:10.1117/12.847945

85. Sikorski W. Acoustic Emission :: Research and applications. Cardiff University. 2014. Available at: http://www.acousticemission.net/research.asp (Accessed: 7 April 2015)

86. Kalicka M. Acoustic emission signal propagation through welded steel bridge joints. 10th European Conference on Non-Destructive Testing (ECNDT): 7-11 June. Moscow; 2010.

87. El-Alej ME. Monitoring sand particle concentration in multiphase flow using acoustic emission technology. PhD Thesis. Cranfield University; 2014.

88. Alssayh M. Slug velocity measurement and flow regime recognition using

acoustic emission technology. PhD Thesis. Cranfield University; 2013.

89. Chen L., Wood S., Moore S., Nguyen B. Acoustic emission of bubbly flow and its size distribution spectrum. Proceedings of Acoustics 21-23 November. Fremantle, Australia: Australian Acoustical Society; 2012.

90. Husin S. An experimental investigation into the correlation between acoustic emission (AE) and bubble dynamics. PhD Thesis. Cranfield University; 2011. Available at: http://dspace.lib.cranfield.ac.uk/handle/1826/7318 (Accessed: 29 January 2017)

91. Addali A. Monitoring gas void fraction in two-phase flow with acoustic emission. PhD Thesis. Cranfield University; 2010. Available at: http://hdl.handle.net/1826/4475 (Accessed: 29 January 2017)

92. Parker Hannifin Manufacturing Ltd. Acoustic emissions monitoring and analysis in power generation. 2015. Available at: http://www.kittiwakeholroyd.com/acoustic-emissions-in-the-power-generation-industry.htm (Accessed: 26 April 2015)

93. Abrahamsen, J. and Bentsen S. Developments in sub-sea leak and condition monitoring. Monitor Publishing Inc. 2013. Available at: http://www.oilgasmonitor.com/developments-in-sub-sea-leak-and-condition-monitoring/4454/ (Accessed: 26 April 2015)

94. Miller RK., Carlos M., Finlayson RD. Helicopter drivetrain damage detection and classification using acoustic emission and a kinematic variable. AHS International Annual Forum, 57th: 9-11 May. Washington, DC; 2001. Available at: https://vtol.org/store/product/helicopter-drivetrain-damage-detection-and-classification-using-acoustic-emission-and-a-kinematic-variable-4503.cfm (Accessed: 26 April 2015)

95. Yilmazer P. Structural health condition monitoring of rails using acoustic emission techniques. The Proceedings of NDT: 11-13 September 2012. Northamptonshire, UK;

96. Shrivastava S. Assessment of bone condition by acoustic emission technique: A review. Journal of Biomedical Science and Engineering. 2009; 2(3): 144–154. Available at: DOI:10.4236/jbise.2009.23025

97. Vallen H. AE testing fundamentals, equipment, applications. The e-Journal of Nondestructive Testing. 2002; 7. Available at: http://www.ndt.net/article/v07n09/05/05.htm

98. Xiaoqi C., Hao Z., Wildermuth D. SIMTech Technical Report AT/01/014/AMP: In-process tool monitoring through acoustic emission sensing. Singapore: Singapore Institute of Manufacturing Technology; 2001. Available at: http%3A%2F%2Fciteseerx.ist.psu.edu%2Fviewdoc%2Fdownload%3Fdoi%3D10.1.1.131.2665%26rep%3Drep1%26type%3Dpdf&usg=AFQjCNHufXgj5UOhuwGnzy7XQImXOzsG8A (Accessed: 27 January 2017)

99. Scruby C. An introduction to acoustic emission. Journal of Physics E: Scientific Instruments. 1987; 20(8): 946–953. Available at: DOI:10.1088/0022-3735/20/8/001

100. Huang M., Jiang L., Liaw PK., Brooks CR., Seeley R., Klarstrom DL. Using acoustic emission in fatigue and fracture materials research. Journal of The Minerals, Metals & Materials Society. 1998; 50(11). Available at: http://www.tms.org/pubs/journals/JOM/9811/Huang/Huang-9811.html

101. Alshammari F., Addali A. Bearing condition monitoring with acoustic emission techniques. International Journal of Mechanical, Aerospace, Industrial, Mechatronic and Manufacturing Engineering. 2015; 9(12): 1863–1867.

102. Balderston HL. The detection of incipient failure in bearings. Materials Evaluation. 1969; 27(6): 121–128. Available at: DOI:10.1016/0041-624X(70)90973-X

103. Sundt PC. Monitoring acoustic emission to detect mechnaical defects. Instrumentation technology. 1979; 26(12): 43–44.

104. Holroyd TJ., Randall N. Use of acoustic emission for machine condition monitoring. British Journal of Non-Destructive Testing. 1993; 35(2): 75–78. Available at: http://www.scopus.com/inward/record.url?eid=2-s2.0-0027542738&partnerID=tZOtx3y1

105. Holroyd TJ. Condition monitoring of very slowly rotating machinery using AE techniques. 14th International congress on Condition monitoring and Diagnostic engineering management (COMADEM'): 4-6 September. Manchester; 2001.

106. Yoshioka T. Detection of rolling contact subsurface fatigue cracks using acoustic emission technique. Journal of Society of Tribologists Lubrication Engineers. 1992; 49(4): 303–308. Available at: http://www.osti.gov/scitech/biblio/6293354 (Accessed: 6 October 2015)

107. Jamaludin, N. , Mba, D. and Bannister RH. Monitoring the lubricant condition in a low-speed rolling element bearing using high frequency stress waves. Process Mechanical Engineering. 2002; 216(Part E): 73–88. Available at: DOI:10.1243/095765004773644076

108. Sato I. Rotating machinery diagnosis with acoustic emission techniques. Electrical Engineering in Japan. 1990; 110(2): 115–127. Available at: DOI:10.1002/eej.4391100211 (Accessed: 25 January 2016)

109. Elforjani M., Mba D. Assessment of natural crack initiation and its propagation in slow speed bearings. Nondestructive Testing and Evaluation. 2009; 24(3): 261–275. Available at: DOI:10.1080/10589750802339687

110. McFadden PD., Smith JD. Acoustic emission transducers for the vibration monitoring of bearings at low speeds. ARCHIVE: Proceedings of the Institution of Mechanical Engineers, Part C: Mechanical Engineering Science 1983-1988 (vols 197-202). 1984; 198(8): 127–130. Available at: DOI:10.1243/PIME_PROC_1984_198_097_02

111. Smith JD. Vibration monitoring of bearings at low speeds. Tribology

International. 1982; 15: 139–144. Available at: DOI:10.1016/0301-679X(82)90130-X

112. Couturier J., Mba D. Operational bearing parameters and acoustic emission generation. Journal of Vibration and Acoustics. 2008; 130: 24502. Available at: DOI:10.1115/1.2776339

113. Oh H., Shibutani T., Pecht M. Precursor monitoring approach for reliability assessment of cooling fans. Journal of Intelligent Manufacturing. 2009; 23(2): 173–178. Available at: DOI:10.1007/s10845-009-0342-2

114. Norton MP., Karczub DG. Fundamentals of noise and vibration analysis for engineers. 2nd edn. Cambridge: Cambridge University Press; 2007. Available at: DOI:10.3397/1.2721371

115. Zhao Q., Swami A., Tong L. Signal Processing and Modulation. 2006. pp. 84–93.

116. Prabhakar S., Mohanty AR., Sekhar AS. Application of discrete wavelet transform for detection of ball bearing race faults. Tribology International. 2002; 35(12): 793–800. Available at: DOI:10.1016/S0301-679X(02)00063-4

117. Immovilli F., Cocconcelli M., Bellini A., Rubini R. Detection of generalized-roughness bearing fault by spectral-kurtosis energy of vibration or current signals. IEEE Transactions on Industrial Electronics. 2009; 56(11): 4710–4717. Available at: DOI:10.1109/TIE.2009.2025288

118. Sandoval H., Pedraza Ramirez CA., Quiroga Mendez JE. Acoustic emission-based early fault detection in tapered roller bearings. Ingeniería E Investigación. 2013; 33(3): 5–10. Available at: http://www.revistas.unal.edu.co/index.php/ingeinv/article/view/41032/43160 (Accessed: 27 January 2017)

119. Lorenzo F De., Calabro M. Kurtosis : A statistical approach to identify defect in roller bearings. 2nd International Conference on Marine Research and Transportation: 28-30 june. Naples, Italy; 2007. pp. 17–24.

120. Mba D. The use of acoustic emission for estimation of bearing defect size. Journal of Failure Analysis and Prevention. 2008; 8(2): 188–192. Available at: DOI:10.1007/s11668-008-9119-8

121. Tandon N., Nakara BC. Defect detection in rolling element bearings by acoustic emission method. Journal of Acoustic Emission. 1990; 9(1): 25–28. Available at: http://cat.inist.fr/?aModele=afficheN&cpsidt=4343383 (Accessed: 10 May 2015)

122. Tan C. Application of acoustic emission to the detection of bearing failures. Tribology conference: 2-5 December. Australia: Institution of Engineers, Australia; 1990. pp. 110–114. Available at: http://search.informit.com.au/documentSummary;dn=377857431358203;res=IELENG (Accessed: 10 May 2015)

123. Tan CK., Irving P., Mba D. A comparative experimental study on the diagnostic and prognostic capabilities of acoustics emission, vibration and spectrometric oil analysis for spur gears. Mechanical Systems and Signal Processing. 2007; 21(1): 208–233. Available at: DOI:10.1016/j.ymssp.2005.09.015

124. Miettinen J., Andersson P. Acoustic emission of rolling bearings lubricated with contaminated grease. Tribology International. 2000; 33(11): 777–787. Available at: DOI:10.1016/S0301-679X(00)00124-9

125. Elmaleeh MAA., Saad N. Development of acoustic emission diagnostic system for condition monitoring of rotating machines. PECon 2008 - 2008 IEEE 2nd International Power and Energy Conference: 1-3 December. Johor Baharu, Malaysia; 2008. pp. 1049–1054. Available at: DOI:10.1109/PECON.2008.4762630

126. Morhain A. Defect diagnosis of lightly loaded bearings with acoustic emissions. MSc Thesis. Cranfield University; 2002. Available at: https://unicorn.dmz.cranfield.ac.uk/uhtbin/cgisirsi/?ps=vM4je489DP/CRANFIELD/46910326/5/0

127. Eric Y Kim, Andy C. C. Tan JM and BY. Development of an online condition monitoring system for slow speed machinery. Proceedings of the 4th World Congress of Engineering Assets Management (WECAEM 2009): 28-30 September 2009. Athens, Greece;

128. Cockerill A., Holford KM., Bradshaw T., Cole P., Pullin R., Clarke A. Use of high frequency analysis of acoustic emission signals to determine rolling element bearing condition. Journal of Physics: Conference Series. 2015; 628(1): 12074. Available at: DOI:10.1088/1742-6596/628/1/012074

129. Cockerill A., Clarke A., Pullin R., Bradshaw T., Cole P., Holford K. Determination of rolling element bearing condition via acoustic emission. Proceedings of the Institution of Mechanical Engineers, Part J: Journal of Engineering Tribology. 2016; 0(0): 1–12. Available at: DOI:10.1177/1350650116638612

130. Graney BP., Starry K. Rolling element bearing analysis crosses threshold. Materials Evaluation. 2011; 70(1): 78–85. Available at: DOI:10.1016/0308-9126(80)90087-5

131. Minebea. Bearing Parts – Component Descriptions and Terminology - NMB. 2014. Available at: http://www.nmbtc.com/bearings/engineering/component-parts/ (Accessed: 8 April 2017)

132. Mathematics. What are the limitations /shortcomings of fourier transform and fourier series? - Mathematics stack exchange. 2016. Available at: http://math.stackexchange.com/questions/1267754/what-are-the-limitations-shortcomings-of-fourier-transform-and-fourier-series (Accessed: 3 February 2016)

133. Smith S. Digital signal processing: A practical guide for engineers and scientists. 1st edn. Elsevier Newnes. 2002.

134. McFadden PD., Smith JD. Vibration monitoring of rolling element bearings by the high-frequency resonance technique - A review. Tribology

International. 1984; 17(1): 3–10. Available at: DOI:10.1016/0301-679X(84)90076-8

135. Ho D., Randall RB. Optimisation of bearing diagnostic techniques using simulated and actual bearing fault signals. Mechanical Systems and Signal Processing. 2000; 14(5): 763–788. Available at: DOI:10.1006/mssp.2000.1304

136. Rai VK., Mohanty AR. Bearing fault diagnosis using FFT of intrinsic mode functions in hilbert-huang transform. Mechanical Systems and Signal Processing. 2007; 21(6): 2607–2615. Available at: DOI:10.1016/j.ymssp.2006.12.004

137. Bechhoefer E. A quick introduction to bearing envelope analysis. Green Power Monitoring Systems; Available at: http://www.mfpt.org/FaultData/MFPT Bearing Envelope Analysis.pdf (Accessed: 27 January 2017)

138. Polikar R. The wavelet tutorial. Internet Resources httpengineering rowan edu polikar waveletswt tutorial html. 1994. pp. 1–67. Available at: DOI:10.1088/1751-8113/44/8/085201

139. Randall RB. Applications of spectral kurtosis in machine diagnostics and prognostics. Key Engineering Materials. 2005; 293–294: 21–32. Available at: DOI:10.4028/www.scientific.net/KEM.293-294.21

140. Antoni J. The spectral kurtosis: A useful tool for characterising non-stationary signals. Mechanical Systems and Signal Processing. 2006; 20(2): 282–307. Available at: DOI:10.1016/j.ymssp.2004.09.001

141. Aherwar, Amit ; Bajpal, Rahul; Khalid S. Investigation to failure analysis of rolling element bearing with various defects. IAEME. 2012; 3(2): 138–149.

142. Hutchings A. Test rig assembly. Cranfield University School of Engineering; 2011.

143. Karditsas S. Investigation of vibration’s influence on the fatigue life of rolling

bearing. MRes thesis. Cranfield University; 2011.

144. SMC Corporate. SMC E2 European product catalogue. 2016. Available at: http://uk.rs-online.com/web/c/?searchTerm=NT-25&sra=oss&r=t (Accessed: 30 March 2016)

145. AEWin. Pci-2 based ae system user's manual rev 3. Physical Acoustics; 2007.

146. National Instruments. Aliasing and sampling at frequencies above the nyquist frequency. ReCALL. 2006. Available at: http://www.ni.com/white-paper/3000/en/ (Accessed: 30 January 2017)

147. National Instruments. Acquiring an analog signal: bandwidth, nyquist sampling theorem, and aliasing. 2015. Available at: http://download.ni.com/evaluation/pxi/Acquiring_Analog_Signal.pdf (Accessed: 30 January 2017)

148. MISTRAS Group. AE sensor calibration certificate. Cambridge: MISTRAS Group; 2015.

149. Acoustic Technology Group. AE calibration and simulators: signal source. Available at: http://www.atgndt.com/ae-calibration-and-simulators/calibration-signal-source/ (Accessed: 18 May 2016)

150. Kiral Z., Karagülle H. Simulation and analysis of vibration signals generated by rolling element bearing with defects. Tribology International. 2003; 36(9): 667–678. Available at: DOI:10.1016/S0301-679X(03)00010-0

151. Tandon N., Choudhury A. An analytical model for the prediction of the vibration response of rolling element bearings due to a localized defect. Journal of Sound and Vibration. 1997; 205(3): 275–292. Available at: DOI:10.1006/jsvi.1997.1031

152. Al Kazzaz SA., Singh GK. Experimental investigations on induction machine condition monitoring and fault diagnosis using digital signal processing techniques. Electric Power Systems Research. 2003; 65(3):

197–221. Available at: DOI:10.1016/S0378-7796(02)00227-4

153. Mba D. Acoustic emissions and monitoring bearing health. Tribology Transactions. 2003; 46(3): 447–451. Available at: DOI:10.1080/10402000308982649

APPENDICES

Appendix A : **Waveform Recoding length**

Table A.1: Waveform recording length for the outer race defect

Speed (rpm)	Recording length (sec)
10	5.94
20	2.97
30	1.99
40	1.49
50	1.20
60	1.00
70	0.86
80	0.75
90	0.67
100	0.60

Table A.2: Waveform recording length for the inner race defect

Speed (rpm)	Recording length (sec)
10	4.04
20	2.03
30	1.35
40	1.02
50	0.82
60	0.68
70	0.59
80	0.51
90	0.46
100	0.41

Appendix B : **Outer Race Fault Data**

B.1 AE RMS Observations

The RMS values of AE signal under three loads and three speeds (30, 50, and 100 rpm) are shown in Figure B.1. These values are for a healthy bearing (ND) and five defects, D1 to D5, in the outer race, as described in Table 4.1 and shown in Figure 4.16.

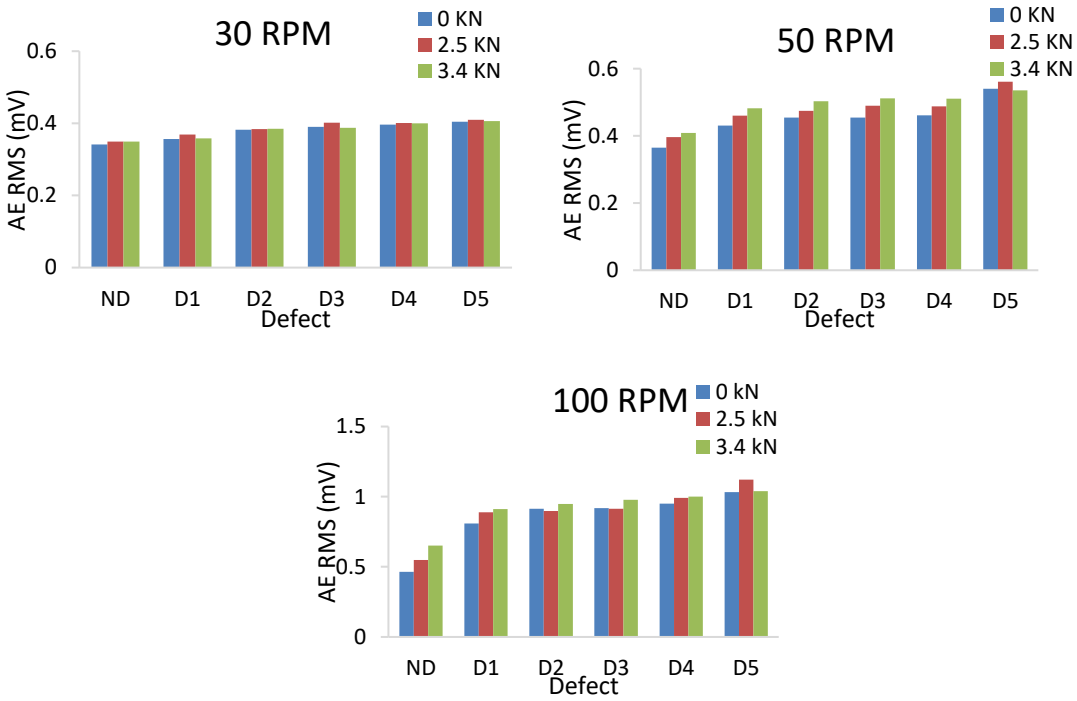

Figure B.1: AE RMS for outer bearing race for healthy and five fault conditions for three loads

The IR values for the measured AE values for each of five defective cases were calculated using Equation (5.1) and shown in Table B.1.

Table B.1: AE RMS IR value for outer bearing race for five fault conditions, at three shaft speeds for three loads

Fault	Defect Dimensions (mm)	AE RMS IR								
		30 RPM			50 RPM			100 RPM		
		0 kN	2.5 kN	3.4 kN	0 kN	2.5 kN	3.4 kN	0 kN	2.5 kN	3.4 kN
D1	Dent (D = 0.5)	1.04	1.06	1.03	1.18	1.16	1.18	1.74	1.62	1.40
D2	2.5 X 0.9	1.12	1.10	1.10	1.24	1.20	1.23	1.96	1.64	1.45
D3	6.0 X 0.9	1.14	1.15	1.11	1.25	1.23	1.25	1.98	1.67	1.50
D4	6.0 X 3.0	1.16	1.15	1.14	1.26	1.23	1.25	2.04	1.81	1.53
D5	12.0 X 6.0	1.18	1.17	1.16	1.48	1.42	1.31	2.22	2.04	1.59

B.2 AE Kurtosis Observations

The kurtosis for AE signal for the given defects at 30, 50, and 100 rpm, under three loads, are shown in Figure B.2. The IR values of the AE kurtosis are presented in Table B.2.

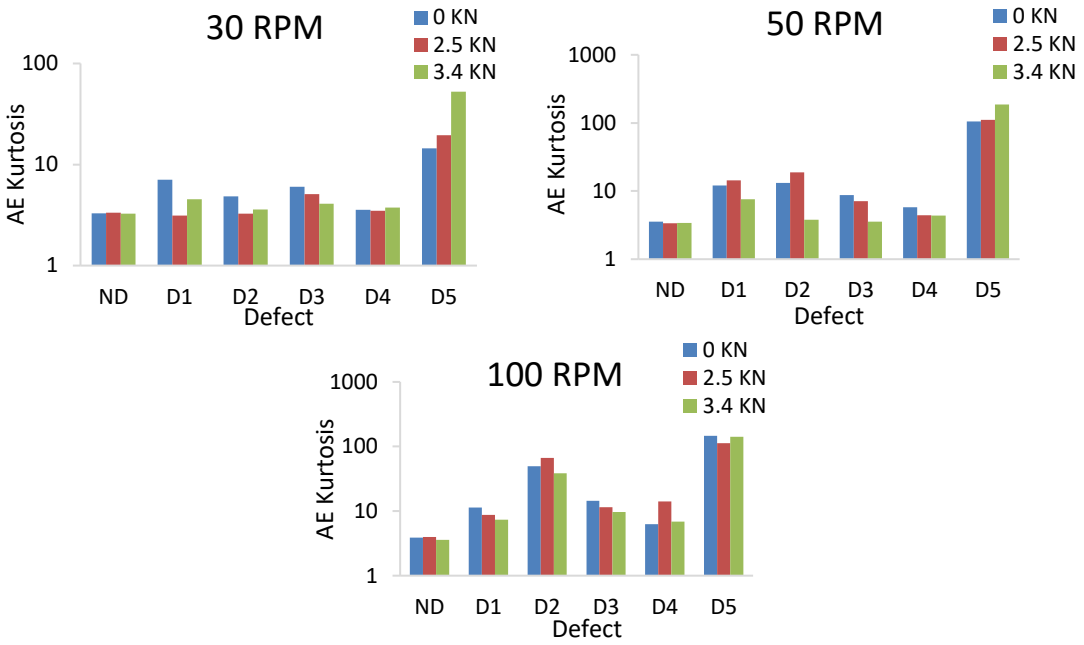

Figure B.2: AE Kurtosis for outer bearing race for healthy and five fault conditions for three loads

Table B.2: AE Kurtosis IR value for outer bearing race for five fault conditions, at three shaft speeds for three loads

Fault	Defect Dimensions (mm)	AE Kurtosis IR								
		30 RPM			50 RPM			100 RPM		
		0 kN	2.5 kN	3.4 kN	0 kN	2.5 kN	3.4 kN	0 kN	2.5 kN	3.4 kN
D1	Dent (D = 0.5)	2.15	0.94	1.39	3.41	4.27	2.22	2.91	2.20	2.05
D2	2.5 X 0.9	1.47	0.98	1.10	3.71	5.61	1.11	12.7	16.86	10.77
D3	6.0 X 0.9	1.84	1.52	1.25	2.45	2.12	1.05	3.69	2.90	2.71
D4	6.0 X 3.0	1.09	1.04	1.15	1.63	1.31	1.28	1.61	3.56	1.92
D5	12.0 X 6.0	4.41	5.84	16.06	29.4	33.13	54.70	37.8	28.39	39.21

B.3 AE Amplitude Observations

The effect of changing the size of the outer race defect on AE amplitude is illustrated in Figure B.3, for shaft speeds of 30, 50, and 100 rpm, and three loads. The IR values, calculated using Equation (5.1) are presented in Table B.3.

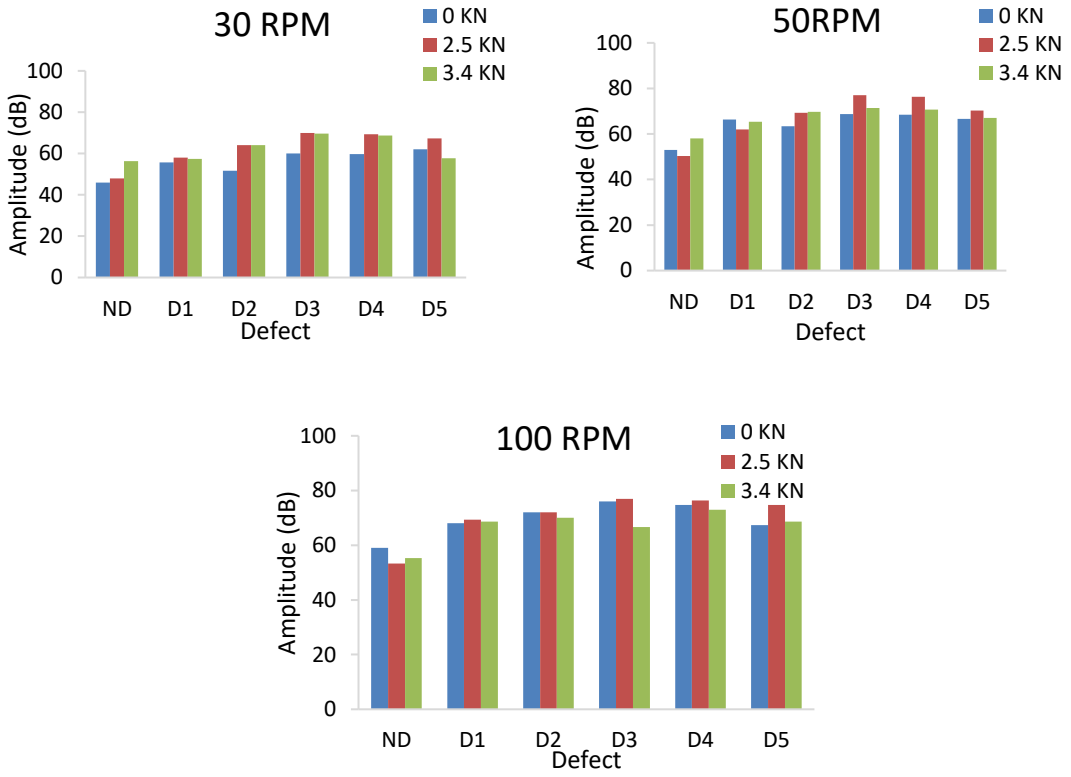

Figure B.3: AE Amplitude for outer bearing race for healthy and five fault conditions for three loads

Table B.3: AE amplitude IR value for outer bearing race for five fault conditions, at three shaft speeds for three loads

Fault	Defect Dimensions (mm)	AE Amplitude IR								
		30 RPM			50 RPM			100 RPM		
		0 kN	2.5 kN	3.4 kN	0 kN	2.5 kN	3.4 kN	0 kN	2.5 kN	3.4 kN
D1	Dent (D = 0.5)	1.21	1.21	1.02	1.25	1.23	1.13	1.15	1.30	1.24
D2	2.5 X 0.9	1.12	1.33	1.14	1.19	1.38	1.20	1.22	1.35	1.27
D3	6.0 X 0.9	1.30	1.46	1.24	1.30	1.53	1.23	1.29	1.44	1.20
D4	6.0 X 3.0	1.30	1.44	1.22	1.29	1.52	1.22	1.27	1.43	1.32
D5	12.0 X 6.0	1.35	1.40	1.02	1.26	1.40	1.16	1.14	1.40	1.24

B.4 AE Counts Observations

The influence of the outer race defect size on the AE counts under three loads is presented in Figure B.4, for shaft speeds of 30, 50, and 100 rpm, and three loads. The corresponding IR values are listed in Table B.4.

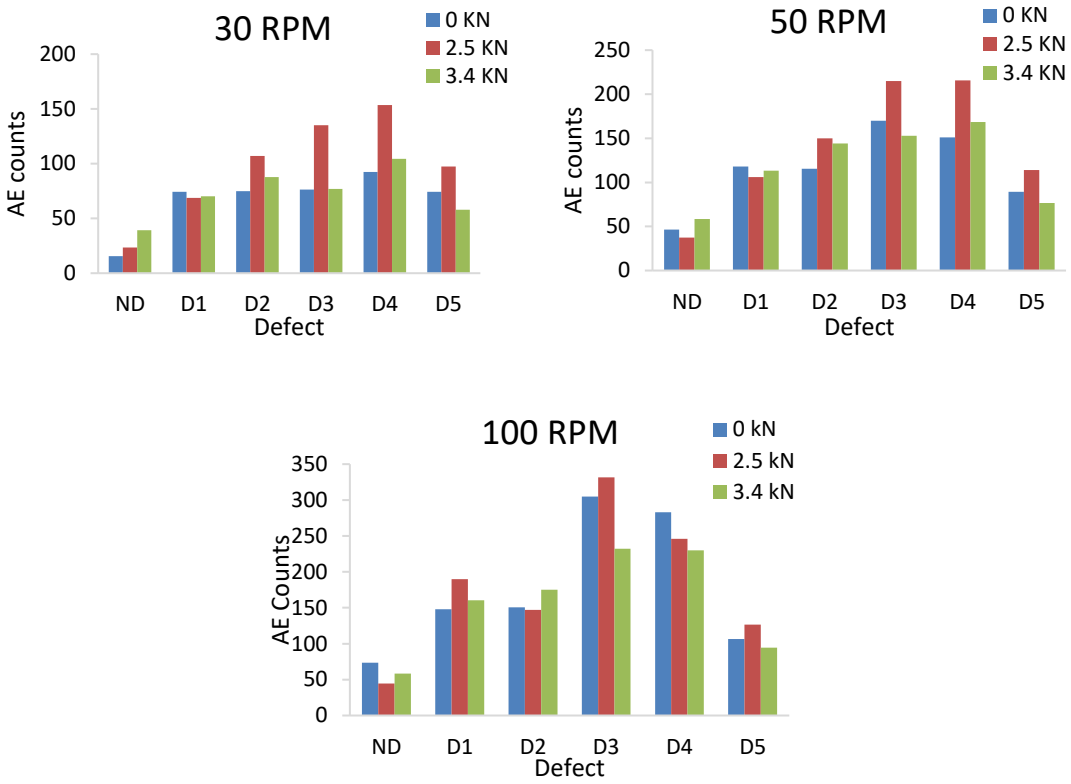

Figure B.4: AE counts for outer bearing race for healthy and five fault conditions for three loads

Table B.4: AE counts IR value for outer bearing race for five fault conditions, at three shaft speeds for three loads

Fault	Defect Dimensions (mm)	AE counts IR								
		30 RPM			50 RPM			100 RPM		
		0 kN	2.5 kN	3.4 kN	0 kN	2.5 kN	3.4 kN	0 kN	2.5 kN	3.4 kN
D1	Dent (D = 0.5)	4.74	2.94	1.79	2.55	2.84	1.94	2.02	4.29	2.75
D2	2.5 X 0.9	4.79	4.59	2.23	2.49	4.02	2.47	2.05	3.32	3.00
D3	6.0 X 0.9	4.87	5.79	1.96	3.67	5.76	2.62	4.15	7.48	3.98
D4	6.0 X 3.0	5.89	6.59	2.65	3.26	5.78	2.89	3.86	5.55	3.94
D5	12.0 X 6.0	4.74	4.17	1.47	1.93	3.05	1.31	1.45	2.86	1.62

Appendix C : **Inner Race Fault Data**

C.1 AE RMS Observations

The RMS values of AE signal under three loads and shaft speeds of 30, 50, and 100 rpm are shown in Figure C.1. These values for a healthy bearing (ND) and five defects, D1 to D5, in the inner race as listed in Table 4.1 and shown in Figure 4.17.

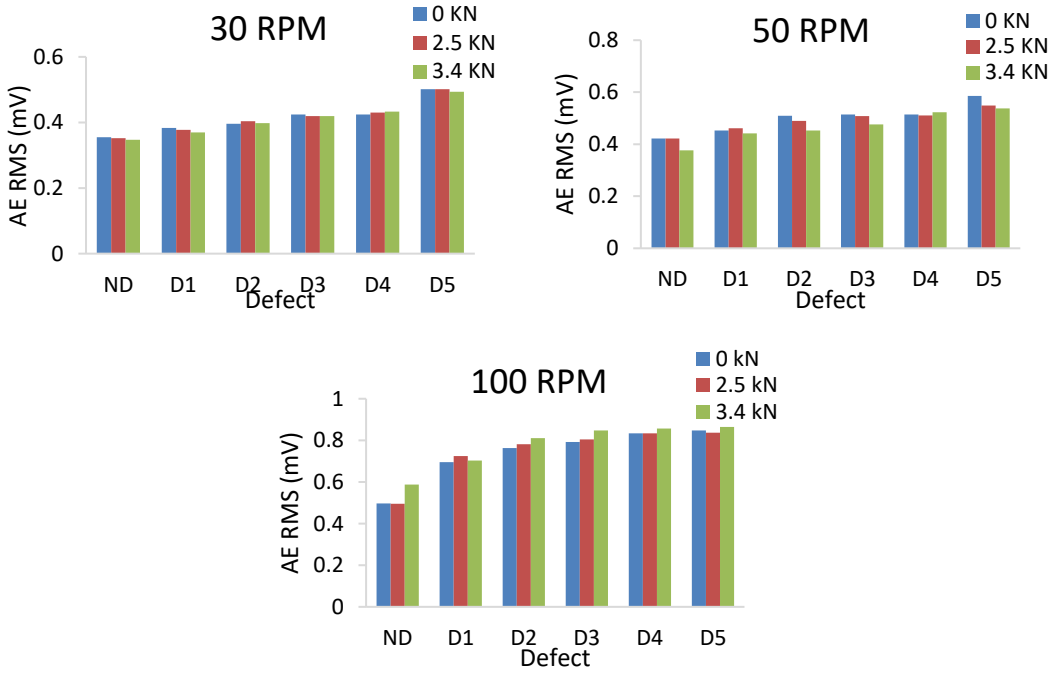

Figure C.1: AE RMS for inner bearing race for healthy and five fault conditions for three loads

The IR values for the measured AE values for each of five defective cases at speeds of 30, 50, and 100 rpm and under three loads was calculated using Equation (5.1) and are shown in Table C.1.

Table C.1: AE RMS IR value for inner bearing race for five fault conditions, at three shaft speeds and for three loads

Fault	Defect Dimensions (mm)	AE RMS IR								
		30 RPM			50 RPM			100 RPM		
		0 kN	2.5 kN	3.4 kN	0 kN	2.5 kN	3.4 kN	0 kN	2.5 kN	3.4 kN
D1	Dent (D = 0.5)	1.08	1.07	1.06	1.08	1.09	1.17	1.40	1.46	1.19
D2	2.5 X 0.9	1.11	1.15	1.15	1.21	1.16	1.20	1.53	1.58	1.38
D3	6.0 X 0.9	1.19	1.19	1.21	1.22	1.20	1.26	1.59	1.62	1.44
D4	6.0 X 3.0	1.19	1.22	1.25	1.22	1.21	1.39	1.68	1.69	1.46
D5	12.0 X 6.0	1.41	1.43	1.42	1.39	1.30	1.43	1.70	1.69	1.47

C.2 AE Kurtosis Observations

The kurtosis for AE signal as a function of defect size, for speeds of 30, 50, and 100 rpm, under three loads, are shown in Figure C.2. The IR of the AE kurtosis values are presented in Table C.2.

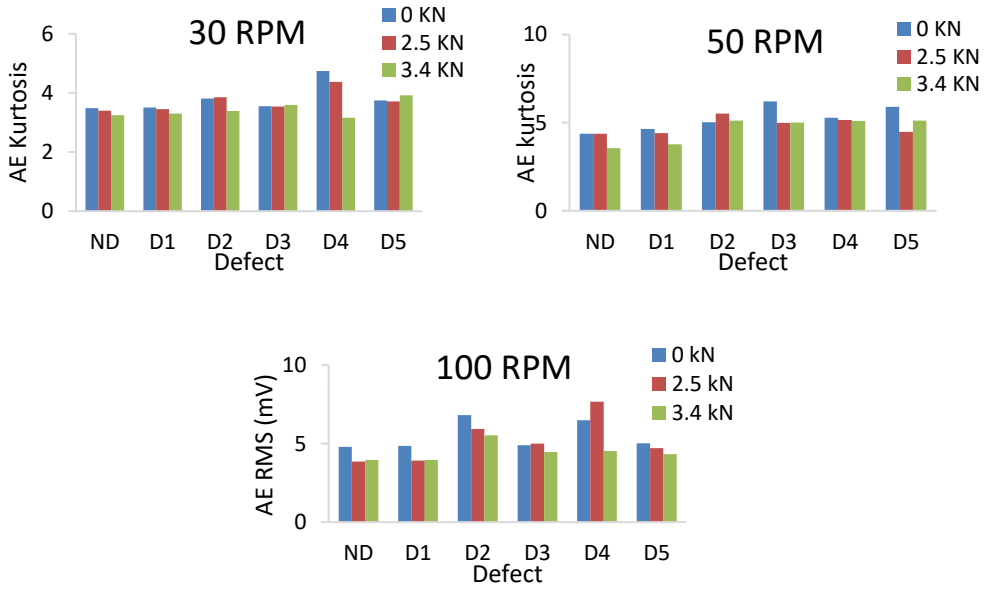

Figure C.2: AE Kurtosis for inner bearing race for healthy and five fault conditions for three loads

Table C.2: AE Kurtosis IR value for inner bearing race for five fault conditions, at three shaft speeds and for three loads

Fault	Defect Dimensions (mm)	AE Kurtosis IR								
		30 RPM			50 RPM			100 RPM		
		0 kN	2.5 kN	3.4 kN	0 kN	2.5 kN	3.4 kN	0 kN	2.5 kN	3.4 kN
D1	Dent (D = 0.5)	1.00	1.02	1.02	1.06	1.01	1.06	1.01	1.01	1.00
D2	2.5 X 0.9	1.09	1.13	1.04	1.15	1.26	1.43	1.42	1.54	1.40
D3	6.0 X 0.9	1.02	1.04	1.11	1.42	1.14	1.40	1.02	1.30	1.13
D4	6.0 X 3.0	1.36	1.29	0.97	1.21	1.18	1.43	1.36	1.99	1.15
D5	12.0 X 6.0	1.07	1.09	1.21	1.35	1.02	1.44	1.05	1.22	1.10

C.3 AE Amplitude Observations

The effect of changing the size of the inner race defect on AE amplitude under three loads, at shaft speeds of 30, 50, and 100 rpm is illustrated in Figure C.3. The IR values, calculated using Equation (5.1) are presented in Table C.3.

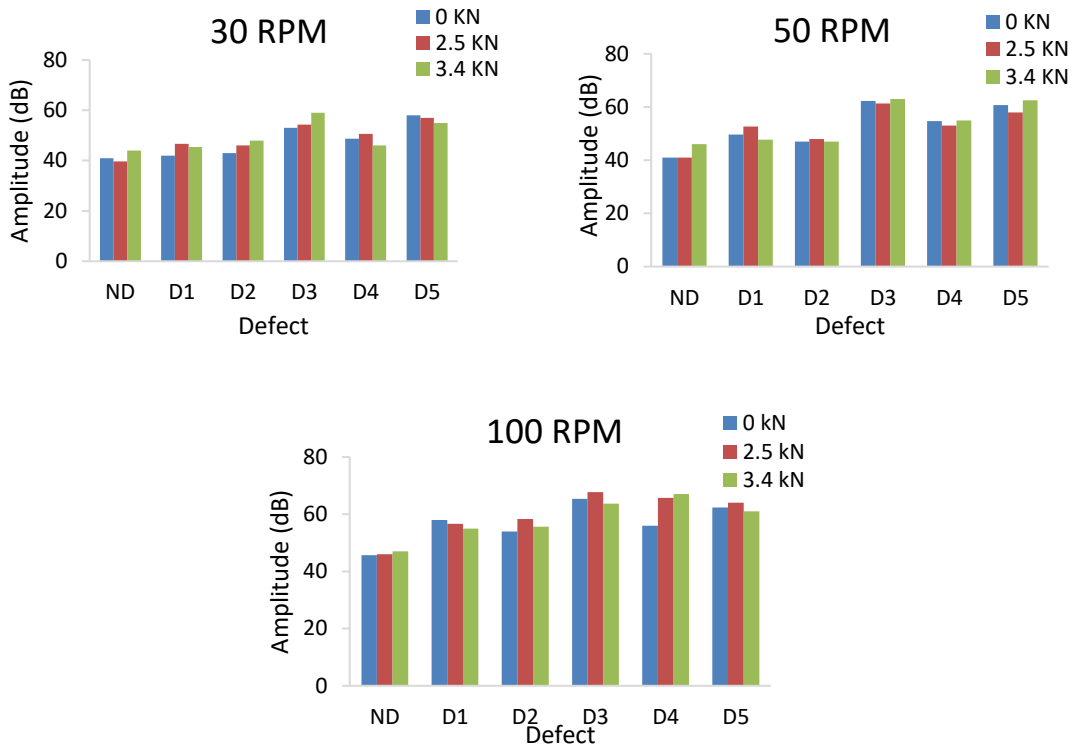

Figure C.3: AE Amplitude for inner bearing race for healthy and five fault conditions for three loads

Table C.3: AE amplitude IR value for inner bearing race for five fault conditions, at three shaft speeds and three loads

Fault	Defect Dimensions (mm)	AE Amplitude IR								
		30 RPM			50 RPM			100 RPM		
		0 kN	2.5 kN	3.4 kN	0 kN	2.5 kN	3.4 kN	0 kN	2.5 kN	3.4 kN
D1	Dent (D = 0.5)	1.02	1.18	1.03	1.21	1.28	1.04	1.27	1.23	1.17
D2	2.5 X 0.9	1.05	1.16	1.09	1.15	1.17	1.02	1.18	1.27	1.18
D3	6.0 X 0.9	1.29	1.37	1.34	1.52	1.50	1.37	1.43	1.47	1.35
D4	6.0 X 3.0	1.19	1.28	1.05	1.33	1.29	1.20	1.23	1.43	1.43
D5	12.0 X 6.0	1.41	1.44	1.25	1.48	1.41	1.36	1.36	1.39	1.30

C.4 AE Counts Observations

The influence of the inner race defect size on the AE counts under three loads is presented in Figure C.4, for shaft speeds of 30, 50, and 100 rpm. The corresponding IR values are listed in Table C.4.

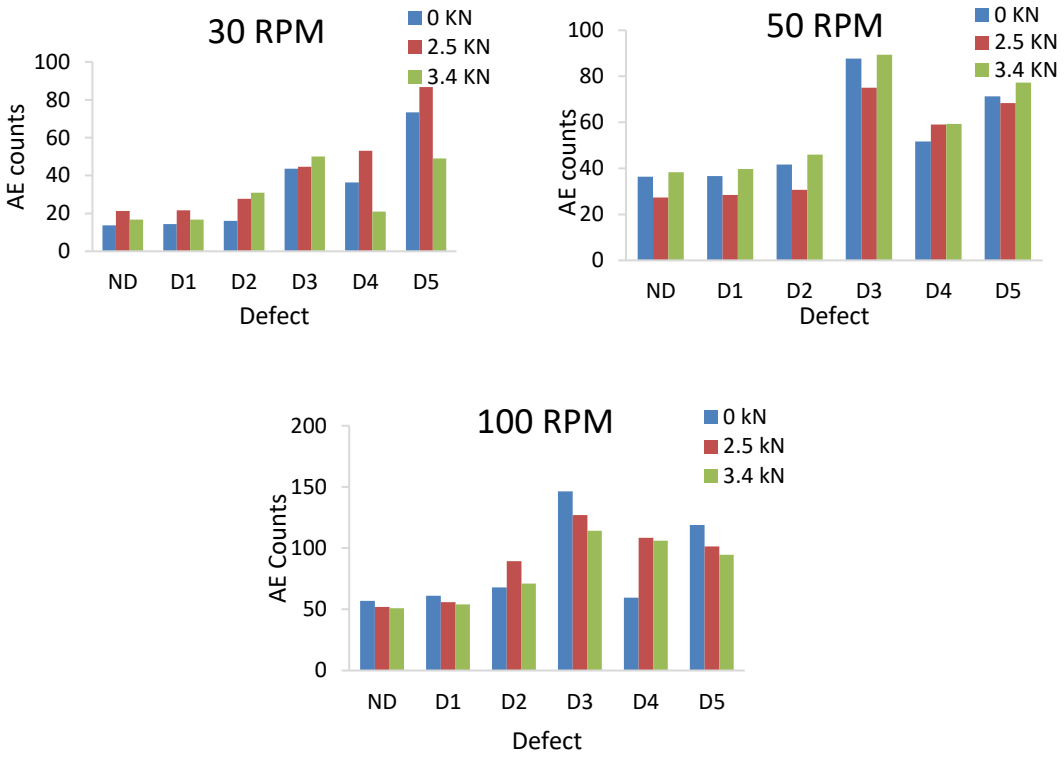

Figure C.4: AE counts for inner bearing race for healthy and five fault conditions for three loads

Table C.4: AE counts IR value for inner bearing race for five fault conditions, at three shaft speeds for three loads

Fault	Defect Dimensions (mm)	AE counts IR								
		30 RPM			50 RPM			100 RPM		
		0 kN	2.5 kN	3.4 kN	0 kN	2.5 kN	3.4 kN	0 kN	2.5 kN	3.4 kN
D1	Dent (D = 0.5)	1.05	1.02	1.00	1.01	1.04	1.03	1.07	1.08	1.06
D2	2.5 X 0.9	1.17	1.30	1.86	1.15	1.12	1.20	1.19	1.72	1.39
D3	6.0 X 0.9	3.19	2.09	3.00	2.41	2.74	2.33	2.57	2.44	2.24
D4	6.0 X 3.0	2.66	2.48	1.26	1.42	2.16	1.55	1.05	2.08	2.08
D5	12.0 X 6.0	5.36	4.06	2.94	1.96	2.50	2.02	2.09	1.95	1.86

Appendix D : **Inner and Outer Race Comparison**

D.1 AE RMS Observations

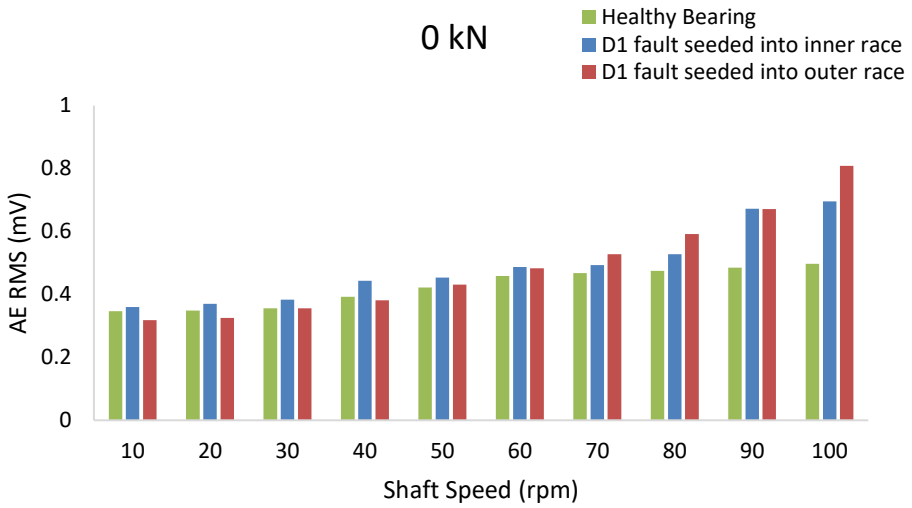

Figure D.1: Comparison of AE RMS as a function of shaft speed at zero applied load, for a healthy bearing and a D1 fault in the inner and outer races

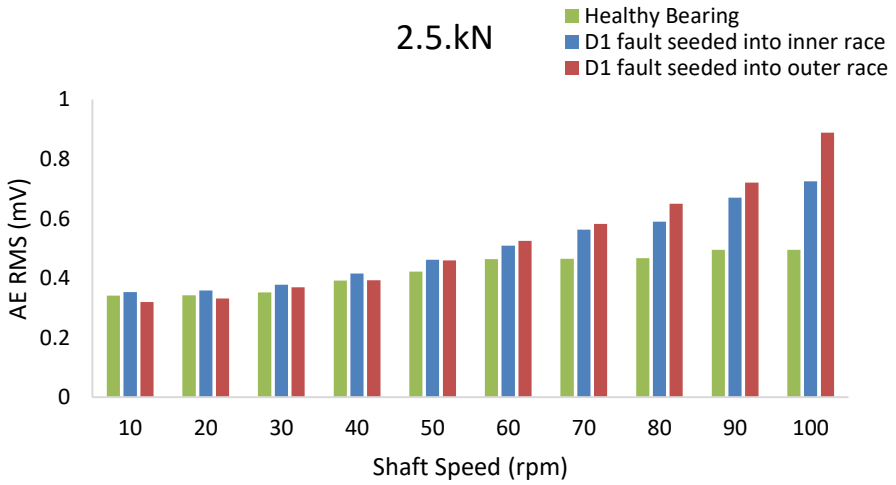

Figure D.2: Comparison of AE RMS as a function of shaft speed at 2.5 kN load, for a healthy bearing and a D1 fault in the inner and outer races

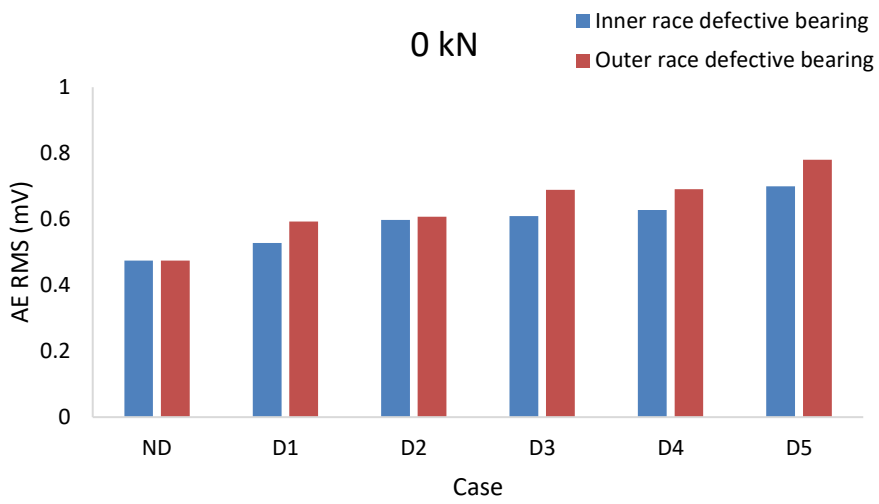

Figure D.3: AE RMS for a healthy bearing and five different faults in the inner and outer races, at 80 rpm and zero applied load

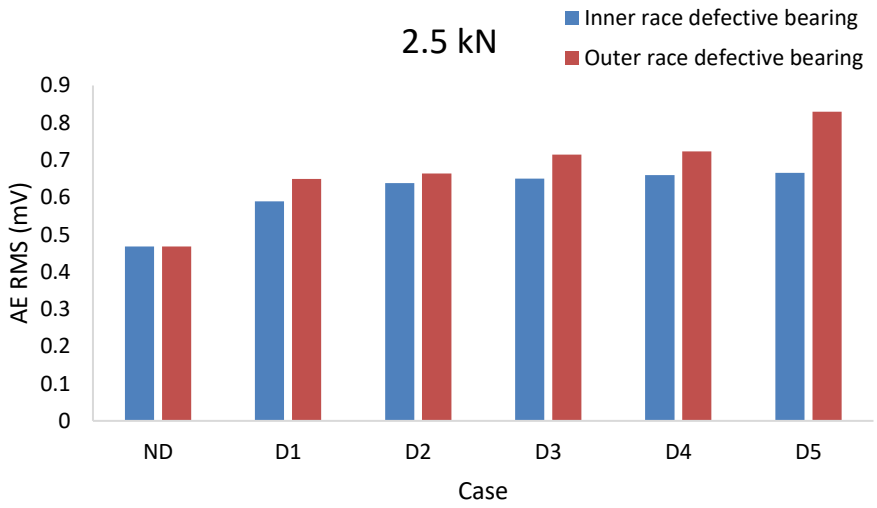

Figure D.4: AE RMS for a healthy bearing and five different faults in the inner and outer races, at 80 rpm and 2.5 kN load.

D.2 AE Kurtosis Observations

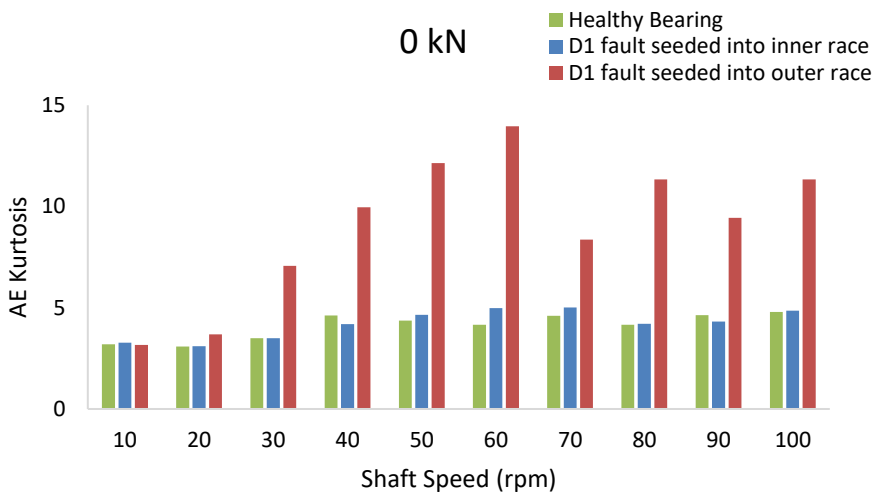

Figure D.5: Comparison of AE kurtosis as a function of shaft speed at zero applied load, for a healthy bearing and a D1 fault in the inner and outer races

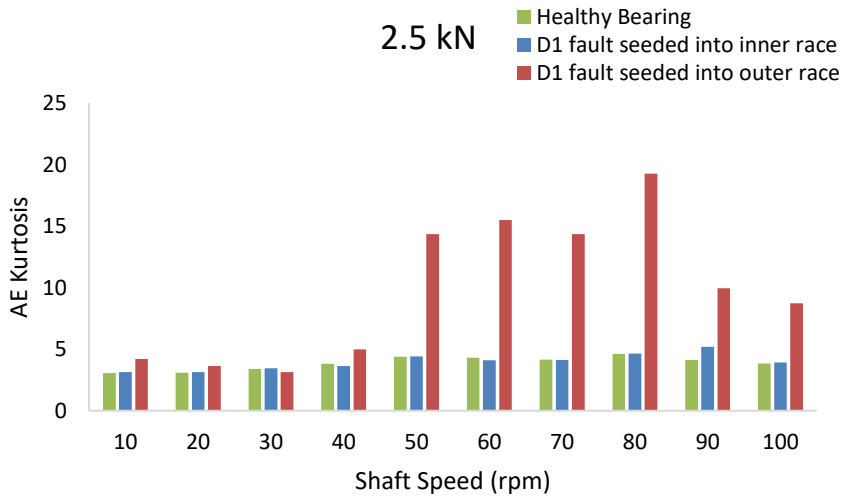

Figure D.6: Comparison of AE kurtosis as a function of shaft speed at 2.5 kN load, for a healthy bearing and a D1 fault in the inner and outer races

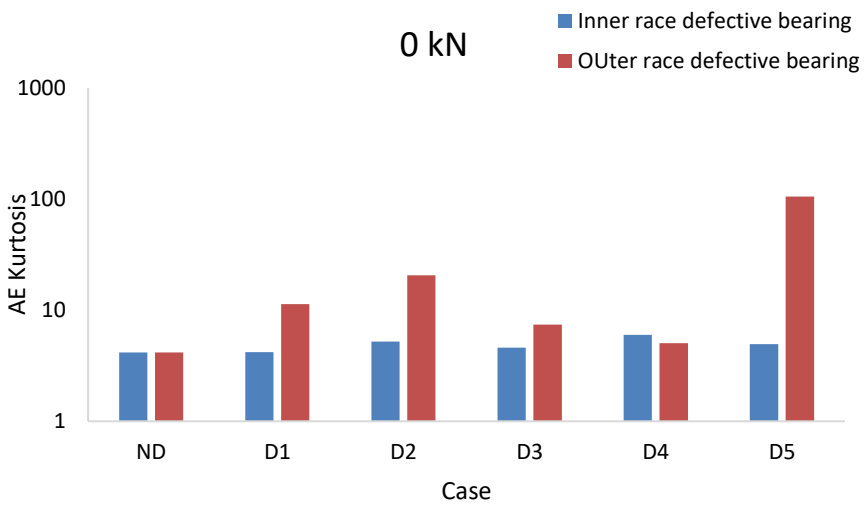

Figure D.7: AE kurtosis for six inner and outer race bearing conditions, at 80 rpm and zero applied load

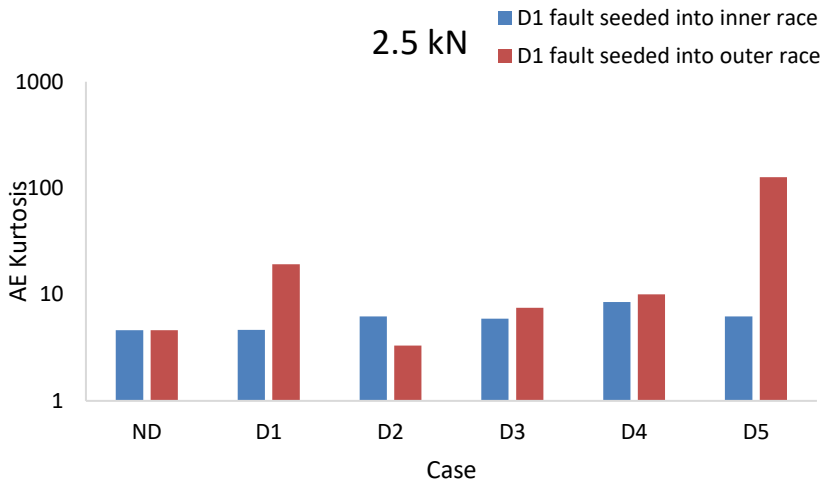

Figure D.8: AE kurtosis for six inner and outer race bearing conditions, at 80 rpm and 2.5 kN load

D.3 Amplitude Observations

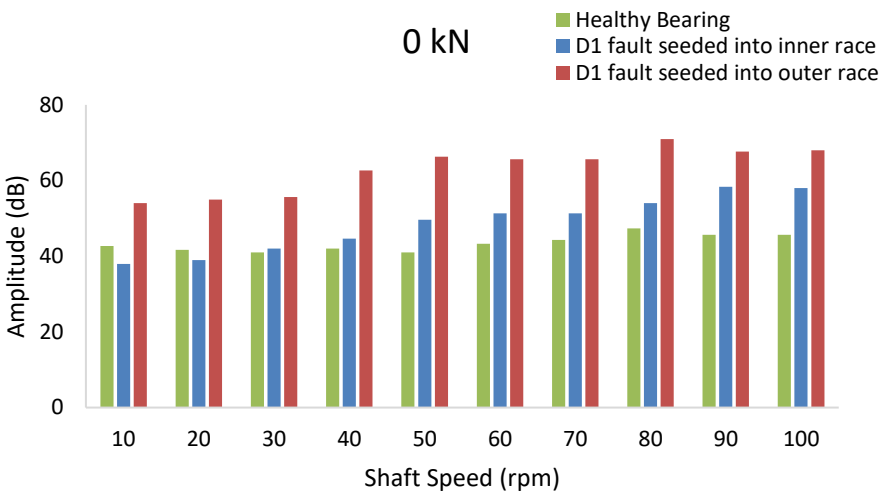

Figure D.9: Comparison of AE amplitude as a function of shaft speed at 0 kN load, for healthy bearing and bearings with a D1 fault in the inner and outer races

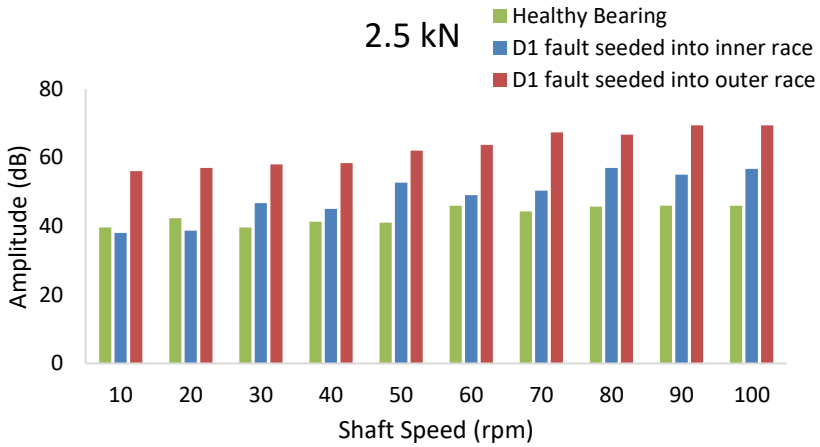

Figure D.10: Comparison of AE amplitude as a function of shaft speed at 2.5 kN load, for healthy bearing and bearings with a D1 fault in the inner and outer races

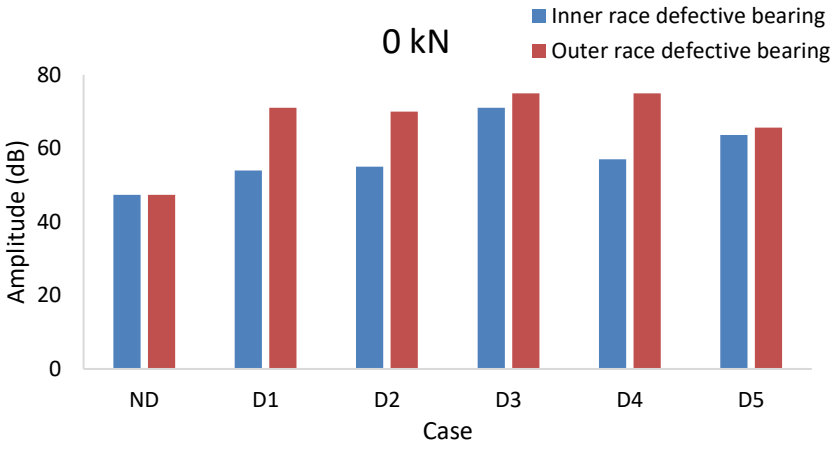

Figure D.11: AE amplitude for six inner and outer races bearing conditions, at 80 rpm and zero applied load

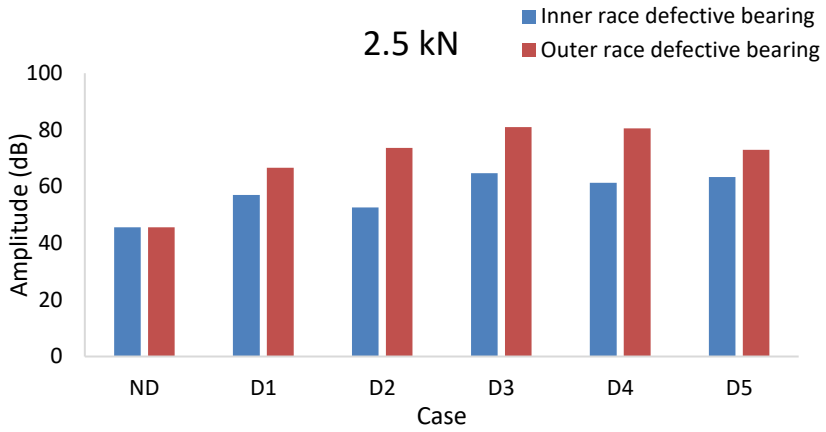

Figure D.12: AE amplitude for six inner and outer races bearing conditions, at 80 rpm and 2.5 kN load

D.4 AE Counts Observations

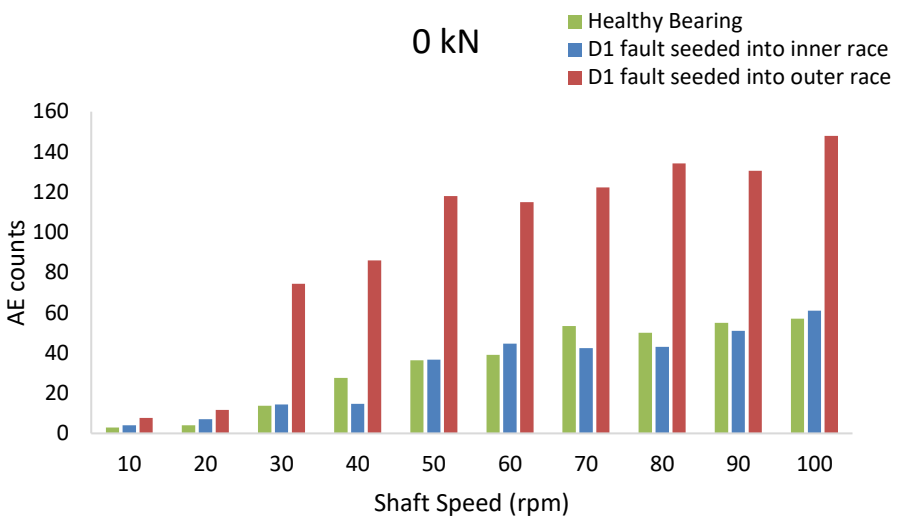

Figure D.13: Comparison of AE counts as a function of shaft speed at zero applied load, for a healthy bearing and bearings with a D1 fault in the inner and outer races

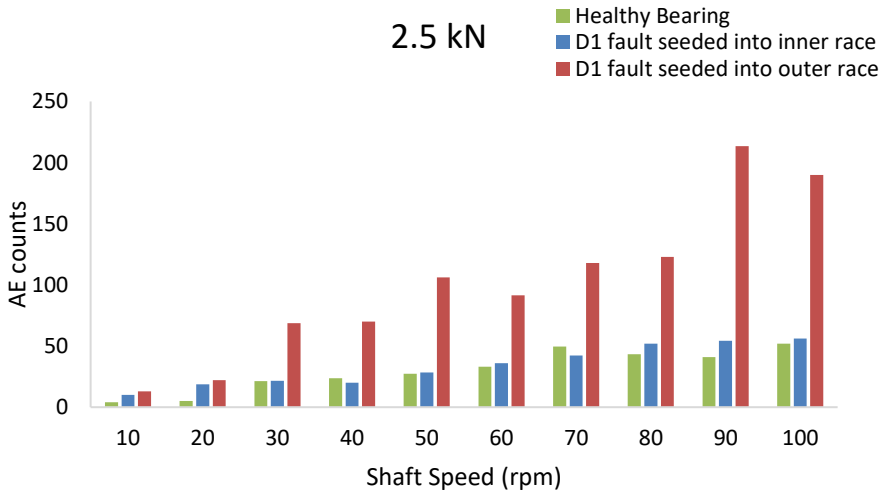

Figure D.14: Comparison of AE counts as a function of shaft speed at 2.5 kN load, for a healthy bearing and bearings with a D1 fault in the inner and outer races

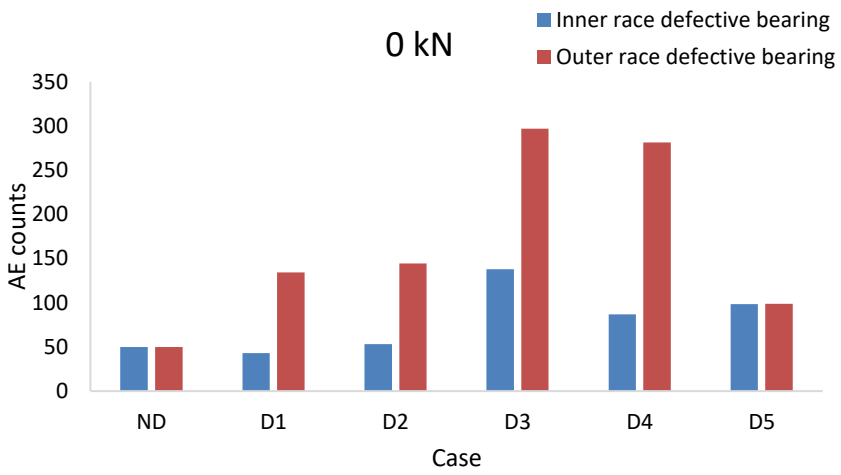

Figure D.15: AE counts for six inner and outer races bearing conditions, at 80 rpm and zero applied load

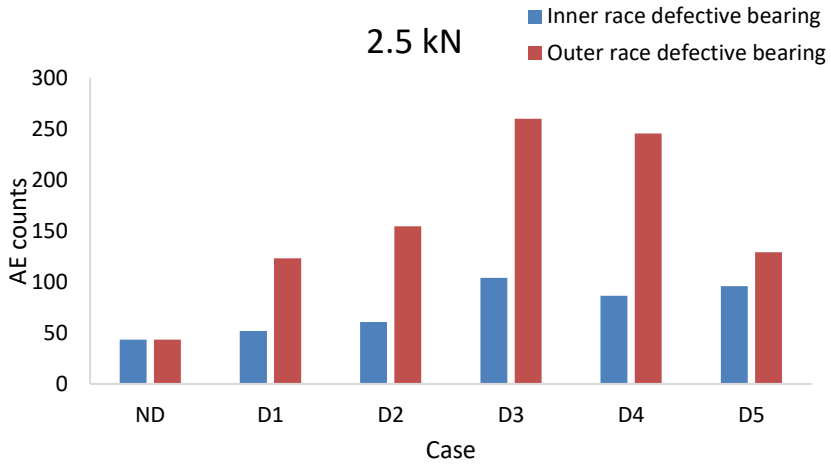

Figure D.16: AE counts for six inner and outer races bearing conditions, at 80 rpm and 2.5 kN load

Appendix E : **Defect Location Comparison**

This section presents the results of a healthy bearing and two bearings with a seeded defect size of (6X3 mm^2) one at the middle (D4) and the other at the edge (D12) of the outer race as shown respectively in Table 4.1 and Figure 4.16 and Figure 4.18 (b).

E.1 RMS Observations

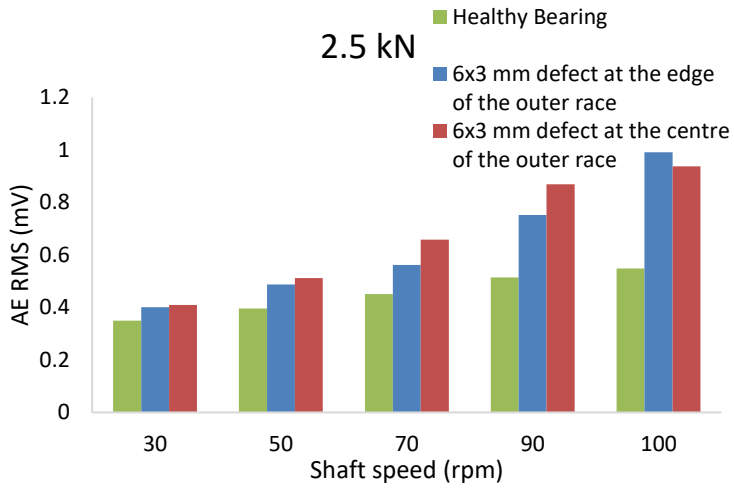

Figure E.1: AE RMS as a function of shaft speed at 2.5 kN, for healthy and two defective bearings (D4 and D12)

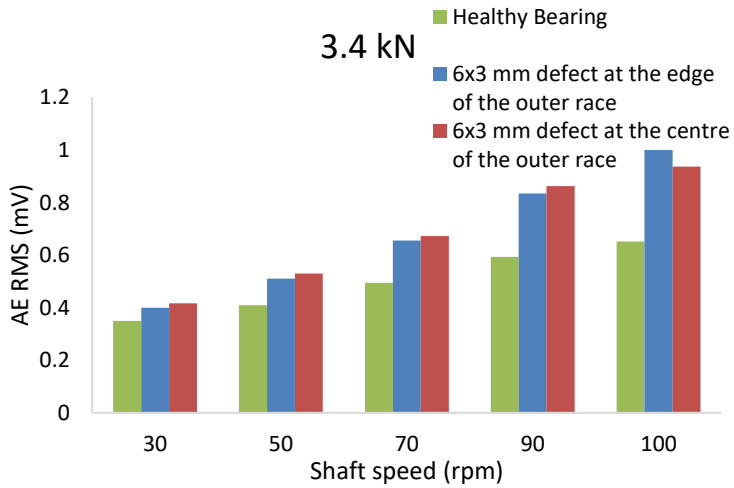

Figure E.2: AE RMS as a function of shaft speed at 3.4 kN, for healthy and two defective bearings (D4 and D12)

E.2 Kurtosis Observations

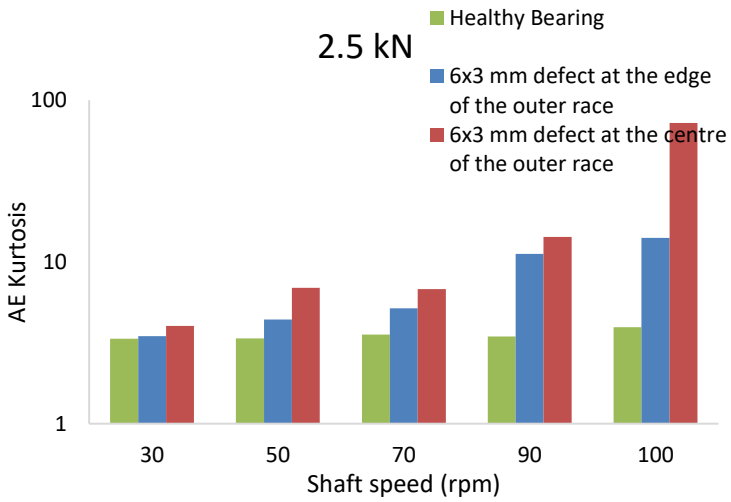

Figure E.3: AE kurtosis as a function of shaft speed at 2.5 kN, for healthy and two defective bearings (D4 and D12)

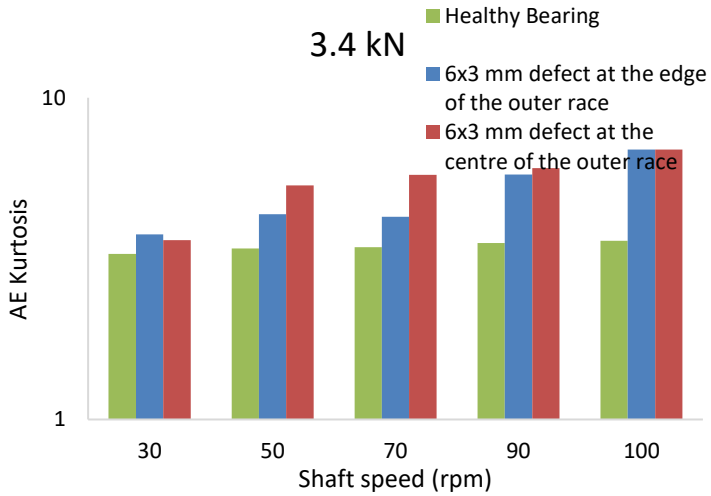

Figure E.4: AE kurtosis as a function of shaft speed at 3.4 kN, for healthy and two defective bearings (D4 and D12)

E.3 Amplitude Observations

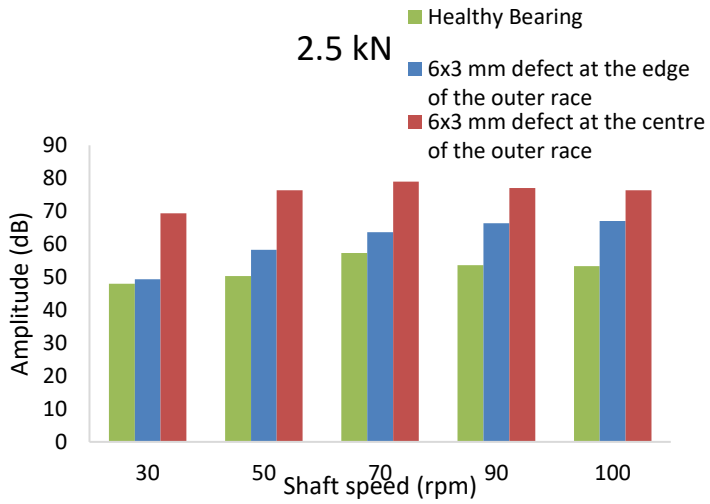

Figure E.5: AE Amplitude as a function of shaft speed at 2.5 kN, for healthy and two defective bearings (D4 and D12)

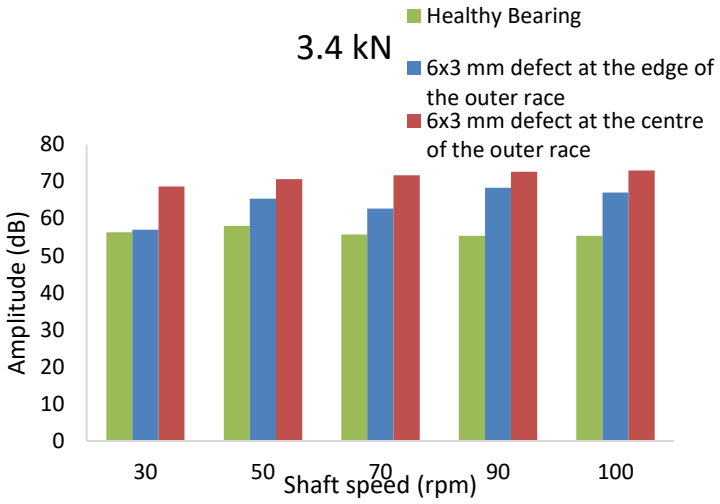

FigureE.6: AE Amplitude as a function of shaft speed at 3.4 kN, for healthy and two defective bearings (D4 and D12)

E.4 AE Counts Observations

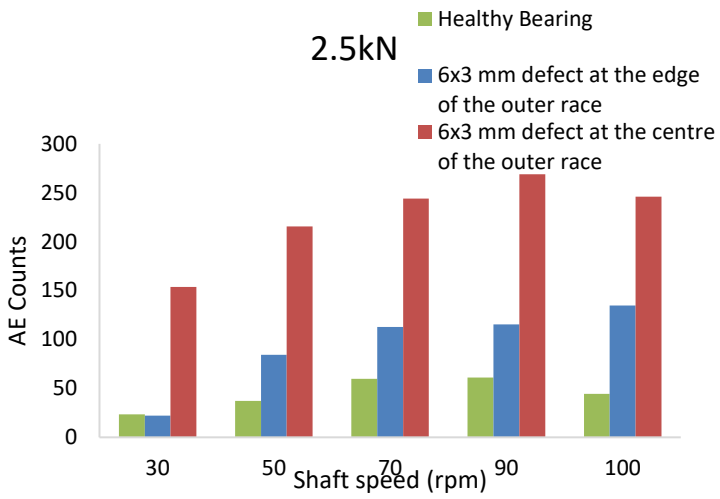

Figure E.7: AE counts as a function of shaft speed at 2.5 kN, for healthy and two defective bearings (D4 and D12)

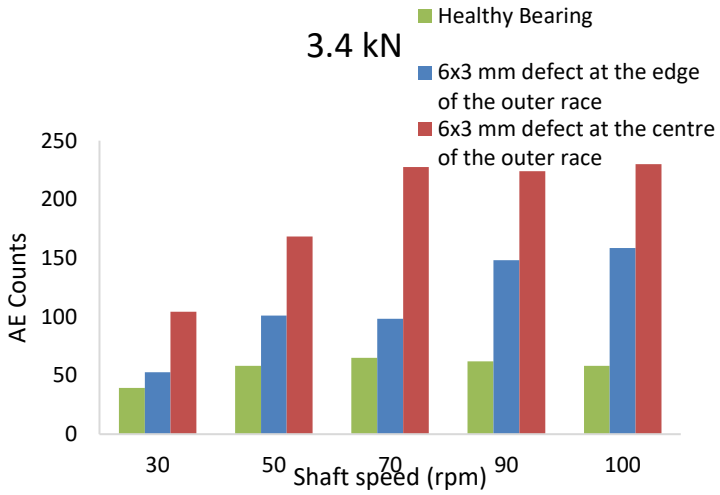

Figure E.8: AE counts as a function of shaft speed at 3.4 kN, for healthy and two defective bearings (D4 and D12)